

Chem Soc Rev

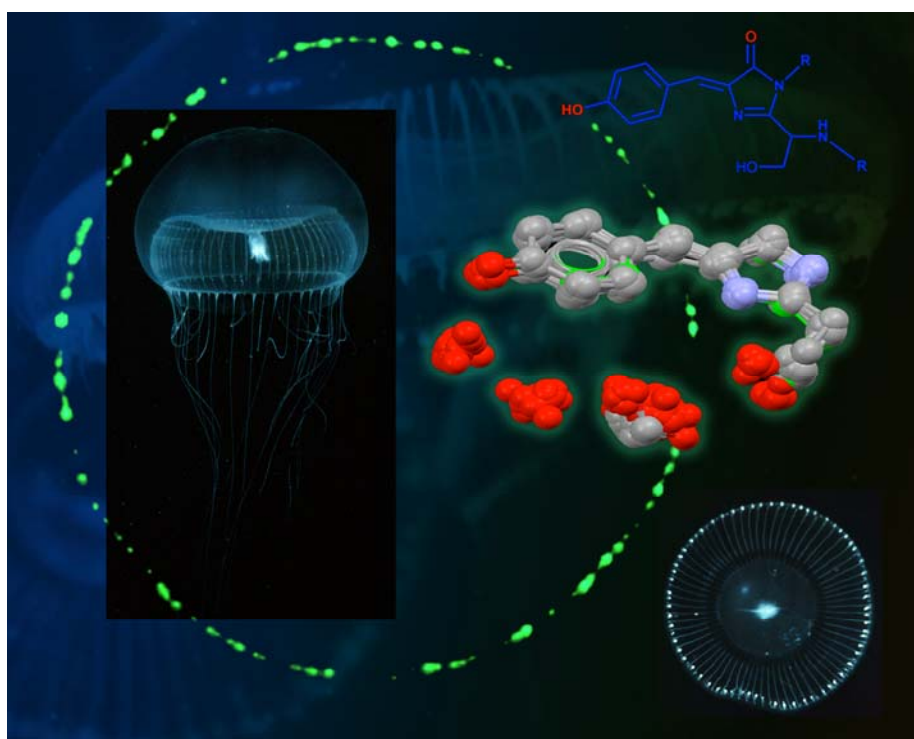
This article was published as part of the
2009 Green Fluorescent Protein issue

Reviewing the latest developments in the science of green
fluorescent protein

Guest Editors Dr Sophie Jackson and Professor Jeremy Sanders

All authors contributed to this issue in honour of the 2008 Nobel Prize winners in
Chemistry, Professors Osamu Shimomura, Martin Chalfie and Roger Y. Tsien

Please take a look at the issue 10 [table of contents](#) to access
the other reviews



The fluorescent protein palette: tools for cellular imaging†

Richard N. Day^{*a} and Michael W. Davidson^b

Received 8th May 2009

First published as an Advance Article on the web 4th August 2009

DOI: 10.1039/b901966a

This critical review provides an overview of the continually expanding family of fluorescent proteins (FPs) that have become essential tools for studies of cell biology and physiology. Here, we describe the characteristics of the genetically encoded fluorescent markers that now span the visible spectrum from deep blue to deep red. We identify some of the novel FPs that have unusual characteristics that make them useful reporters of the dynamic behaviors of proteins inside cells, and describe how many different optical methods can be combined with the FPs to provide quantitative measurements in living systems (227 references).

“If wood is rubbed with the *Pulmo marinus*, it will have all the appearance of being on fire; so much so, indeed, that a walking-stick, thus treated, will light the way like a torch” (translation of Pliny the Elder from John Bostock, 1855).

1. Introduction

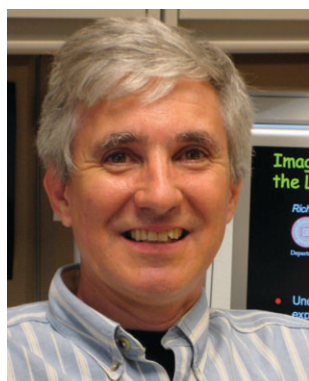
There has long been a fascination with things in nature that glow—illustrated by the comments of Pliny the Elder in AD77.¹ It is now well appreciated that, aside from the jellyfish found in the Bay of Naples (*Pulmo marinus*) first described by

Pliny the Elder, many marine organisms produce light through chemiluminescent or fluorescence (and as we will see, sometimes both) processes.² Efforts to identify the molecular basis for the glow of the jellyfish began with Osamu Shimomura’s studies of the *Aequorea* jellyfish in the early 1960’s. Then at Princeton University, Shimomura traveled with Frank Johnson to Friday Harbor Laboratories at the University of Washington with the goal of developing a method to extract the light emitting components from *Aequorea victoria*. They observed that when the circumoral ring on the underside of the jellyfish, which contains the luminescent organs, was removed and squeezed through a sieve, the “squeezate” was dimly luminescent.³ In a heroic effort, involving the collection and processing of many thousands of jellyfish into squeezate, they isolated and purified

^a Department of Cellular and Integrative Physiology, Indiana University School of Medicine, 635 Barnhill Dr., Indianapolis, IN 46202, USA. E-mail: rnday@iupui.edu; Fax: +1 317 274 3318; Tel: +1 317 274 2166

^b National High Magnetic Field Laboratory and Department of Biological Science, The Florida State University, 1800 E. Paul Dirac Dr., Tallahassee, FL 32310, USA

† Part of a themed issue on the topic of Green Fluorescent Protein (GFP) in honour of the 2008 Nobel Prize winners in Chemistry, Professors Osamu Shimomura, Martin Chalfie and Roger Y. Tsien.



Richard N. Day

Richard N. Day is a Professor in the Department of Cellular and Integrative Physiology at the Indiana University School of Medicine. His research focuses on understanding the network of regulatory protein interactions that function to control cell-type specific gene expression. His laboratory group uses biochemical and molecular approaches to define networks of protein interactions that are coordinated by specific transcription factors. These in vitro

approaches are then complemented by non-invasive live-cell imaging techniques using the many different color variants of the marine invertebrate fluorescent proteins. Recent studies from the laboratory have used Förster resonance energy transfer (FRET)-based microscopy approaches to begin to define networks of protein interactions in living cells.



Michael W. Davidson

Michael W. Davidson is an Associate in Research affiliated with the Department of Biological Science and the National High Magnetic Field Laboratory at the Florida State University. Davidson’s laboratory is involved in development of educational websites that address all phases of optical microscopy, including bright field, phase contrast, DIC, fluorescence, confocal, TIRF, and multi-photon. In addition to his interest in educational activities, Davidson is also involved in research involving the performance of traditional fluorescent proteins and optical highlighters in fusions for targeting and dynamics studies in live cells.

the chemiluminescent protein aequorin.⁴ Aequorin is a luciferase that catalyzes the oxidization of the substrate coelenterazine in a calcium-dependent reaction that leads to the emission of blue light. This discovery was curious,

however, since the luminescent organs of the intact jellyfish produce green light. Importantly, during the purification Shimomura had observed a protein in the jellyfish extracts "exhibiting a very bright, greenish fluorescence" under

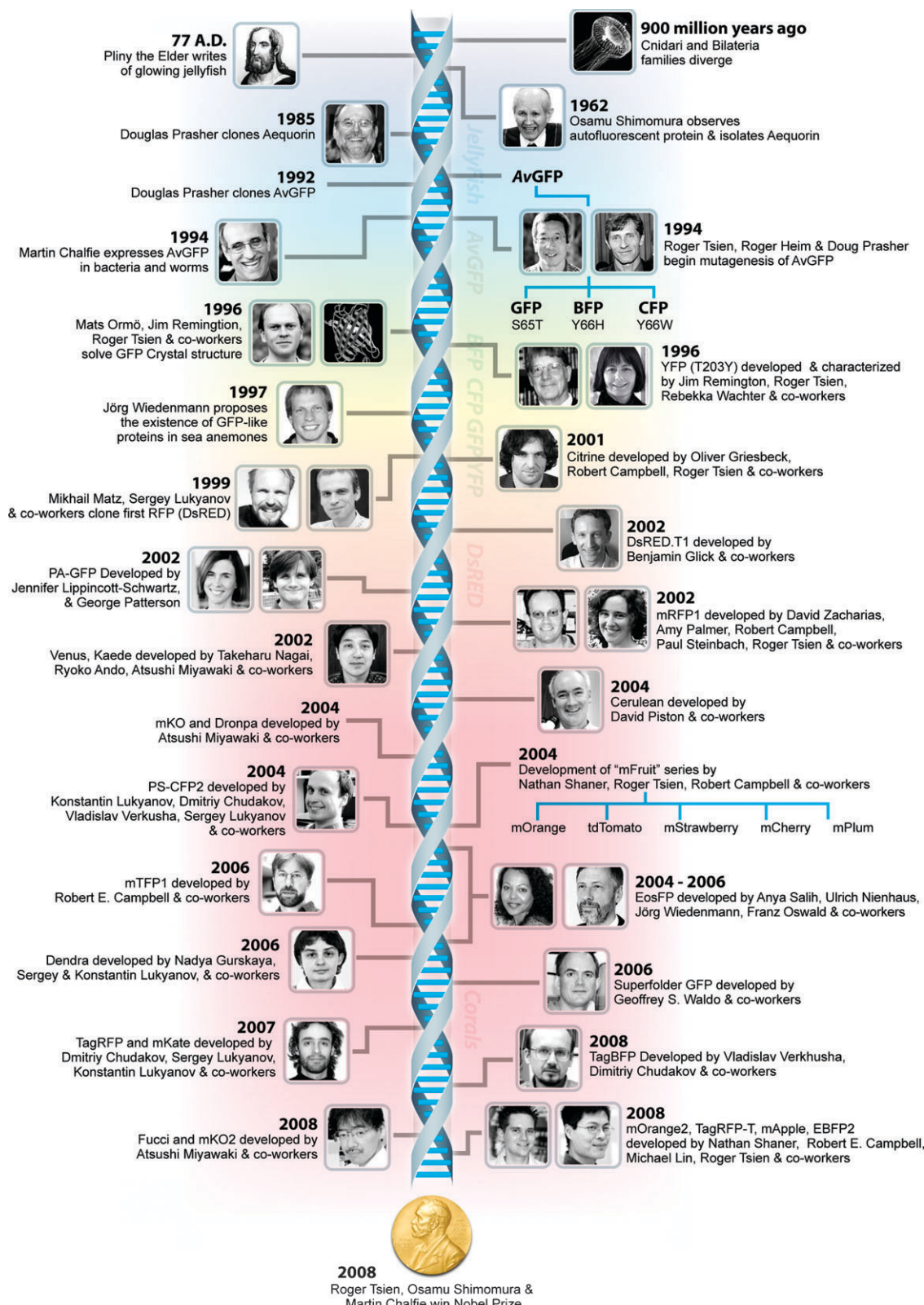


Fig. 1 Timeline of important events in fluorescent protein technology.

ultraviolet (UV) light illumination.⁴ It was later determined that this autofluorescent protein was a companion protein for the chemiluminescent aequorin—the protein now known as the jellyfish green fluorescent protein (GFP). In the 1970's, Shimomura and colleagues⁵ purified this autofluorescent protein and showed for the first time that GFP, *via* an energy transfer process, absorbed the excited state energy from aequorin and emitted green light.

The identification of GFP from *Aequorea* was the first step in what has often been described as a "revolution" in cell biology, although it would be some years before the true significance of this observation became apparent.⁶ Early in the 1980's, while working with Milton Cormier at the University of Georgia, Douglas Prasher prepared a cDNA library from *A. victoria* mRNA, and used this to clone the gene encoding the aequorin.⁷ Later, using the same cDNA library, Prasher isolated a clone that contained part of the sequence encoding the companion protein, GFP (pGFP1). Then, by creating a new cDNA library in the λgt10 cloning vector, and screening it with the pGFP1 clone, Prasher obtained a single full-length clone (*gfp10*) that encoded the complete *Aequorea* GFP sequence in 1992.⁸ Prasher recognized the great potential of GFP as a tool for cell biologists, but since no information was available regarding the biosynthesis pathway leading to chromophore formation and fluorescence, he was cautious of the difficulties associated with producing the protein in biological systems other than the jellyfish.³

Fortunately, Prasher's concerns regarding the difficulties of expressing *Aequorea* GFP in other biological systems proved to be unwarranted. Using the clone isolated by Prasher, Martin Chalfie successfully expressed GFP in both bacteria and the sensory neurons of *Caenorhabditis elegans* nematode worms, demonstrating for the first time that chromophore formation (and fluorescence) required no additional factors that were specific to the jellyfish.⁹ Many other studies rapidly followed, which demonstrated the utility of this new genetically encoded probe for *in vivo* fluorescence labeling in a variety of different cellular systems and transgenic organisms.^{10–14}

As it turns out, the GFP chromophore is encoded by the primary amino acid sequence, and it forms spontaneously without the requirement for cofactors or external enzyme components (other than molecular oxygen), through a self-catalyzed protein folding mechanism and intramolecular rearrangement (for more on this subject, see other articles in this themed issue). The genetically encoded GFP provided for the first time the ability to label specific proteins inside the living cell without the need for exogenous synthetic or antibody-labeled fluorescent tags. When coupled with the astonishing advances in live-cell imaging instrument (microscope and camera) technologies that have occurred over the past decade, the fluorescent proteins (FPs) have truly ushered in a new era for investigations related to cell biology, medicine, and physiology. Presented in Fig. 1 is a timeline of important events in the development of the fluorescent proteins described throughout this review article. These tools now provide an important complement to the classical biochemical studies, extending the analysis of protein–protein interactions, protein conformational changes, and the

behavior of signaling molecules to their natural environment within the intact cell.

2. The *A. victoria* GFP

Early studies by Shimomura¹⁵ using the purified *Aequorea* GFP showed that the entire protein sequence was necessary for its characteristic fluorescence. However, the digestion of the purified protein with papain, followed by high-performance liquid chromatography to isolate the fragments, revealed that a single hexapeptide sequence starting at amino acid 64 was responsible for all the light absorption properties of GFP.¹⁶ This discovery led to the demonstration that the chromophore absorbing the blue light energy from aequorin was formed by the cyclization of the adjacent Ser65-Tyr66-Gly67 (the number denotes the position in the intact peptide sequence) residues within this hexapeptide sequence.¹⁶ The most popular model describing the formation of the chromophore (outlined in Fig. 2) during the maturation of GFP has a series of torsional peptide and side-chain bond adjustments that position the carboxyl carbon of Ser65 close to the amino nitrogen atom of Gly67. This leads to a nucleophilic attack by the amide nitrogen of glycine on the serine carbonyl carbon atom, which is followed by dehydration, resulting in the formation of an imidazolin-5-one heterocyclic ring system.¹⁶ Fluorescence occurs when oxidization of the Tyr66 α–β carbon bond by molecular oxygen extends the conjugation of electron orbitals of the imidazoline ring system to include the tyrosine phenyl ring, and its *para*-oxygen substituent.^{3,17,18} Participation of molecular oxygen is a critical factor in chromophore development, and at least one oxygen molecule is required for dehydrogenation.^{18,19} Additionally, Arg96 and Glu222, two residues that are invariant in every FP yet discovered, are thought to catalyze the reaction. The end result of chromophore maturation is a highly conjugated π-electron resonance system that largely accounts for the spectroscopic and photophysical properties of the protein.

In 1996, the crystal structure for GFP was solved, revealing that the cyclic tripeptide chromophore is buried in the center

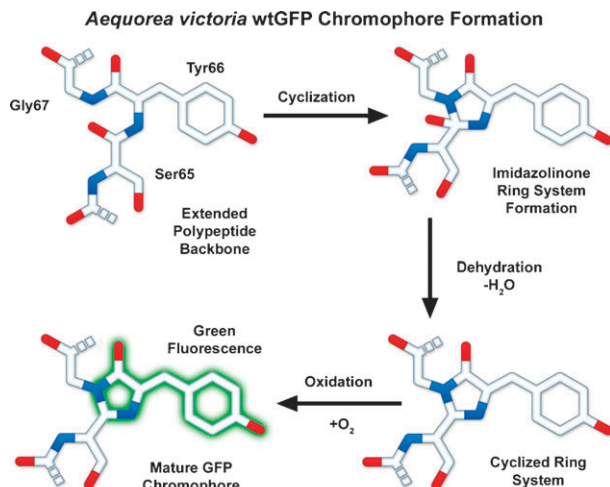


Fig. 2 Steps in the formation of the *A. victoria* wtGFP chromophore.

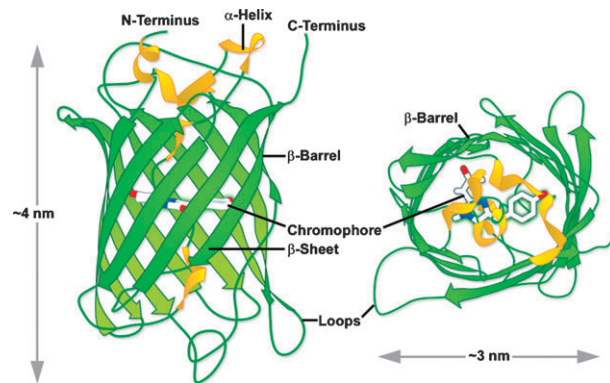


Fig. 3 *A. victoria* GFP β -barrel architecture and approximate dimensions. Drawing based on Protein Data Bank ID: 1w7s.

of a nearly perfect cylinder formed by a tightly interwoven eleven-stranded “ β -barrel” structure^{20,21} (see Fig. 3). As the protein folds, the tripeptide sequence is positioned at the core of the β -barrel, driving the cyclization and dehydration reactions necessary to form the mature chromophore.^{3,18} Visualization of the intact structure of GFP explained the earlier observations that nearly the entire protein sequence is required to generate a functional chromophore.^{15,22} The remarkable cylindrical geometry of GFP is conserved in all the FPs yet discovered, and appears to be ideally suited to the primary function of protecting the chromophore. The β -barrel structure has dimensions of approximately 25 Å \times 40 Å,²⁰ and the tight packing of amino acid residues imparts a high level of stability to the protein. A lack of clefts and gaps for access of small ligands (such as ions and oxygen), combined with the fact that the chromophore is located near the exact center of the protein (almost perpendicular to the long axis of the barrel), partially explains the extraordinary photostability

and high quantum yields that are observed (for more on this subject, see other articles in this themed issue). Fortunately for the cell biologists, both the amino and carboxy termini are exposed on the surface of the barrel, and therefore are available to be employed as linkers to fusion proteins without significantly affecting the structural integrity of the fluorophore. The compact protein structure also enhances resistance to changes in pH, temperature, fixation with paraformaldehyde, and the disruptive action of many common denaturing agents, such as urea and guanidinium hydrochloride.¹⁸

2.1 Spectral variants from the *Aequorea* GFP

Over the last decade, the application of both site-directed and random mutagenesis approaches to the cDNA encoding the *Aequorea*-GFP have demonstrated that its fluorescence properties are very dependent on the three-dimensional structure of amino acid residues surrounding the chromophore.^{18,23,24} As will be discussed below, mutations that alter the residues immediately adjacent to the chromophore generally have a significant impact on the spectral properties of the protein. Surprisingly, however, several amino acid substitutions in regions of the polypeptide far removed from the chromophore were also found to profoundly affect the spectral characteristics of the protein.²⁴ These protein engineering approaches have generated many different spectral variants from the *Aequorea* GFP, and some of the more significant derivatives are discussed below and catalogued in Table 1. Just as important, site-directed mutagenesis was also used to introduce substitutions that improved the efficiency of protein maturation and expression in many different heterologous cell systems. For example, preferred human codon usage was incorporated for improved expression in mammalian cells, as well as silent mutations that increased

Table 1 Properties of selected *Aequorea*-GFP derivatives. The peak excitation (Ex) and emission (Em) wavelengths, molar extinction coefficient (EC), quantum yield (QY), relative brightness, and physiological quaternary structure are listed (* signifies a weak dimer, see Section 2.6). The computed brightness values were derived from the product of the molar extinction coefficient and quantum yield, divided by the value for EGFP

Protein (acronym)	Ex/nm	Em/nm	EC/ 10^{-3} M $^{-1}$ cm $^{-1}$	QY	Quaternary structure	Relative brightness (% of EGFP)	Ref.
Blue fluorescent proteins							
Sirius	355	424	15.0	0.24	Monomer*	11	54
Azurite	384	448	26.2	0.55	Monomer*	43	52
EBFP	383	445	29.0	0.31	Monomer*	27	35
EBFP2	383	448	32.0	0.56	Monomer*	53	50
Cyan fluorescent proteins							
ECFP	439	476	32.5	0.40	Monomer*	39	22
Cerulean	433	475	43.0	0.62	Monomer*	79	56
CyPet	435	477	35.0	0.51	Monomer*	53	68
SCFP	433	474	30.0	0.50	Monomer*	45	60
Green fluorescent proteins							
EGFP	488	507	56.0	0.60	Monomer*	100	23
Emerald	487	509	57.5	0.68	Monomer*	116	30
Superfolder avGFP	485	510	83.3	0.65	Monomer*	160	32
T-Sapphire	399	511	44.0	0.60	Monomer*	79	27
Yellow fluorescent proteins							
EYFP	514	527	83.4	0.61	Monomer*	151	62
Topaz	514	527	94.5	0.60	Monomer*	169	18
Venus	515	528	92.2	0.57	Monomer*	156	25
Citrine	516	529	77.0	0.76	Monomer*	174	67
YPet	517	530	104	0.77	Monomer*	238	68
SYFP	515	527	101	0.68	Monomer*	204	60
mAmetrine	406	526	45.0	0.58	Monomer	78	222

the efficiency of folding and maturation of the protein at physiological temperatures.^{18,25–27} These variants are collectively termed the “enhanced” (E) FPs.

2.2 Green *Aequorea* fluorescent proteins

The wild-type (wt) *Aequorea* GFP displays a complex absorption spectrum, with maximal excitation occurring at 397 nm, and a minor secondary peak residing at 476 nm (Fig. 4A). Boxer and colleagues²⁸ examined the dynamics of wtGFP protein in the excited state, and showed that fluorescence resulted from deprotonation of the Tyr66 residue within the chromophore that resulted in an ionic species favoring excitation at 476 nm. The predominate ground state species contains a protonated Tyr66 residue and is responsible for the larger 397 nm absorption peak. In addition, it is thought that the charged intermediate state exists as a minor population of the ground (non-excited) state, accounting for the minor secondary absorption peak at 476 nm.²⁸ The complex absorption spectrum featuring a significantly higher extinction coefficient at near UV wavelengths, coupled with the low quantum yield of wtGFP, has severely limited its utility for cellular imaging applications.

Mutagenesis strategies were initially applied to the sequence encoding wtGFP to determine whether different amino acid substitutions might be used to “fine-tune” its spectral characteristics. This approach has yielded a broad range of derivative FPs with fluorescence emission ranging from the blue to the yellow regions of the visible spectrum.^{18,26} For example, an interesting variant of wtGFP, named Sapphire,¹⁸ resulted from the substitution of the isoleucine for threonine at position 203 (T203I). This residue is located in one of the β -sheet strands that surround a central α -helix containing the chromophore, and is positioned close to the chromophore, where it influences the local environment. The consequence of the T203I substitution is a loss of the secondary absorption peak of GFP at 475 nm, resulting in a derivative exhibiting peak absorption at 399 nm and emission in the green spectral region (maxima at 511 nm; Table 1). The separation between the peak excitation and the peak emission, known as the Stokes shift, is more than 100 nm for Sapphire, and is one

of the largest for the current FPs. Several improved Sapphire variants were subsequently developed with more efficient maturation, including a probe known as T-Sapphire.²⁷

Early studies on the structure–function relationships in the GFP chromophore region by Roger Tsien’s laboratory (reviewed in ref. 18) showed that mutations that altered the first amino acid in the chromophore, Ser65, to cysteine, leucine, alanine, or threonine simplified the excitation spectrum to a single peak ranging from 471 to 489 nm.²² For example, changing the Ser65 to threonine (S65T) stabilized the hydrogen-bonding network in the chromophore, resulting in a permanently ionized form of the chromophore absorbing at 489 nm.^{17,29,30} This GFP^{S65T} variant was a distinct improvement over wtGFP for applications as a fluorescent marker in living cells, because it had a well-defined absorption profile with a single peak at 489 nm (see Fig. 4B).²³ In addition, the GFP^{S65T} derivative is about five-fold brighter than wtGFP, and it matures more rapidly, allowing fluorescence to be detected at earlier time points after cell transfection.²³ The GFP^{S65T} variant was further modified by replacing phenylalanine for leucine at position 64 (F64L), which improved the efficiency of protein maturation at 37 °C, yielding EGFP (enhanced GFP). This enhanced derivative features an excitation spectral profile that overlays nicely with the 488 nm argon-ion laser line and is similar in profile to fluorescein and related synthetic fluorophores that are readily imaged using commonly available filter sets designed for fluorescein (FITC). Furthermore, EGFP is among the brightest and most photostable of the *Aequorea*-based FPs (Fig. 5C).^{26,31} The only drawbacks to the use of EGFP as a fusion tag are a slight sensitivity to pH and a weak tendency to dimerize (this important aspect is discussed in Section 2.6).

Continued engineering of EGFP has yielded several green variants with improved characteristics. Among the best of these is the variant named Emerald (after the precious gemstone), which has improved photostability and brightness (see Table 1).^{30,31} Until recently, there was no commercial source for plasmids encoding Emerald (it is now available from Invitrogen), so there has been limited use of this green

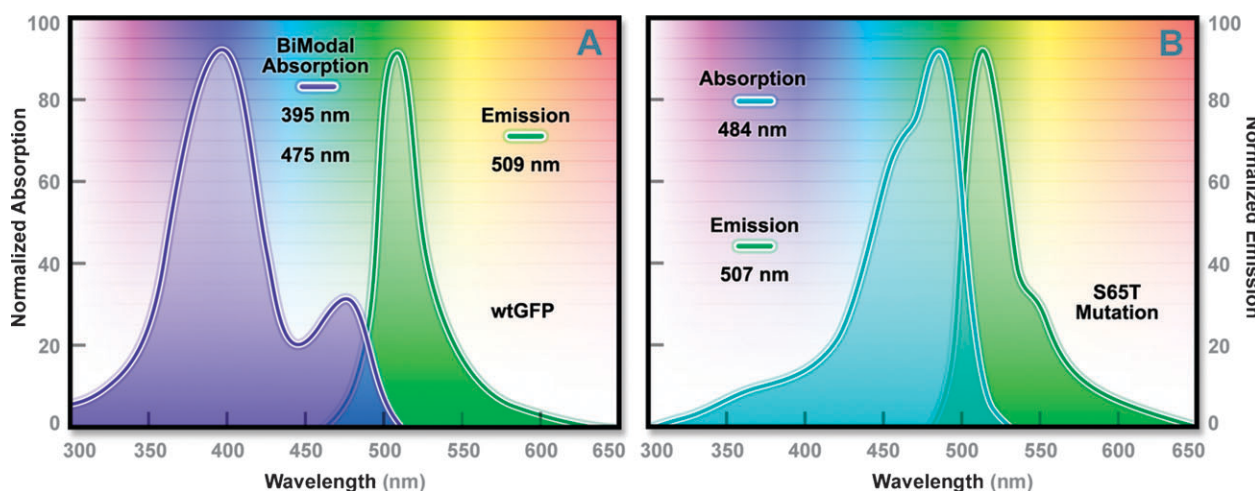


Fig. 4 Absorption and emission spectral profiles of (A) wild-type *A. victoria* GFP; and (B) the improved S65T derivative.

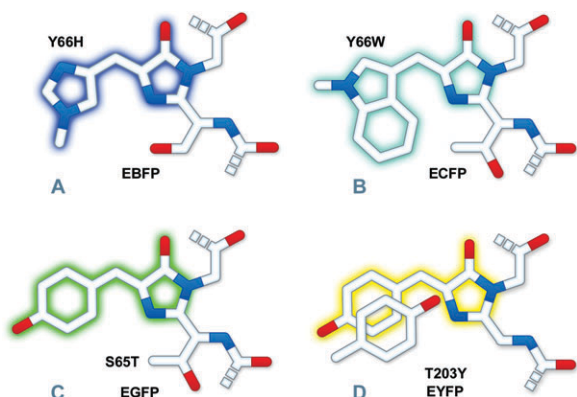


Fig. 5 Chromophore structures of: (A) BFP derivatives; (B) CFP derivatives; (C) EGFP derivatives; (D) YFP derivatives. The tryptophan residue (Trp66) in (B) is illustrated in the *cis* conformation as occurs for Cerulean derivatives rather than the *trans* isomer that is common to CFP and related variants. Portions of the chromophores that are conjugated and give rise to fluorescence are shaded with colors corresponding to the emission spectral profile.

variant. The Emerald derivative contains the S65T, and F64L mutations featured in EGFP, but also has four additional point mutations that further improve the efficiency of maturation and folding at 37 °C, and increase the intrinsic brightness. Although Emerald is more efficient than EGFP in folding and developing fluorescence in mammalian cells, it has a fast photobleaching component that might affect quantitative imaging in some environments.

Among the most interesting new developments in the *Aequorea* GFP palette over the past several years is the “superfolder” GFP,³² which was designed to fold even when fused to insoluble proteins. As an added benefit, superfolder GFP is slightly brighter and more acid resistant than either EGFP or Emerald. Waldo and colleagues³² engineered superfolder GFP by fusing libraries of shuffled GFP sequences to relatively insoluble “bait” polypeptides known to interfere with GFP folding when expressed in bacteria. Starting with cycle-3 GFP,³³ the EGFP mutations F64L and S65T were added, and after 4 rounds of DNA shuffling, the investigators

isolated a brightly fluorescent fusion clone (superfolder GFP) that contained 6 new mutations in addition to the cycle-3 and EGFP mutations. The work with superfolder GFP is clear evidence that there is significantly more room for engineering improvements even in the highly optimized GFP derivatives.

2.3 Blue *Aequorea* fluorescent proteins

One of the earliest color variants derived from the wtGFP was a blue FP (BFP), which contains the substitution of Tyr66 with histidine (Y66H).^{30,34} The Y66H mutation (Fig. 5A) produced a chromophore having a broad absorption band centered close to 380 nm (Fig. 6A), with blue light emission peaking at 448 nm (Fig. 6B).^{17,30} The original version of BFP had a low quantum yield and exhibited only about 15–20% of the brightness of the parent GFP (Table 1), so there was a need for additional mutations to improve the characteristics of the protein. The introduction of these mutations led to the improved EBFP variant, but this FP was still only 25% as bright as EGFP and its use as a cellular marker was severely limited by poor photostability.^{35–37}

In the mid-to-late 1990’s, investigators had a keen interest in creating matched pairs of FPs for Förster (or Fluorescence) resonance energy transfer (FRET; described in Section 5.3) experiments, as well as investigations requiring multicolor labeling.¹⁸ Because the fluorescence emission profile of EBFP is readily distinguishable from EGFP, this FP combination was the first utilized for dual color imaging.^{34,38} EBFP also has the distinction of being incorporated into the first genetically encoded biosensor reporter proteins as a direct fusion to EGFP. The broad emission peak of EBFP overlaps significantly with the absorption band of EGFP, allowing this pair to be used in FRET microscopy.³⁹ The linkage of EBFP to EGFP through an intervening protease-sensitive spacer allowed FRET to be used to demonstrate the cleavage of the biosensor protein (the biosensor technique will be described in detail in Section 5).^{34,40} In addition, EBFP was used in combination with different GFP derivatives in FRET experiments designed to monitor transcription factor dimerization,^{41,42} calcium fluctuations,^{43,44} and apoptosis.⁴⁵

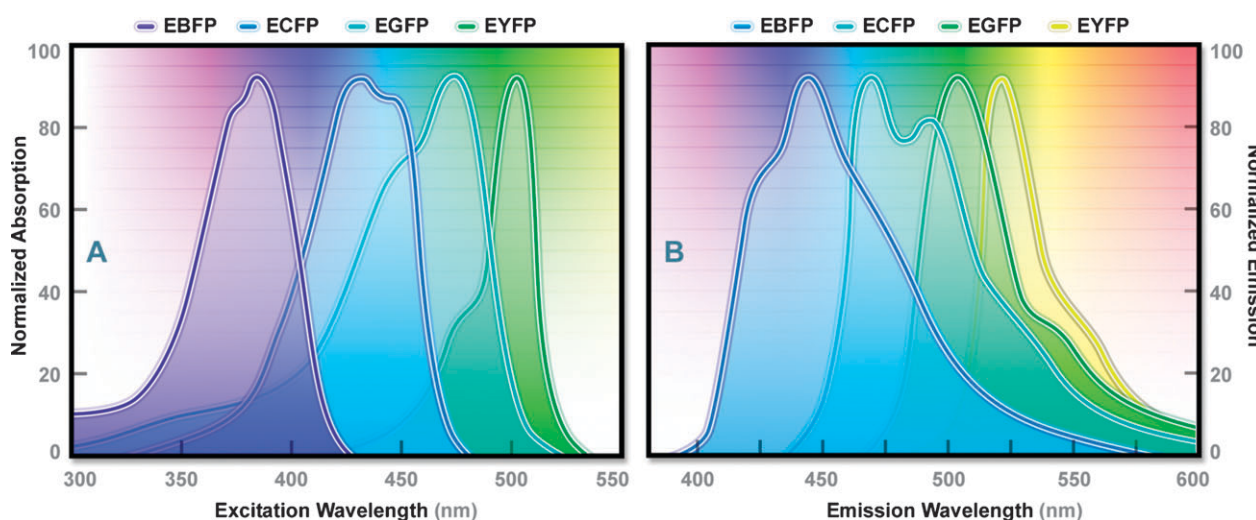


Fig. 6 Absorption (A) and emission (B) spectral profiles of the enhanced *Aequorea*-GFP derivatives: EBFP, ECFP, EGFP, and EYFP.

Aside from its low intrinsic brightness and sensitivity to photobleaching, the usefulness of EBFP for cellular imaging was also limited by its requirement for excitation with near-UV light, which is phototoxic to mammalian cells, even under limited illumination.^{46–48} Further, substantially more cellular autofluorescence and light scattering is observed when exciting fluorophores in this spectral region, and microscope systems require specialized light sources, optics, and filter combinations for imaging at near-UV wavelengths.⁴⁹ Because of these problems, there was limited interest in developing more efficient EBFPs for almost a decade. Recently, however, several groups used advanced mutagenesis strategies to develop new BFP variants with much higher quantum yields and photostabilities, greatly improving the utility of these deep blue probes.^{50–52} These new BFPs (Table 1) are named Azurite,⁵² SBFP2 (strongly enhanced blue fluorescent protein),⁵¹ and EBFP2.⁵⁰ The most promising derivative, EBFP2, is the brightest and most photostable of the BFP variants yet discovered, and has been shown to be an excellent donor for FRET studies.³¹ EBFP2 should be useful for long-term imaging in living cells in situations where a blue probe is required, especially when two-photon excitation is used, which avoids cellular damage by near UV excitation.⁵³ All BFP variants can be readily imaged using standard BFP and DAPI fluorescence filter sets.

Substitution of Tyr66 with phenylalanine in wtGFP also produces a blue FP, but in this case the spectral profiles are shifted to even shorter wavelengths than are observed with histidine at the same position (peaks for excitation at 360 nm and emission at 442 nm),¹⁸ and the resulting variant is extremely dim. Renewed interest in this chromophore was initiated with the introduction of an advanced derivative named Sirius⁵⁴ that is much brighter than the parent Phe66 variant, more photostable than EBFP2, and extremely insensitive to pH fluctuations. Although Sirius is only approximately 10% as bright as EGFP, it features the shortest emission wavelength yet reported among fluorescent proteins (424 nm). Sirius was demonstrated to be stable at pH values ranging from 3 to 9 and exhibits potential as a FRET donor for cyan FPs, but the requirement for excitation in the ultraviolet region (355 nm) will hinder attempts at long-term time-lapse imaging of living cells because of problems associated with phototoxicity and autofluorescence (discussed above).

2.4 Cyan *Aequorea* fluorescent proteins

The development of cyan (CFP) color variants from the *Aequorea* GFP provided an early alternative to the BFPs. Cyan fluorescence results from substitution of Tyr66 with tryptophan (Y66W; Fig. 5B), and an enhanced version (ECFP) was generated by including several additional substitutions within the surrounding β-barrel structure.^{17,30} The original Y66W mutation yielded a chromophore featuring a broad, bimodal absorption spectrum that peaks at 433 and 445 nm (Fig. 6A), and an equally broad, bimodal fluorescence emission profile with maxima at 475 and 503 nm (Fig. 6B). Subsequent refinements, including the addition of the F64L substitution that improves maturation and the S65T mutation (discussed above), resulted in an enhanced version (ECFP)

with improved brightness and photostability.^{22,36} Even with these modifications, however, the brightness of ECFP is still only about 40% of that of EGFP. Additionally, as was observed for the wtGFP, the complex excitation spectrum of ECFP indicates that there is more than one excited state species for ECFP, and this has been subsequently confirmed using fluorescence lifetime measurements.⁵⁵ This attribute has limited the usefulness of ECFP as a probe for fluorescence lifetime imaging microscopy (FLIM), and will be discussed in Section 5.

Efforts to address the complex excited state characteristics of ECFP have yielded a high-performance variant, termed Cerulean (after the sky-blue color; Table 1), which resulted from targeted substitutions on the solvent-exposed surface of ECFP (Tyr145 and His148). Cerulean has a higher extinction coefficient, increased quantum yield, and is reported to have a simplified excited state when compared to ECFP.⁵⁶ Cerulean is at least 1.5-fold brighter than ECFP, and demonstrates increased contrast and signal-to-noise when coupled with yellow-emitting FPs, such as Venus, in FRET investigations (discussed in Section 5.3). Indeed, the combination of Cerulean and one of the high-performance yellow-emitting *Aequorea* FPs (Venus and Citrine, Section 2.5) is currently the most popular pairing for FRET-based measurements.⁵⁷ The advantageous features afforded by Cerulean make this protein one of the most useful *Aequorea*-based derivatives. However, when Cerulean is expressed in living cells, its fluorescence decay kinetics still indicate the presence of more than one excited state species.^{58,59} As will be discussed below (Section 5.3), techniques that measure the fluorescence lifetime of a fluorophore are most accurate when the probe has simple decay kinetics.

The introduction of beneficial “folding” mutations into ECFP resulted in new monomeric variants featuring enhanced brightness, solubility, and improved performance for FRET-based imaging approaches. Announced by the authors⁶⁰ as “super” CFPs (SCFPs), the engineered variants are significantly brighter than the parent protein when expressed in bacteria and almost two-fold brighter in mammalian cells. The authors speculate that these high-performance FPs should have improved utility for labeling cellular proteins, and may also be useful for creating new CFP-based FRET biosensors with an improved dynamic range.⁶⁰ The optimal detection of CFPs using widefield fluorescence microscopy requires a specialized filter set that is available from the microscope companies or aftermarket filter manufacturers. When the CFPs are used for laser scanning confocal microscopy, the most efficient excitation is achieved with a 440 nm diode laser, but the more commonly available 405 nm and 458 nm laser lines can also be employed, albeit with significantly reduced excitation efficiency.

2.5 Yellowish-green *Aequorea* fluorescent proteins

The longest-wavelength emitting variants of *Aequorea* GFP were generated after careful inspection of the native GFP crystal structure.²⁰ The X-ray studies indicated that the Thr203 residue in the β-barrel lies in close proximity to the chromophore, and the Sapphire mutation (T203I; discussed above) had already demonstrated that substitutions at this

position had the potential to change the spectral profile of the protein. The targeted substitution of Thr203 with tyrosine (T203Y; Fig. 5D) was expected to induce π -orbital stacking, leading to the stabilization of the chromophore excited state dipole moment.⁶¹ The T203Y substitution (originally named “mutant 10C”) resulted in almost a 20 nm shift to longer wavelengths for both the excitation and emission spectra (Fig. 6), generating a new FP with yellowish-green emission (YFP).^{18,20,61} The enhanced version, EYFP, has become one of the brightest and most widely utilized of the FPs.^{26,62,63} Unfortunately, EYFP is very sensitive to acidic pH, losing ~50% of its fluorescence at pH 6.5. In addition, EYFP is also very sensitive to chloride ions, and exhibits poor photostability when compared to many of the other *Aequorea* FP variants. Nevertheless, several investigators have exploited the environmental sensitivity of YFP to develop biosensors to measure cytoplasmic pH,⁶⁴ and chloride ion concentrations.^{65,66}

Continued efforts to improve the YFP family led to the discovery that substitution of the glutamine at position 69 for methionine (Q69M) dramatically increases the acid stability of the protein, while simultaneously reducing its chloride sensitivity.⁶⁷ This variant has been named Citrine in recognition of the yellow color and acid resistance (Table 1). In addition, Citrine is expressed more efficiently in mammalian cell culture (especially when targeted to acidic organelles) and is more photostable than many previous yellow fluorescent proteins. Citrine features absorption and fluorescence emission maxima at 516 and 529 nm, respectively, and is 75% brighter than EGFP, although it is still much less photostable. During continued studies, Nagai and colleagues²⁵ demonstrated that substitution of the phenylalanine at position 46 with leucine (F46L) dramatically improved the maturation efficiency and reduced the halide sensitivity of YFP to yield a derivative that they named Venus (after the brightest object in the nighttime sky). Additional mutations were introduced that increased the tolerance of Venus to acidic environments. However, the photostability of Venus is only about 25% that of EYFP, which is a significant problem for long-term imaging experiments. Unfortunately, most of the *Aequorea*-based YFP derivatives (EYFP, Citrine, and Venus) are not available from commercial sources. A similar, but less well-characterized *Aequorea* derivative, named after the birthstone Topaz,³⁰ is currently available from Invitrogen.

Several other EYFP variants have been introduced and may be useful for specialized applications (Table 1). For example, the comprehensive site-directed mutagenesis strategies that yielded optimized monomeric variants of ECFP (discussed above) were also applied to EYFP to select for derivatives having enhanced brightness, folding efficiency, solubility, and utility in FRET applications.⁶⁰ These efforts resulted in what has been termed a “super” yellow fluorescent protein derivative, SYFP, which is significantly brighter than the parent protein when expressed in bacteria and mammalian cells. Another potentially useful variant of EYFP was generated using an evolutionary mutagenesis strategy that was applied to cDNAs encoding a linked CFP–YFP pair. Here, the goal was to simultaneously mutate CFP and YFP, and select for pairs with improved FRET efficiency.⁶⁸ The cDNA libraries were screened directly for FRET efficiency and

the best clones were subjected to several evolutionary cycles of random mutagenesis and synthetic DNA shuffling. This resulted in the generation of a new CFP–YFP pair, named CyPet–YPet (for cyan or yellow fluorescent protein for energy transfer) that displayed a four-fold improvement in the ratiometric FRET signal.⁶⁸

A total of seven mutations were accumulated in CFP during the directed evolution to yield CyPet, which features absorption and emission maxima positioned at 435 nm and 477 nm, respectively. However, CyPet is only two-thirds as bright as Cerulean, and is not optimally expressed in cells grown at 37 °C, limiting its use for stand-alone applications.²⁶ In contrast, YPet is the brightest of the YFP variants yet developed and demonstrates excellent photostability. In addition, YPet is more resistant to acidic environments than other YFP derivatives, which will enhance its utility in biosensor combinations targeted at acidic organelles. However, although the CyPet–YPet pair was selected as an optimized pairing for FRET studies, the poor quantum yield of CyPet has raised doubts about the origin of the improved FRET response. Recently, it was shown that the enhanced FRET signals resulted from the S208F and V224L mutations, which act to stabilize an intramolecular complex formed between the linked CyPet and YPet.^{69,70} This artifact illustrates how the potential for the *Aequorea*-based FPs to self-associate can be an important consideration for many different types of studies using these cellular markers.

2.6 Oligomerization of the fluorescent proteins

Virtually all the FPs discovered to date display varying degrees of quaternary structure. For example, there is a weak tendency of native *Aequorea* GFP and its derivatives to dimerize if they are immobilized at high concentrations, such as when constrained to membranes or when incorporated as fusions to proteins that form biopolymers.^{71,72} Similarly, FPs isolated from *Renilla* sea pansies⁷³ have been verified to form obligate dimers, which are necessary for solubility. To further complicate matters, there appears to be a strict tetramerization motif for most of the native yellow, orange, and red fluorescent proteins (Fig. 7) isolated in reef corals and anemones.^{74–77} FP oligomerization can be a significant problem for many applications in cell biology, particularly in cases where the FP is fused to a partner host protein that is targeted at a specific subcellular location. Once expressed, the formation of dimers and higher order oligomers induced by the FP portion of the chimera can produce atypical localization, disrupt normal function, interfere with signaling cascades, or restrict the fusion product to aggregation within a specific organelle or the cytoplasm. This effect is particularly evident when the FP is fused to partners such as actin, tubulin, gap junction connexins, or histones, which naturally form oligomeric structures *in vivo*. Fusion products with proteins that form only weak dimers (*i.e.*, most of the *Aequorea* GFP variants) may not exhibit aggregation or improper targeting, provided the localized concentration remains low. However, when dimeric FPs are targeted to specific cellular compartments, such as the tight, two-dimensional constraints of the plasma membrane,⁷² the localized FP concentration can become high

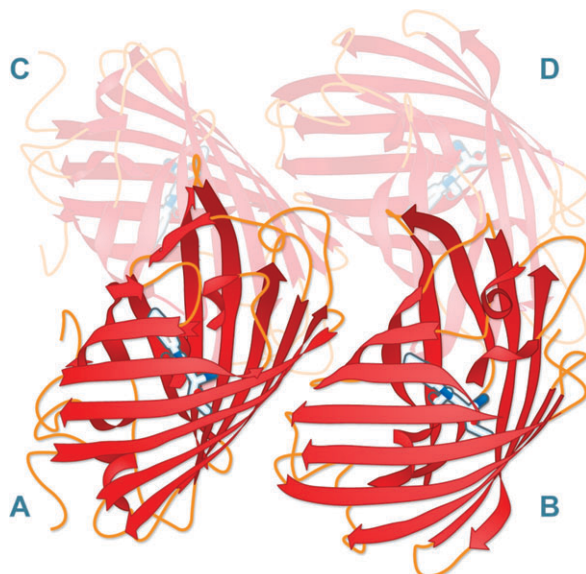


Fig. 7 Tetramer formation in native DsRed FP. Each of the protomers are individually lettered (A–D). Drawing based on Protein Data Bank ID: 1g7k.

enough to permit dimerization or even aggregation in some circumstances. This is of particular concern when conducting FRET experiments, which can yield complex data sets that are easily compromised by dimerization artifacts.

The basic strategy for overcoming oligomerization is to modify the FP amino acid sequence to include residues that disrupt intermolecular binding, a procedure that varies in complexity depending on the nature and origin of the FP. For many *Aequorea*-based variants, dimerization can be either significantly reduced or eliminated completely⁷⁸ by replacing the hydrophobic amino acid side chains in the dimer interface with positively charged residues at several key sequence positions. The three most successful mutations, in increasing order of effectiveness, are F223R, L221K, and A206K, where the non-polar amino acids phenylalanine, leucine, and alanine are replaced by hydrophilic alternatives (arginine or lysine). In cases where close molecular associations are suspected involving a fusion protein and where quantitative FRET interactions are being investigated, it is highly recommended that *Aequorea* GFP variants are converted into monomers using one of these point mutations (preferably A206K).^{24,26,31}

Creating FP monomers from the tetrameric reef coral and sea anemone proteins has proven to be far more difficult. For example, the FP isolated from the sea anemone *Discosoma striata*, called DsRed (discussed further in Section 3.1), is an obligate tetramer even at exceedingly low concentrations,^{74,79,80} and cannot be dissociated without irreversible denaturation of the polypeptides.⁸¹ In the tetrameric unit, each DsRed protein interacts with two adjacent neighbors, one through a hydrophobic interface and the other through a hydrophilic interface.^{71,74,76} Other Anthozoa proteins, such as the *Zoanthus* variants and eqFP611^{82,83} discussed below, have simpler interfaces that may prove easier to break apart into functional monomers. The most successful approaches^{24,71} utilized so far to generate FP monomers with

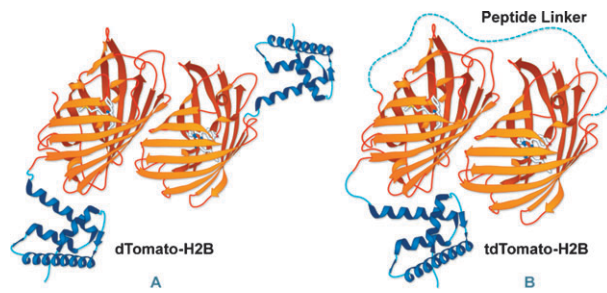


Fig. 8 Using tandem dimers to simulate “pseudo-monomer” function in FPs. (A) dimeric Tomato FP constrains fusion tags due to intermolecular dimerization, which can be relieved (B) by linking two copies of the dimeric FP with a short peptide linker.

Anthozoa species have involved repeated site-directed mutagenesis to disrupt the tetrameric interfaces, usually by substitution of hydrophilic or charged amino acids for hydrophobic and neutral moieties. Because a significant decrease in fluorescence emission quantum yield usually accompanies these genetic modifications, a second round of random mutagenesis is often necessary to rescue fluorescence.

Another technique for generating “pseudo” monomers from FPs that exist naturally as dimeric complexes involves linking two copies of the FP cDNA with a short intervening DNA sequence encoding simple neutral or hydrophilic amino acids (glycine, alanine, and serine) to form “tandem dimers” (Fig. 8). Upon expression in live cells, the fused FPs preferentially bind to each other to form an intramolecular dimeric unit that performs essentially as a monomer although at twice the molecular weight (and size). This method was successfully applied with HcRed by fusing two copies of the DNA sequence, separated by a short linker of four amino acids, to several subcellular localization proteins.⁸⁴ Tandem dimer constructs have also been developed with DsRed⁷¹ and a photoconversion FP known as Eos⁸⁵ as will be discussed in more detail below. Other mechanisms for reducing FP oligomerization and aggregation effects include removing several basic residues from the N-terminus⁸⁶ and simultaneous co-expression of FP tagged proteins with an excess of a non-fluorescent mutant of the marker protein to generate heterodimers or heterotetramers that contain only a single target polypeptide and can thus be considered pseudo-monomeric.^{87,88}

3. Fluorescent proteins from Anthozoa

The search for a red-emitting fluorescent protein with performance attributes similar to EGFP (*i.e.*, brightness, photostability, and utility in fusions) has been seen as a critical avenue to providing an important tool for multicolor imaging and in generating new FRET biosensors with spectral profiles in the longer wavelength regions.³¹ Another driver for the development of red FPs is that cellular autofluorescence is significantly reduced in this spectral region, allowing the probes to be detected deeper into biological tissue.⁸⁹ Furthermore, living cells and tissues better tolerate illumination by the longer excitation wavelengths, allowing extended periods for imaging. Unfortunately, after years of unsuccessful mutagenesis attempts

to develop RFPs from the *Aequorea*-based FPs, the YFPs remain the most red-shifted of the GFP derivatives.^{18,31}

To address this problem, several groups of investigators demonstrated that much of the color diversity in reef corals is a result of GFP-like proteins.^{2,90,91} It is widely thought that these proteins evolved in the corals to fulfill roles that are distinct from those in the luminescent jellyfish. For instance, the production of FPs and related chromoproteins (FP-like proteins that absorb but do not fluoresce) in the sessile corals might function in a photo-protective role.^{92,93} Alternatively, the FPs might function to support the symbiotic relationships between the corals and algae.⁹⁴ Regardless of their evolutionary origin or biological function, many corals and other Anthozoa species have been identified that produce the FP-like proteins. These marine organisms are currently being mined for novel proteins that fill the gaps in FP color palette.

Over the past decade, FP-like proteins spanning the entire visible light spectrum have been characterized and cloned from Anthozoa, and some of these have been optimized for imaging applications (see Table 2 and Fig. 9).^{95–97} One of the first Anthozoa-derived FPs to be extensively characterized was isolated from the sea anemone *D. striata*. This novel FP was originally called drFP583, but is now commonly known as DsRed.⁹⁵ When expressed in cells, the fully matured DsRed protein is optimally excited at 558 nm, and has an emission maximum at 583 nm. However, there are multiple problems associated with DsRed when used for live-cell imaging. Among the most acute of these problems is that maturation of DsRed is slow, and proceeds through an intermediate chromophore stage where most of the fluorescence emission occurs in the green spectral region.⁷⁴ This “green state” introduces signal crosstalk that limits the usefulness of DsRed for multiple labeling experiments. In addition, as mentioned above, DsRed is an obligate tetramer (see Fig. 7) with the tendency to form oligomers, and this can lead to protein aggregation and interference with the localization of linked protein in living cells. Although these side effects are not important when the probe is utilized simply as a reporter for gene expression, the utility of DsRed for a wide variety of investigations in cell biology is severely compromised.⁷¹ Thus, in contrast to the *Aequorea*-based proteins that have been used to successfully label hundreds of different proteins, protein fusions to DsRed have proven far more problematic. These shortcomings have required strategies to improve DsRed through mutagenesis, or alternatively, to search for other FPs from corals with more optimal characteristics for live-cell imaging.

3.1 Fluorescent protein variants based on DsRed

The major problems associated with DsRed have been overcome in the past few years by site-directed and random mutagenesis approaches. This effort yielded a second-generation version of DsRed, appropriately called DsRed2, which contains a series of silent nucleotide substitutions corresponding to human codon preferences, as well as several mutations that increase the maturation rate.⁹⁸ In addition, the elimination of a string of basic amino acid residues at the amino terminus of DsRed2 (by mutation to acidic or neutral

moieties) significantly reduces the tendency of the protein to form aggregates.⁸⁶ DsRed2 still forms a tetramer in solution (see Fig. 7), but the increased maturation rate greatly reduces the intermediate green species, making it more useful for multiple labeling experiments.⁹⁸ Further increase in the rate of maturation was realized with the third generation of DsRed mutants, which also display an increased intrinsic brightness. For example, the DsRed-Express variant (available from Clontech) can be detected within an hour after transfection of cells, compared to approximately six hours for DsRed2 and 11–15 hours for DsRed.⁹⁸ Still further improved versions of the tetrameric DsRed, named DsRed-Express2 and DsRed-Max,⁹⁹ exhibit faster maturation rates and improved solubility. However, since all these direct descendants of DsRed remain obligate tetramers, there has been a concerted effort to generate newer dimeric and monomeric red FP variants.

The generation of truly monomeric DsRed variants, as well as monomers from proteins derived from a host of different Anthozoa species, has proven to be a difficult task.^{31,49} For example, site-directed mutagenesis to break the tetramer formation by DsRed2 resulted in the generation of a non-fluorescent monomer.⁷¹ To rescue fluorescence, Tsien and colleagues⁷¹ applied successive rounds of random mutagenesis to the monomer, selecting for proteins in each round with improved red fluorescence (this approach is called “directed evolution”). A total of 33 amino acid substitutions were required to generate the first-generation monomeric red fluorescent protein, which was termed mRFP1.⁷¹ The rapid maturing mRFP1 overcame many critical problems associated with DsRed, while shifting the fluorescence emission about 25 nm deeper into the red spectrum. Unfortunately, mRFP1 exhibits significantly reduced fluorescence emission intensity (as expected, the quantum yield of the monomer is about 25% of DsRed2) and it is very sensitive to photobleaching. Furthermore, mRFP1 has an absorbance peak at 503 nm that arises from a non-fluorescent species, which likely indicates a significant fraction of the protein that never fully matures. Over the past several years, extensive mutagenesis efforts,^{100,101} including novel techniques such as iterative somatic hypermutation,¹⁰² have successfully been applied to mRFP1 to yield a new generation (catalogued in Table 2) of orange, red, and far-red FP variants.^{26,31}

3.2 The “mFruit” series of fluorescent proteins

One of the most productive developments in the efforts to generate useful FPs in the orange and red spectral regions resulted from the directed evolution of mRFP1.¹⁰⁰ Shaner and colleagues¹⁰⁰ speculated that the chromophore amino acids Q66 and Y67, which are critical determinants of the spectral characteristics of the *Aequorea* proteins, would play a similar role in determining color of mRFP1 derivatives as well. Here, the directed evolution approach was applied to mRFP1, targeting these amino acid residues followed by selecting for new color variants. The result was a group of six new monomeric FPs exhibiting emission maxima ranging from 540 nm to 610 nm (Table 2). These new FPs were named mHoneydew, mBanana, mOrange, mTangerine, mStrawberry, and mCherry (the “m” referring to monomer), referencing the common fruits that bear colors similar to their respective emission

Table 2 Properties of selected Anthozoa FP derivatives. The peak excitation (Ex) and emission (Em) wavelengths, molar extinction coefficient (EC), quantum yield (QY), relative brightness, and physiological quaternary structure are listed. The computed brightness values were derived from the product of the molar extinction coefficient and quantum yield, divided by the value for EGFP

Protein (acronym)	Ex/nm	Em/nm	EC/ 10^{-3} M $^{-1}$ cm $^{-1}$	QY	Quaternary structure	Relative brightness (% of EGFP)	Ref.
Blue fluorescent proteins							
mTagBFP	399	456	52.0	0.63	Monomer	98	113
Cyan fluorescent proteins							
TagCFP	458	480	37.0	0.57	Monomer	63	224
AmCyan	458	489	44.0	0.24	Tetramer	31	95
Midoriishi Cyan	472	495	27.3	0.90	Dimer	73	96
mTFP1	462	492	64	0.85	Monomer	162	117
Green fluorescent proteins							
Azami Green	492	505	55.0	0.74	Monomer	121	120
mWasabi	493	509	70.0	0.80	Monomer	167	225
ZsGreen	493	505	43.0	0.91	Tetramer	117	95
TagGFP	482	505	58.2	0.59	Monomer	102	224
TagGFP2	483	506	56.5	0.60	Monomer	105	113
TurboGFP	482	502	70.0	0.53	Dimer	112	91
CopGFP	482	502	70.0	0.60	Tetramer	125	91
AceGFP	480	505	50.0	0.55	Monomer	82	119
Yellow fluorescent proteins							
TagYFP	508	524	64.0	0.60	Monomer	118	224
TurboYFP	525	538	105.0	0.53	Monomer	169	91
ZsYellow	529	539	20.2	0.42	Tetramer	25	95
PhiYFP	525	537	130.0	0.40	Dimer	158	91
Orange fluorescent proteins							
Kusabira Orange	548	559	51.6	0.60	Monomer	92	96
Kusabira Orange2	551	565	63.8	0.62	Monomer	118	127
mOrange	548	562	71.0	0.69	Monomer	146	100
mOrange2	549	565	58.0	0.60	Monomer	104	101
dTomato	554	581	69.0	0.69	Dimer	142	100
dTomato-Tandem	554	581	138	0.69	Pseudo-monomer	283	100
DsRed	558	583	75.0	0.79	Tetramer	176	95
DsRed2	563	582	43.8	0.55	Tetramer	72	98
DsRed-Express (T1)	555	584	38.0	0.51	Tetramer	58	98
DsRed-Express2	554	586	35.6	0.42	Tetramer	45	99
DsRed-Max	560	589	48.0	0.41	Tetramer	59	99
DsRed-Monomer	556	586	35.0	0.10	Monomer	10	Clontech
TurboRFP	553	574	92.0	0.67	Dimer	187	114
TagRFP	555	584	100.0	0.48	Monomer	142	114
TagRFP-T	555	584	81.0	0.41	Monomer	99	101
Red fluorescent proteins							
mRuby	558	605	112.0	0.35	Monomer	117	134
mApple	568	592	75.0	0.49	Monomer	109	101
mStrawberry	574	596	90.0	0.29	Monomer	78	100
AsRed2	576	592	56.2	0.05	Tetramer	8	95
mRFP1	584	607	50.0	0.25	Monomer	37	71
JRed	584	610	44.0	0.20	Dimer	26	91
mCherry	587	610	72.0	0.22	Monomer	47	100
eqFP611	559	611	78.0	0.45	Tetramer	106	131
tdRFP611	558	609	70.0	0.47	Pseudo-monomer	98	133
HcRed1	588	618	20.0	0.015	Dimer	1	130
mRaspberry	598	625	86.0	0.15	Monomer	38	102
Far-red fluorescent proteins							
tdRFP639	589	631	90.4	0.16	Pseudo-monomer	43	133
mKate	588	635	31.5	0.28	Monomer	26	97
mKate2	588	633	62.5	0.40	Monomer	74	89
Katushka	588	635	65.0	0.34	Dimer	67	97
tdKatushka	588	633	132.5	0.37	Pseudo-monomer	146	89
HcRed-Tandem	590	637	160	0.04	Pseudo-monomer	19	84
mPlum	590	649	41.0	0.10	Monomer	12	102
AQ143	595	655	90.0	0.04	Tetramer	11	107

profiles, and thus, these new FPs are commonly known as the “mFruits”. Although the mFruits were a tour de force, yielding tremendous information about FP structure and function, several mFruit FPs, including mHoneydew, mBanana, and mTangerine, suffer from low intrinsic brightness and poor photostability. The most promising

aspect of these probes is that the mere existence of mHoneydew (a cyan-type Y67W mutant) demonstrates that the tryptophan-based chromophore of CFP can undergo a further maturation into a longer-wavelength emitting species,¹⁰⁰ which may serve as a basis for further improvement using site-specific mutagenesis or directed evolution.

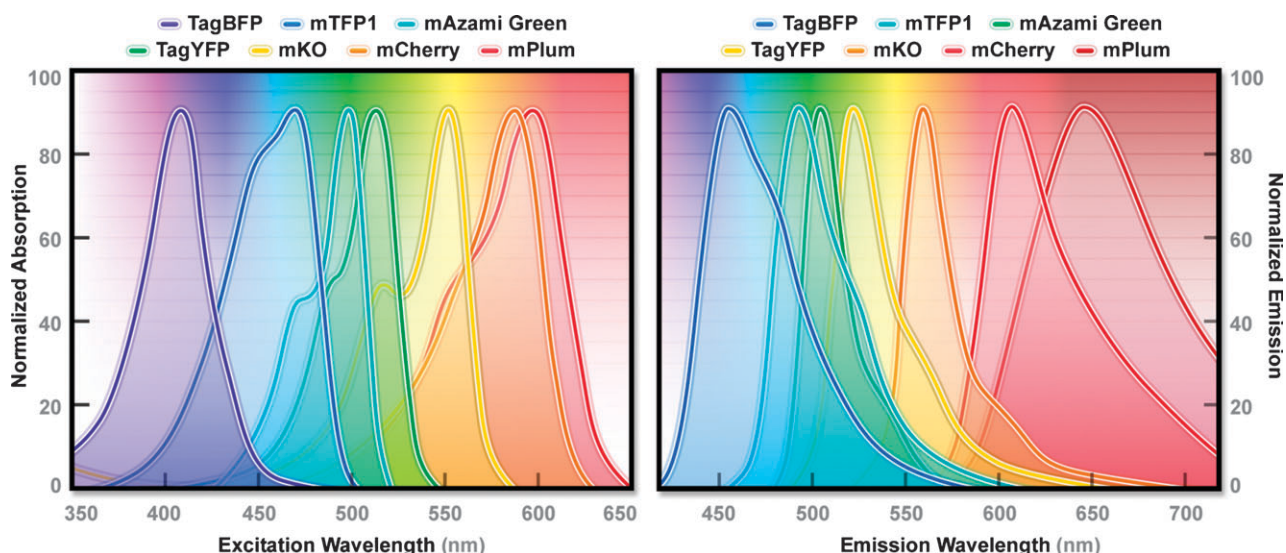


Fig. 9 Absorption (A) and emission (B) spectral profiles of high-performance Anthozoa FP derivatives: mTagBFP, mTFP1, mAzami Green, TagYFP, mCherry, and mPlum.

The most promising members in the mFruit series are mOrange, mStrawberry, and mCherry. The structure of mCherry is shown in Fig. 10, illustrating a general feature of the Anthozoa FPs—a more elliptical symmetry to the β -barrel than the *Aequorea* FP derivatives (compare Fig. 3 and 10). The mOrange FP is the brightest of the mFruit proteins and has spectral characteristics allowing it to be paired with other FPs in the cyan and green spectral region for multicolor imaging and as a potential FRET acceptor. Unfortunately, the photostability of mOrange is only $\sim 5\%$ that of EGFP. Recently, the photobleaching deficiency was corrected by using a directed evolution approach that selected for enhanced photostability.¹⁰¹ This approach yielded the mOrange2 derivative, which is about 30% more photostable than EGFP. mOrange2 also performs well as a tag for cellular proteins and the improved photostability should enable long-term imaging studies of cellular dynamics. The most useful red mFruit proteins, mCherry (610 nm emission peak) and mStrawberry (596 nm emission peak), have intrinsic brightness levels of

$\sim 50\%$ and $\sim 75\%$ that of EGFP, respectively. However, mCherry is more photostable than mStrawberry, so it is the preferred choice for cellular imaging. Recently, another red FP, named mApple, was generated in the same photostability screen that yielded mOrange2, and it features spectral characteristics close to mStrawberry, but with significantly improved photostability.¹⁰¹ The mApple variant is a rapid maturing, bright, and photostable RFP that might prove to be better choice for tagging cellular proteins that are difficult to label (*i.e.*, histones, tubulin, and connexins).

Another FP that arose from the fruit series screen was an obligate dimer FP called dTomato. To exploit its characteristics while controlling the dimer formation, two dTomato units were joined (head-to-tail) through a sequence that encodes an optimized 12-amino acid linker, yielding a tandem dimer FP, called tdTomato (see Fig. 8).¹⁰⁰ The tdTomato derivative is the brightest FP yet reported, featuring an orange-red emission maximum at 581 nm, and is one of the most photostable FPs under widefield illumination.^{26,31} Although the tandem dimer is twice the size of the other mFruits, as discussed above, it has been proven useful in many fusions to cellular proteins, and is more easily detected, allowing it to be used in live-cell imaging studies at very low light levels.

The mFruit protein family was extended further by using a clever technique termed “iterative somatic hypermutation”.¹⁰² This approach yielded FPs with the deepest-red emission of any of the mFruit proteins, allowing imaging in the far-red (630 to 700 nm) region of the spectrum. The most useful probe is mPlum, which despite its low intrinsic brightness ($\sim 10\%$ of EGFP), has a good signal-to-noise ratio because of the reduced autofluorescence in this spectral region. The mPlum variant also has excellent photostability, and should be useful for multicolor applications when combined with FPs emitting in the cyan, green, yellow, and orange spectral regions. These mFruit proteins, along with a multitude of new reef coral orange and red fluorescent proteins (discussed in Section 3.3),

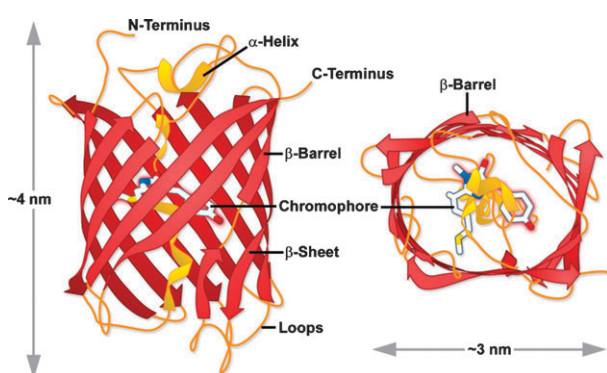


Fig. 10 mCherry FP β -barrel architecture and approximate dimensions. In general, Anthozoa FPs have a more elliptical symmetry to the β -barrel than do *A. victoria* GFP derivatives (see Fig. 3). Drawing based on Protein Data Bank ID: 2h5q.

have filled essential gaps in the FP color palette to enable multicolor imaging scenarios (for example, see Fig. 11). The continued efforts to evolve proteins with optimal characteristics may ultimately yield the elusive RFP that has equivalent utility to EGFP. Among the important characteristics that still need to be addressed are photostability, maturation time, brightness, acid resistance, and utility as tags for cellular proteins that have been difficult to label. Although

many new FPs feature properties that meet or exceed those of EGFP in some categories, no single FP yet discovered excels in all of them.

3.3 Novel fluorescent proteins from Anthozoa

A variety of novel and potentially useful FPs in virtually every color class have recently been cloned from Anthozoa,^{76,103} copepods,^{104,105} and amphioxus,¹⁰⁶ and researchers have

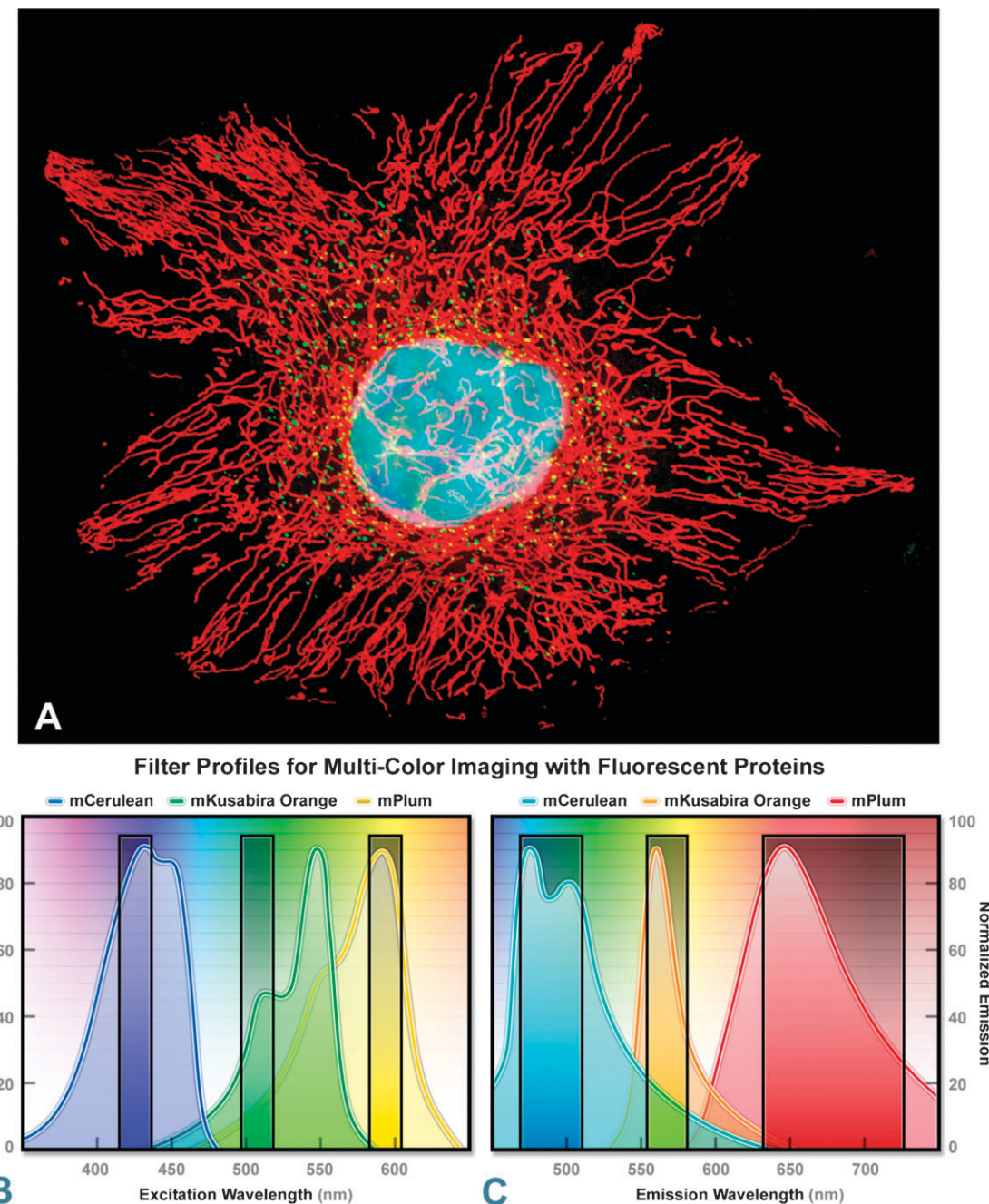


Fig. 11 Optimized fluorescence filter combinations for multicolor imaging of three FPs spanning the cyan to far-red wavelength regions. (A) Widefield fluorescence image of a single HeLa cells labeled with mCerulean (human histone H2B; nucleus; pseudocolored cyan), mKusabira Orange (peroxisomes; pseudocolored green), and mPlum (mitochondrial targeting signal; pseudocolored red). (B) Excitation filters optimized to avoid cross excitation for mCerulean, mKusabira Orange, and mPlum FPs having center wavelengths of 425, 508, and 585 nm, respectively. The bandwidth of the excitation filters is 20 nm. (C) Emission filters optimized for the same probes having center wavelengths of 480, 564, and 675 nm with bandwidths of 40, 28, and 100 nm, respectively.

extensively engineered these new probes to improve their utility for live-cell imaging.^{26,31,103} Structural investigations of the stereochemical nature of the fluorophore and the effects of its surrounding environment on fluorescent properties have been essential for understanding of spectral diversity in the wide range of fluorescent proteins discovered so far. Aside from the *Aequorea*-protein derivatives, there appears to be a high degree of variation in the fluorophores of red-shifted fluorescent proteins.¹⁰⁷ Although the DsRed fluorophore configuration, termed planar *cis*, appears to be the predominant structure in most proteins that emit in the orange and red regions, there are at least two additional motifs, planar *trans* and non-planar *trans*, which have been elucidated through X-ray diffraction studies.

A planar *trans* motif found in the red fluorescent protein eqFP611 (discussed in Section 3.9), isolated from the sea anemone *Entacmaea quadricolor*,¹⁰⁸ displays one of the largest Stokes shift of any naturally occurring Anthozoan fluorescent protein. In contrast, the non-planar *trans* conformation is characteristic of the non-fluorescent chromoprotein Rms5 from *Montipora efflorescens*.¹⁰⁹ Aside from the stereochemical variations, several proteins isolated from Anthozoa also have markedly different chromophore structures compared to the *Aequorea* variants (see Fig. 12). The maturation of orange and red Anthozoa FPs is believed to follow the same initial pathway as *Aequorea* GFP, but it continues with a second oxidation step⁷⁵ that generates an acylimine moiety integrated into the peptide backbone between the amino acid residue preceding the chromophore and the first residue of the

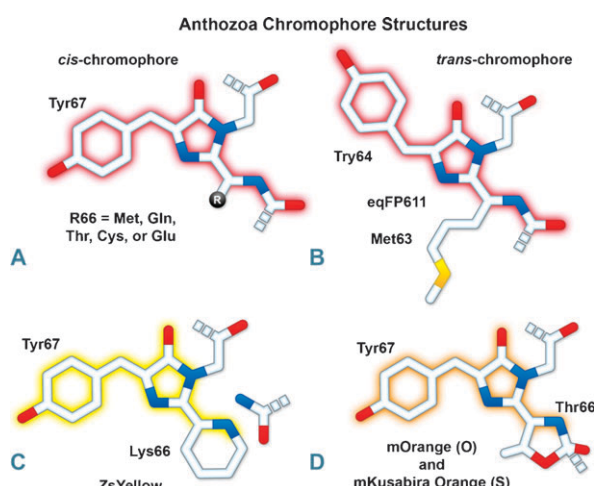


Fig. 12 Chromophore structural variation in yellow, orange, and red FPs. (A) FPs derived from DsRed and other reef coral organisms thought to have a *cis*-chromophore. The residue at position 66 can be Met, Gln, Thr, Cys, or Glu. (B) eqFP611, a red variant derived from *E. quadricolor*, is the only known FP featuring a *trans*-chromophore (see Section 3.3). (C) ZsYellow (also zFP538), derived from the button polyp *Zoanthus*, features a novel three-ring chromophore that is created when the lysine residue at position 66 cyclizes with its own α -carbon to form a tetrahydropyridine ring conjugated to the chromophore. (D) mOrange and mKO also feature a three-ring chromophore where Thr66 or the equivalent cysteine cyclizes with the preceding carbonyl carbon to yield a partially conjugated oxazole or thiazole ring.

chromophore (usually methionine, glutamine, cysteine, or glutamic acid in Anthozoan FPs). In several cases, the first residue of the chromophore also undergoes a cyclization reaction to form a third ring system, which further influences the emission spectrum.^{110–112}

As further studies into the complex characteristics of fluorescent protein chromophores yield clues about the structure–function relationship with the polypeptide backbone, the task of genetically engineering more finely-tuned color variants and broadening the spectral range of useful proteins will undoubtedly become easier. The diverse chromophore amino acid triplets uncovered so far in the Anthozoan proteins produce a huge range in emission maxima that probably arise from variations in the β -barrel structures. For example, the range of emission maxima for β -barrels with the MYG chromophore is 177 nm, 137 nm for QYG, 91 nm for TYG, and 80 nm for CYG. Therefore, additional mutations should be possible that will optimize the spectral characteristics and other properties of the FPs derived from these organisms. The following discussion will target novel non-*Aequorea* FPs that demonstrate potential for applications in live-cell imaging experiments.

3.4 Blue Anthozoa fluorescent proteins

Similar to the situation with *Aequorea* FPs, mining the Anthozoan species for blue FP variants with high brightness, pH resistance, and photostability has proven to be a challenging task. However, in recent years mutagenesis efforts have made significant progress in this area.¹¹³ Capitalizing on the fact that many Anthozoan red FPs have chromophores that are formed *via* a blue intermediate, Subach and colleagues applied random and site-directed mutagenesis on a variety of Anthozoan FPs, including TagRFP,¹¹⁴ mCherry,¹⁰⁰ and HcRed1,⁸⁴ to convert these orange and red proteins into blue FPs. The strategy was to introduce site-specific mutations that prevent maturation of the tyrosine-containing chromophore beyond the blue protonated intermediate, while simultaneously stabilizing the chromophore. The most promising candidate to emerge from this study was derived from TagRFP and named mTagBFP. When compared to blue *Aequorea* FPs having histidine in the chromophore (see Section 2.3, above), mTagBFP demonstrates superior brightness, faster chromophore maturation, and higher pH stability (see Tables 1 and 2). Regarding photostability, mTagBFP is less stable than EBFP2 under arc lamp illumination, but more than twice as stable when illuminated with laser light. mTagBFP has been demonstrated to perform well in most fusions with partner proteins and is an excellent FRET donor when coupled to green and yellow FPs from both *Aequorea* and Anthozoa.

3.5 Cyan Anthozoa fluorescent proteins

Several potentially useful cyan proteins have been isolated in Anthozoan species and improved versions of these FPs will likely see significant duty in live-cell imaging. Derived from the reef coral *Anemonia majano*, the AmCyan FP,⁹⁵ which is now commercially available (as AmCyan1; Clontech), has been optimized with human codons for enhanced expression in mammalian cell systems.¹¹⁵ Originally named amFP486

(am for *A. majano*; FP for fluorescent protein; 486 emission maximum) in accordance with a nomenclature scheme⁹⁵ devised to simplify the classification of Anthozoan proteins, this variant exhibits a similar brightness level, but a significantly better resistance to photobleaching than *Aequorea* CFP. The absorption and emission maxima of AmCyan occur at 458 nm and 489 nm, respectively. Both peaks are shifted to longer wavelengths by 19 and 13 nm, respectively, compared to ECFP. Unfortunately, similar to most of the other reef coral proteins, AmCyan forms tetramers, which will significantly complicate attempts to employ this protein as a fusion tag or a FRET biosensor.

Another potentially useful cyan Anthozoa protein, first isolated by Miyawaki and associates from an *Acropora* stony coral species,⁹⁶ is a cyan-emitting derivative named Midoriishi Cyan (abbreviated MiCy). MiCy was originally designed as the donor in a novel FRET combination with the monomeric Kusabira Orange FP (discussed below) to generate a biosensor probe with an excellent spectral overlap (discussed in Section 5.3). The fluorescence emission of MiCy features the longest absorption and emission wavelength profiles (472 and 495 nm, respectively) reported for any probe in the cyan spectral class. Furthermore, the high molar extinction coefficient and quantum yield exhibited by MiCy render the FP of equal brightness to Cerulean, although the spectra are far more sensitive to pH. Also similar to Cerulean, MiCy features a single exponential lifetime decay component with a time constant of 3.4 ns, which should be useful for measurements of FRET in combination with fluorescence lifetime imaging microscopy (FLIM). An unusual feature of MiCy is that it forms a homodimeric complex similar to the GFP variant isolated from the bioluminescent sea pansy, *Renilla reniformis*,¹¹⁶ instead of the obligate tetramer observed in most coral reef species. Although the dimerization motif may be a problem in some fusion proteins, it should be far easier (than a tetramer) to mutate MiCy into a true monomer.

Recently, a new monomeric cyan fluorescent protein having superior brightness, pH resistance, and photostability has been introduced for live-cell imaging applications of fusion partners and as a FRET donor for yellow and orange acceptor fluorescent proteins in biosensors.¹¹⁷ Termed mTFP1 (monomeric teal fluorescent protein 1; see Table 2 and Fig. 9), the variant was produced from a synthetic gene library built around the tetrameric cyan protein, cFP484, originating from a *Clavularia* soft coral. Displaying red-shifted spectral profiles (excitation and emission maxima at 462 and 492 nm, respectively) when compared to most other cyan members of this spectral class, mTFP1 has a total of 31 amino acid substitutions relative to the wild-type tetramer. This probe is classified as teal instead of cyan because it fills the spectral gap between the cyan and green FPs, and is optimally excited by the 457 nm argon-ion laser line that is available on most confocal microscopes. Unlike members of the *Aequorea* cyan FP group that feature the aromatic amino acid tryptophan at position 66 in the chromophore, mTFP1 contains the classical tyrosine residue at this location. Substituting tyrosine for tryptophan reduces the broad fluorescence emission spectral width from approximately 60 nm to a narrower 30 nm, a factor that is useful for reducing bleed-through in multicolor

imaging experiments. In addition, mTFP1 has a high quantum yield and the relatively narrow emission spectrum strongly overlaps the excitation spectrum of the yellow and orange FPs. This new blue-green protein is also an excellent donor fluorophore for FRET studies using the Venus FP¹¹⁸ (discussed in Section 5.3).

3.6 Green Anthozoa fluorescent proteins

A wide variety of FPs emitting in the green spectral region have been isolated from reef corals and sea anemones, and other variants will probably be discovered in even more diverse organisms.¹⁰⁵ One of the most promising of these probes was derived by random mutagenesis of a colorless chromoprotein isolated from *Aequorea coerulescens*, and is known as aceGFP.¹¹⁹ The substitution of glutamic acid for glycine at position 222 (E222G) transformed the wild-type chromoprotein into a highly fluorescent species with a relatively symmetrical spectral profile, with an absorption maximum at 480 nm and an emission peak at 505 nm. The high molar extinction coefficient and quantum yield of aceGFP combine to produce a brightness level similar to that displayed by EGFP. Demonstrated to exist as a monomer by electrophoresis and gel filtration, this protein is commercially available from several sources (Clontech and Evrogen, as AcGFP1 and AceGFP, respectively) with human-optimized codon replacements. Proper localization of fusion products targeted at specific subcellular components and organelles (such as filamentous actin, the Golgi, nucleus, and mitochondria) indicates that aceGFP is quite useful as a marker and could have potential for pairing with red-emitting proteins in a novel FRET combination. However, the photostability characteristics of aceGFP remain unknown, and there are no clear advantages to the use of this protein over the more common *Aequorea* EGFP and Emerald variants.

Several closely related GFP-like proteins have been isolated from an assortment of copepod aquatic crustacean species. The brightest of these probes was originally called plluGFP2,⁹¹ and is now commercially available (Evrogen) under the names CopGFP and TurboGFP (an enhanced variant). CopGFP is efficiently excited using an argon-ion laser or FITC filter set (absorption maximum at 482 nm) and produces green fluorescence at 502 nm with a brightness value approximately 30% higher than EGFP and much greater resistance to changes in pH. It is reported to be a monomer in dilute solution, and CopGFP matures significantly faster than EGFP and is ideal for applications as a fusion partner targeted at expression in subcellular regions of low pH. However, stable cell lines that expressed this probe could not be isolated, which could indicate that toxicity might be associated with the formation of aggregates in long-term cultures. An improved version, TurboGFP, derived from site-directed and random mutagenesis,⁹¹ retains the fast maturation kinetics of the parent protein with a slight loss in brightness and substantially lower resistance to acidic environments. Despite the improved folding kinetics and excellent optical properties of these proteins, however, photostability data have not been reported and no compelling evidence exists to demonstrate a significant benefit over the application of the extensively studied original GFP derivatives.

Surprisingly, a green FP has recently been isolated from amphioxus,¹⁰⁶ representing the first report of an endogenous FP to be discovered in any representative of the deuterostome branch of the Animal Kingdom. Although not completely characterized, the amphioxus FP (named AmphiGFP) features an amino acid sequence that predicts the standard β -barrel structure and emits green fluorescence peaking at approximately 526 nm. Phylogenetic analysis indicates that AmphiGFP is more closely related to CopGFP than to the jellyfish versions. Several AmphiGFP variants were isolated from three species, which all express the protein in the anterior region of these shallow-water lancelets.

Green FPs have also been extensively mined from reef corals and several of these are commercially available. A bright FP termed Azami Green,¹²⁰ bearing only a surprisingly scant (less than 6%) sequence homology to EGFP, was isolated from the stony coral *Galaxeidae* and has been demonstrated to mature rapidly during expression in mammalian cell lines. Similarly, one of the original Anthozoa coral reef proteins from *Zoanthus* reported by Matz and colleagues⁹⁵ has also been transformed into a commercial product (Clontech) under the trade name ZsGreen. The probes have absorption maxima at 492 and 496 nm and emission peaks at 505 and 506 nm, respectively, allowing visualization and imaging with standard lasers and filter combinations in confocal and widefield microscopy. However, similar to most of the other proteins isolated in corals, Azami Green and ZsGreen (see Table 2) both exist as tetramers in the natural state, which significantly interferes with their use as fusion partners and as a FRET donor or acceptor in biosensors. Both site-directed and random mutagenesis efforts were successful in creating a monomeric version of Azami Green (mAG), but this type of effort has not been reported for ZsGreen although the protein has been re-engineered with human codons to optimize expression (resulting in a variant termed ZsGreen1). Because reliable fusion performance and photostability data are lacking, it is unclear whether either of these proteins will outperform EGFP in long-term imaging experiments.

The sea pansy, an Anthozoa soft coral, is the source of several green FPs that have been characterized and are now commercially available.^{121–123} However, there is a general lack of reliable data concerning extinction coefficients, quantum yields, and photostability for the commercial *Renilla* proteins, so valid comparisons to EGFP regarding brightness and photobleaching are not possible. Furthermore, the *Renilla* GFP is an obligate dimer.⁷³ Despite the oligomerization problem, *Renilla* GFPs may be useful in many applications and have been expressed in a wide variety of organisms, including bacteria, fungi, and mammalian cells. Versions with human codon sequences are available from the commercial distributors, as are derivatives optimized for expression in other species. In summary, although a wide variety of green FPs have been obtained from species other than *Aequorea*, most exist natively as dimers or tetramers and have not been extensively characterized. Furthermore, it is unlikely that any Anthozoa green FPs will ultimately be determined to outperform EGFP or Emerald in routine live-cell imaging applications.

3.7 Yellow Anthozoa fluorescent proteins

In contrast to the many green variants that have been isolated, few proteins emitting in the true yellow spectral region (~ 540 – 555 nm) have been identified. The longest emission achieved for the *Aequorea* FPs is 530 nm, which appears green, not yellow when viewed in a widefield fluorescence microscope. Although the potential for new discoveries of yellow and green FPs in Hydrozoan species other than *Aequorea* is significant, only one candidate has surfaced so far. The protein termed phiYFP⁹¹ was isolated from the *Phialidium* jellyfish that has very bright fluorescence (absorption and emission at 525 and 537 nm, respectively), and was shown to be useful for N-terminal (but not C-terminal) fusion tags. An extraordinary feature of phiYFP is that the naturally occurring protein ironically contains two mutations that were discovered in the protein engineering efforts using the *Aequorea* FPs. Mutations introduced into *Aequorea* derivatives at position 64 (leucine), which increases the folding efficiency,²⁵ as well as the tyrosine at position 203²⁰ that produces yellow fluorescence, are also present in phiYFP. This remarkable discovery of a natural similarity between the structure of phiYFP and genetically modified *Aequorea* proteins is a testament to the efficacy of protein engineering efforts directed at GFP to adjust the spectral properties. phiYFP has been improved further by random mutagenesis to produce a monomeric version without compromising the spectral properties, but this FP has yet to see extensive use in live-cell imaging or FRET applications.

ZsYellow (originally called zFP538) is a yellow FP that was discovered in the Anthozoan button polyp *Zoanthus*.^{95,124,125} One of the most important features of the ZsYellow fluorescence emission spectrum is that the peak (538 nm) occurs almost midway between those of EGFP (508 nm) and DsRed (583 nm), presenting an opportunity to investigate the photophysical properties of proteins emitting fluorescence in the yellow portion of the visible light spectrum. The ZsYellow chromophore features a novel three-ring system (see Fig. 12) and peptide backbone cleavage resulting from the substitution of lysine for serine as the first amino acid residue in the chromophore tripeptide sequence.^{110,126} Because of the unique chromophore motif, the conjugation observed in ZsYellow is intermediate between that observed for EGFP and DsRed (one double bond more than EGFP, and one less than DsRed), which accounts for the positioning of peak emission wavelengths in the yellow region. Unfortunately, ZsYellow exhibits a marked tendency to form tetramers when expressed *in vivo*, hampering the use of this protein as a fusion partner for localization investigations. Furthermore, the reduced brightness level of ZsYellow (25% of EGFP) also limits the utility of this reporter in fluorescence microscopy (the human codon-optimized version is commercially available from Clontech as ZsYellow1). The unique emission spectral profile of ZsYellow, however, should encourage the search for genetic modifications that overcome the tendency to form tetramers while simultaneously increasing the quantum yield and extinction coefficient, an effort that could ultimately yield a high-performance monomeric yellow FP.

3.8 Orange Anthozoa fluorescent proteins

In recent years, many potentially useful orange FPs have been identified in various Anthozoa species. One of the first is a protein named Kusabira orange (KO),⁹⁶ which was isolated from the mushroom coral *Fungia concinna* (known in Japanese as Kusabira-Ishi). The sequence encoding KO was engineered to add ten amino acids to the N-terminus, resulting in an FP having an absorption maximum at 548 nm (ideal for excitation with a 543 nm laser) while emitting bright orange fluorescence at 561 nm. In an effort similar to the strategy used to generate mRFP1, a monomeric version of Kusabira Orange (mKO) was created after site-directed and random mutagenesis of 20 amino acids.⁹⁶ The monomer exhibits similar spectral properties to the tetramer and has a brightness value approximately equal to EGFP, but is slightly more sensitive to acidic environments than the tetramer. However, the photostability of this FP under arc lamp illumination is exceptional, making mKO an excellent choice for long-term imaging experiments. Furthermore, the emission spectral profile is sufficiently well separated from cyan FPs to increase the FRET efficiency in biosensors incorporating mKO, and the probe is useful in multicolor investigations with a combination of cyan, green, yellow, and red FPs (see Fig. 11). Recently, a fast-folding variant containing eight additional mutations, named mKO2, was developed and should improve the utility of this probe for live-cell imaging.¹²⁷

Another bright monomeric orange protein, named TagRFP, has been derived from the dimeric protein known as TurboRFP, originally cloned from the sea anemone *Entacmaea quadricolor*.¹¹⁴ TagRFP was generated by site-directed mutagenesis to replace several key amino acid residues involved in the dimer interface, while simultaneously performing random mutagenesis to rescue folding properties. Eight rounds of mutagenesis resulted in the final variant, which features excellent photophysical properties. TagRFP features an excitation peak at 555 nm, an emission peak at 584 nm, and is well tolerated as a fusion partner for many different proteins expressed in a variety of mammalian cell systems. The only drawback of TagRFP is relatively poor photostability under arc lamp and laser illumination when compared to other FPs in this spectral class. However, during the same investigation that uncovered a highly photostable variant mOrange2, similar mutagenesis of TagRFP yielded a single mutation (S158T) that increases the photostability almost 10-fold.¹⁰¹ The resulting FP, named TagRFP-T, has spectral properties similar to the parent and is among the most photostable of the FPs yet discovered (see Table 2).

3.9 Red and far-red Anthozoa fluorescent proteins

The relentless search for a high-performance red-emitting FP to act as a complement to EGFP has begun to yield promising results.^{31,105,128} Aside from DsRed and its variants (discussed in Section 3.1), a wide spectrum of potentially useful red FPs has been reported (spanning the emission wavelength range of 600 to 650 nm). However, many red FPs isolated from the reef coral organisms still suffer from some degree of the obligatory quaternary structure owing to their species of origin.^{26,76,103,129} Unlike the jellyfish proteins, most of the

native and genetically engineered variants of coral reef proteins mature very efficiently at 37 °C, presumably a result of the differing water temperatures of their respective habitats.^{63,103}

One of the first to be adapted for mammalian cell applications is HcRed,¹³⁰ which was isolated from the anemone *Heteractis crispa* and is now commercially available (as HcRed1; Clontech). HcRed was originally derived from a non-fluorescent chromoprotein that absorbs orange light through site-directed and random mutagenesis. A total of six amino acid substitutions were necessary to create a red fluorescent species that matured rapidly and efficiently at 37 °C (absorption and emission at 588 and 618 nm, respectively). However, like so many other reef coral proteins, the HcRed forms obligate tetramers when expressed in bacteria. Additional mutagenesis efforts resulted in a brighter dimeric variant,¹²⁴ but a monomeric version of the protein has not yet been reported. To generate a derivative of HcRed that is useful as a fusion partner for protein localization studies, a tandem dimer of HcRed has been constructed.⁸⁴ When fused to proteins that associate in biopolymers (such as actin or tubulin), the HcRed tandem dimer (tdHcRed) forms an intramolecular complex (mimicking a monomeric tag) that apparently does not interfere with the biological activity of the resulting chimera. However, because the intrinsic brightness and photostability of tdHcRed have not yet been improved, it remains a secondary choice for routine applications in live-cell microscopy.

A potentially useful far-red FP, named eqFP611 (see Fig. 12), was isolated from the sea anemone *E. quadricolor* and has a peak excitation at 559 nm, with an emission maxima at 611 nm.¹³¹ The quantum yield and extinction coefficient of eqFP611 combine to yield a probe approximately as bright as EGFP. During the *in vivo* fluorophore maturation process, which occurs in about 12 hours at 30 °C (this protein does not mature at 37 °C), the protein passes through a green intermediate state. After maturation, however, only a small fraction of this green species (less than 1%) can be detected. In contrast to other Anthozoan FPs, eqFP611 has a reduced tendency to oligomerize at lower concentrations as evidenced by electrophoresis and single molecule experiments,¹³² although at high concentrations the FP does form tetramers. Initial site-directed mutagenesis efforts have yielded functional dimeric variants of eqFP611,⁸³ but use of these FPs is hampered by the low maturation temperature that is not compatible with mammalian cells.

Additional work on eqFP611 using random and site-directed mutagenesis has led to a series of red FPs that feature long Stokes shifts and emission maxima extending to 639 nm.¹³³ Introduction of several mutations into the parent FP yielded a dimeric variant termed RFP611, which was subsequently converted into a tandem dimer (tdRFP611). This improved version of eqFP611 features a high extinction coefficient and quantum yield that is significantly brighter than EGFP, but less photostable. In addition, a new far-red derivative (RFP639) and its tandem dimer were developed, but these FPs are only about half as bright as EGFP. Continued mutagenesis efforts produced a bright, monomeric version of eqFP611, named mRuby, which contains 29 mutations relative to the parent.¹³⁴ mRuby has excitation

and emission maxima at 558 nm and 605 nm (similar to mCherry), respectively, and is one of the brightest monomeric red FPs yet developed (see Table 2). As an added bonus, mRuby retains the high Stokes shift of eqFP611 and is resistant to acidic environments ($pK_a = 4.4$). Fusions of mRuby to over 30 targeting peptides and proteins have demonstrated excellent localization in most fusions (Davidson, unpublished).

Two additional reef coral red FPs, AsRed2 and JRed, are commercially available (Clontech and Evrogen), but these probes form tetrameric and dimeric complexes, respectively, hampering their use in fusions. AsRed2 was originally isolated⁹⁵ as a chromoprotein from *Anemonia sulcata* and modified through mutagenesis¹³⁵ to yield a protein having an absorption maximum at 576 nm and an emission peak at 595 nm with a very modest quantum yield (0.05). Although the protein has been optimized with human codons for expression in mammalian cell lines, it exhibits only about 10% the brightness level of EGFP and the photostability has not been reported. The dimeric protein, JRed, was derived through extensive mutagenesis of a jellyfish chromoprotein⁹¹ to produce a novel red fluorescent marker with peak absorption and emission wavelengths of 584 and 610 nm, respectively. The probe has been demonstrated to produce useful fusion tags that tolerate dimers but is unsuitable for expression in prokaryotes because of folding problems (no tandem dimer version has yet been reported). JRed is about 25% as bright as EGFP and exhibits limited photostability when illuminated in the 560 to 580 nm region, but can be successfully employed for long-term imaging experiments when excited with a 543 nm laser.

In a search for far-red FPs, Chudakov and colleagues⁹⁷ applied a directed evolution and random mutagenesis approach to the *E. quadricolor* protein known as eqFP578 and selected for novel FPs with deep red emission. This screen yielded a dimeric RFP called Katushka (emission maxima of 635 nm). Although only two-thirds as bright as EGFP, Katushka exhibits the highest brightness levels of any FP emitting in the deep red spectral window (650–800 nm), a region that is important for deep tissue imaging. A tandem dimer version of Katushka⁸⁹ performs well in many fusions and is approximately 4 times brighter than mCherry and 20 times brighter than mPlum.

Introduction of the four principal Katushka mutations into TagRFP generated a monomeric, far-red protein named mKate that has similar spectral characteristics. The photostability of mKate is reported to be exceptional, and the protein displays brightness similar to mCherry, which makes it an excellent candidate for localization experiments in the far-red portion of the spectrum. Continued mutagenesis of mKate led to a brighter variant, mKate2,⁸⁹ which is three times brighter, but retains similar spectral properties (see Table 2). mKate2 features excellent pH resistance and photostability, and transgenic studies in *Xenopus* embryos revealed that the protein has low toxicity for imaging applications in living animals.

Another far-red fluorescent protein, termed AQ143, has been derived from mutagenesis efforts on a chromoprotein isolated from the anemone *Actinia equina*.¹⁰⁷ The excitation

and emission maxima of AQ143 are 595 and 655 nm, respectively, and the brightness is comparable to mPlum. AQ143 features the longest emission wavelength maximum of any FP yet reported, but it forms an obligate tetramer and thus, will probably see little action as a fusion tag. Despite the problems associated with current red and far-red FPs, the fact that FPs are capable of emission at such long wavelengths provides hope that protein engineers will someday be able to fine-tune the emission properties of existing or still undiscovered FPs into useful near-infrared probes.

Although promising imaging candidates are now available in every FP spectral class from either *Aequorea* or Anthozoa species, there remains no equivalent to EGFP in terms of photostability, brightness, and performance in fusions, for much of the color palette. New additions to the blue and cyan region derived from several species exhibit substantially improved brightness and photostability, and many new orange proteins are excellent choices for long-term multicolor imaging. In addition, although brighter than EGFP, photostability is still suboptimal for the yellow proteins, whereas the red and far-red proteins are among the dimmest FPs in all spectral classes. Furthermore, many supposedly “monomeric” FPs do not, sometimes, localize as expected and are subject to aggregation artifacts. Even so, many newly reported FP derivatives can be combined for dual and triple color imaging to yield excellent results. Given that most of the orange and red FPs have only been introduced in the past several years, we remain optimistic that further studies into the complex characteristics of FP chromophores will yield clues about the structure–function relationship with the polypeptide backbone to render the task of genetically engineering more finely-tuned color variants and broadening the spectral range of useful FPs much easier.

3.10 Increasing the Stokes shift in fluorescent proteins

Imaging requirements for FRET, fluorescence cross-correlation spectroscopy (FCCS), and multicolor fluorescence has prompted protein engineers to attempt to modify the Stokes shift for the FPs through random and site-directed mutagenesis. In one of the first efforts, introducing the T203I mutation into wtGFP produces a variant, Sapphire,¹⁸ devoid of the minor excitation peak at 475 nm, which was briefly discussed above (Section 2.2). Sapphire exhibits a dramatic Stokes shift of 112 nm, with excitation and emission maxima at 399 nm and 511 nm, respectively. A derivative with improved folding and brighter fluorescence, T-Sapphire (T for Turbo), was constructed by introducing four additional mutations.²⁷ These variants should be excellent donors in FRET combinations with orange and red proteins (see Fig. 13) because of their ability to be excited in the ultraviolet region.

Extending the Sapphire strategy to red FPs, Miyawaki and associates¹³⁶ used a far more rigorous approach to construct the longest Stokes shift FP variant yet developed (180 nm) starting with a non-fluorescent chromoprotein derived from the *Montipora* stony coral. Mutagenesis of five residues surrounding the chromophore led to a red FP having a bimodal excitation spectrum (peaks at 452 nm and 580 nm) with emission at 606 nm. An additional four mutations

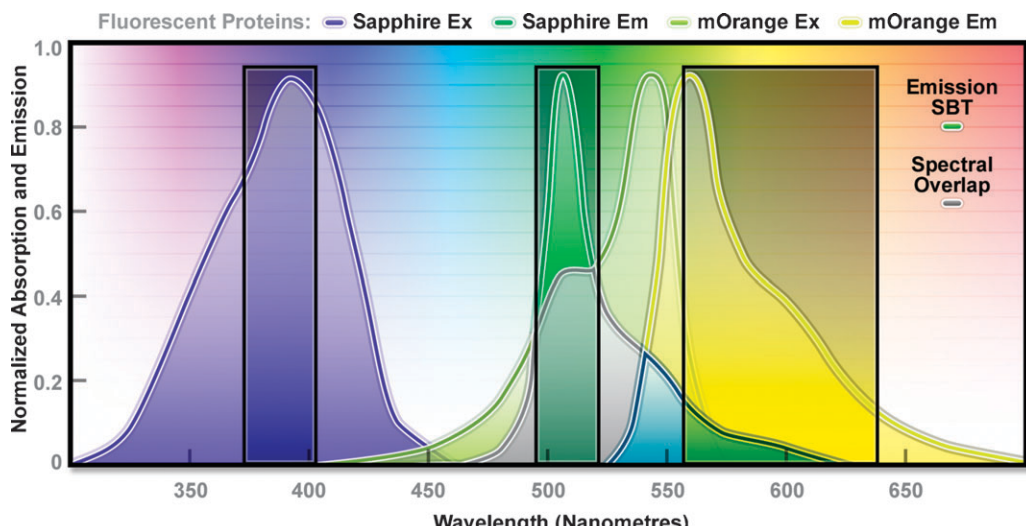


Fig. 13 The combination of Sapphire and mOrange fluorescent proteins as a FRET pair. Illustrated are the absorption and emission spectral profiles of the two probes along with the recommended filter sets. The overlap region between the emission spectrum of Sapphire and the absorption spectrum of mOrange is presented with a gray fill, while the emission spectral bleed-through is depicted by the blue fill (see Section 5.3.2). The excitation filter is centered at 395 nm with a 30 nm bandwidth (395/30), and the 512/26 emission filter enables analysis of the donor fluorescence emission (Sapphire) without contamination of signal from the acceptor (mOrange). The wideband 600/80 acceptor filter collects a significant amount of signal from mOrange with less than 10% bleed-through of the Sapphire fluorescence. A dichromatic mirror having a cut-on wavelength of 500 nm (not illustrated) should be utilized with this filter combination.

substantially reduced the 580 nm peak and blue-shifted the other absorption peak to 440 nm. This derivative, named Keima (after the Japanese chess piece), exhibits an emission maximum at 616 nm, but is tetrameric. Several more rounds of mutagenesis produced a dimer (dKeima) having similar spectral properties, and a monomer (mKeima; emission peak at 620 nm) was subsequently obtained. mKeima exhibits limited brightness (similar to the value for mPlum) and requires a specialized filter combination for imaging, but it has been demonstrated to be useful in FCCS and multicolor imaging experiments.¹³⁶ Recently, a tandem dimer¹³⁷ version (tdKeima) has been created from the brightest variant, dKeima, for use in fusions. Among the primary advantages of large Stokes shift FPs is the potential for coupling several colors together, such as tdKeima, mCerulean, and EGFP, which can be excited with a single laser line in multicolor experiments, thus reducing phototoxicity due to excitation illumination.

4. Optical highlighter fluorescent proteins

The photophysical properties of many FPs are often extremely complex and can involve several distinct emissive and non-emissive (dark) states, as well as on-and-off “blinking” behavior when observed at the single molecule level. One of the first observations of photoswitching in FPs was reported in wtGFP and several of its enhanced derivatives.¹³⁸ As we will see, the photoswitching properties can allow the investigator to change the color or the emission state of a FP, providing unique opportunities to track the dynamic behavior of proteins in living cells and animals. This quality can be extremely useful since, unlike the standard FPs that are uniformly fluorescent from the time they are produced, photosensitive FPs can be “switched on” at a particular time and location within the cell to track the behavior of a tagged protein.

Although FPs are known to undergo a variety of light-induced switching characteristics, the most useful are photoactivation, photoconversion, and photoswitching, functions that are collectively termed *optical highlighting*. *Photoactivatable* FPs are capable of being activated from very low level to bright fluorescence emission upon illumination with ultraviolet or violet light, whereas *photoconvertible* FPs can be optically converted from one fluorescence emission bandwidth to another. In contrast, *photoswitchable* FPs have emission characteristics that can alternatively be turned “on” or “off” with specific illumination (see Table 3).

As a class, optical highlighters allow direct and controlled activation of distinct molecular pools of the FPs within the cell.^{129,139,140} The investigator selects the population of photoactivated or photoconverted molecules to be followed, so dynamic behavior can be monitored over time, independent of other newly synthesized proteins. An ideal optical highlighter protein should be readily photoconvertable (through the process of fluorescence activation and/or emission wavelength shifts) to produce a high level of contrast, as well as being monomeric for optimum expression in the target system. These probes are especially useful since measurements of the photoactivated or photoconverted populations of proteins are not influenced by newly synthesized or non-converted proteins, which either remain invisible or continue to emit the original wavelengths.¹³⁹ In addition, the time required for photoactivation is typically very brief (often less than a second), which allows direct investigations of extremely rapid cellular processes. By repeated excitation in the region of interest, optical highlighters can be continuously photoconverted at a specific intracellular location. Optical highlighters are also emerging as important tools in superresolution microscopy^{141–144} where their switching properties can be utilized to selectively convert limited numbers of molecules in a much larger pool.

Table 3 Properties of selected optical highlighter FP derivatives. The peak excitation (Ex) and emission (Em) wavelengths, molar extinction coefficient (EC), quantum yield (QY), relative brightness, and physiological quaternary structure are listed. The computed brightness values were derived from the product of the molar extinction coefficient and quantum yield, divided by the value for EGFP

Protein (acronym)	Ex/nm	Em/nm	EC/ 10^{-3} M $^{-1}$ cm $^{-1}$	QY	Quaternary structure	Relative brightness (% of EGFP)	Ref.
Photoactivatable fluorescent proteins							
PA-GFP (N)	400	515	20.7	0.13	Monomer	8	145
PA-GFP (G)	504	517	17.4	0.79	Monomer	41	145
PS-CFP2 (C)	400	468	43.0	0.20	Monomer	26	147
PS-CFP2 (G)	490	511	47.0	0.23	Monomer	32	147
PA-mRFP1 (R)	578	605	10.0	0.08	Monomer	3	149
PA-mCherry1 (R)	564	595	18.0	0.46	Monomer	25	150
Phamret (C)	458	475	32.5	0.40	Monomer	39	151
Phamret (G)	458	517	17.4	0.79	Monomer	41	151
Photoconvertable fluorescent proteins							
Kaede (G)	508	518	98.8	0.88	Tetramer	259	152
Kaede (R)	572	580	60.4	0.33	Tetramer	59	152
wtKikGR (G)	507	517	53.7	0.70	Tetramer	112	165
wtKikGR (R)	583	593	35.1	0.65	Tetramer	68	165
mKikGR (G)	505	515	49.0	0.69	Monomer	101	166
mKikGR (R)	580	591	28.0	0.63	Monomer	53	166
wtEosFP (G)	506	516	72.0	0.70	Tetramer	150	163
wtEosFP (R)	571	581	41.0	0.55	Tetramer	67	163
dEos (G)	506	516	84.0	0.66	Dimer	165	163
dEos (R)	569	581	33.0	0.60	Dimer	59	163
tdEos (G)	506	516	84.0	0.66	Tandem dimer	165	85
tdEos (R)	569	581	33.0	0.60	Tandem dimer	59	85
mEos2 (G)	506	519	56.0	0.84	Monomer	140	164
mEos2 (R)	573	584	46.0	0.66	Monomer	90	164
Dendra2 (G)	490	507	45.0	0.50	Monomer	67	160
Dendra2 (R)	553	573	35.0	0.55	Monomer	57	160
Photoswitchable fluorescent proteins							
Dronpa	503	517	95.0	0.85	Monomer	240	171
Dronpa-3	487	514	58.0	0.33	Monomer	56	226
rsFastLine	496	518	39.1	0.77	Monomer	89	176
Padron	503	522	43.0	0.64	Monomer	82	175
bsDronpa	460	504	45.0	0.50	Monomer	67	175
KFP1	580	600	59.0	0.07	Tetramer	12	177
mTFP0.7	453	488	60.0	0.50	Monomer	89	174
E2GFP	515	523	29.3	0.91	Monomer	79	227
rsCherry	572	610	80.0	0.02	Monomer	5	150
rsCherryRev	572	608	84.0	0.005	Monomer	1	150
Photoconvertable/photoswitchable fluorescent proteins							
IrisFP (G)	488	516	52.2	0.43	Tetramer	67	179
IrisFP (R)	551	580	35.4	0.47	Tetramer	50	179

4.1 Photoactivatable fluorescent proteins

The unique photophysical properties of wtGFP were thoroughly investigated during the mid-1990's,^{28,73,138} and served as a foundation for the creation of the first useful optical highlighter designed specifically for photoactivation studies. Termed PA-GFP (for photoactivatable green fluorescent protein), this optical highlighter was developed by improving the photoconversion efficiency of the native chromophore from a predominately neutral form to a species that is anionic in character.^{145,146} By replacing the threonine at position 203 with a histidine residue (T203H) in wtGFP, Lippincott-Schwartz and Patterson¹⁴⁵ produced a variant having negligible absorbance in the region between 450 and 550 nm, thus dramatically enhancing contrast between the non-activated and activated species. PA-GFP is optimally excited at 400 nm, but has negligible absorbance in the region between 450 and 550 nm. However, after photoactivation with violet light, the absorption maximum of PA-GFP is shifted to 504 nm, increasing green fluorescence when excited at 488 nm

approximately 100-fold and providing very high contrast differences between the converted and unconverted pools (Fig. 14). When PA-GFP-labeled proteins are photoactivated inside the living cell (Fig. 15A–C), the diffusion of the newly fluorescent FPs provides a direct measure of the mobility of the labeled proteins.¹³⁹ The major drawback in the use of PA-GFP is that the non-activated form is not readily distinguishable before photoactivation, making it difficult to specifically identify the regions that are expressing the FP.

An optical highlighter derived from aceGFP, isolated from *A. coerulescens*, has been reported to transition from cyan (468 nm) to green fluorescence (511 nm) upon illumination at 405 nm.¹⁴⁷ Named PS-CFP (photoswitchable cyan FP), this unique highlighter is particularly advantageous because a significant level of cyan fluorescence is present prior to photoconversion, a feature that enables investigators to track and selectively illuminate specific intracellular regions. Unfortunately, the fluorescence emission intensity of PS-CFP (and its commercially available version, PS-CFP2; Evrogen) is approximately 2-fold less than PA-GFP, significantly reducing

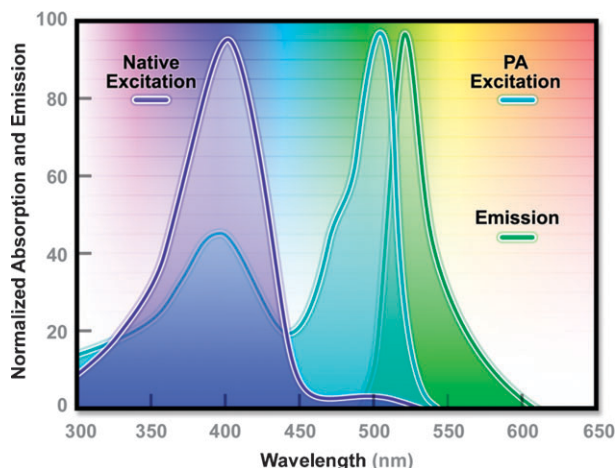


Fig. 14 Absorption and emission spectral profiles of PA-GFP.

the contrast ratio (Table 3). The photoactivation mechanism of both PA-GFP and PS-CFP is believed to be light-induced decarboxylation of the glutamic acid side chain in residue 222 (see Fig. 16A and B), which shifts the chromophore equilibrium to the anionic form.¹⁴⁸

Several photoactivatable optical highlighters have been produced using site-directed mutagenesis of monomeric red-shifted reef coral FPs. The first variant, derived from mRFP1, was named PA-mRFP1, and exhibits a 70-fold increase in fluorescence intensity upon activation using UV illumination.¹⁴⁹ However, the low level of fluorescence observed with PA-mRFP1 (approximately 7% of PA-GFP) has prevented the widespread use of this highlighter. Shifting the focus to more advanced red FPs, Verkushina and colleagues¹⁵⁰ recently reported a photoactivatable variant of mCherry having excitation and emission spectra at 564 and 595 nm, respectively. Compared to PA-mRFP1 the mCherry version features faster maturation, better pH stability, faster photoactivation, improved photostability, and higher contrast. This highlighter should be an excellent complement to PA-GFP for dual color photoactivation labeling in living cells and for superresolution microscopy investigations.

PA-GFP also serves as the activation agent in a new optical highlighter design based on FRET.¹⁵¹ Termed Phamret (an acronym for photoactivation-mediated resonance energy transfer), this unique probe couples PA-GFP to a high-performance ECFP variant through a two amino acid linker to form a photoactivatable tandem dimer. When excited with 458 nm light, Phamret fluoresces cyan so that fusion with targeting peptides or proteins can be readily identified and selected for photoconversion. The PA-GFP portion of Phamret can then be photoactivated with 405 nm illumination to evoke FRET between the ECFP and activated PA-GFP. After photoactivation, Phamret exhibits green fluorescence (520 nm peak) upon illumination at 458 nm and can therefore be used as an optical highlighter. One of the advantages of Phamret is that imaging can be conducted using only a single excitation wavelength for both the native and photoactivated species. The major downside of Phamret is that two FP units were used to construct the probe, increasing the size, and possibly creating steric hindrance in some fusions.

Although there has been significant progress in the development of photoactivatable probes, there remains much room for improvement. The PA-FP color palette is still very limited, and these probes are difficult to track in the non-activated form. Furthermore, the brightness of the photoactivated species in all reported variants is less than 50% that of EGFP and their photostability is significantly diminished compared to the parent FPs. Continued progress in this area likely will yield an expanded color palette of photostable optical highlighters that are useful in a variety of studies.

4.2 Photoconvertable fluorescent proteins

One of the most useful classes of optical highlighters comprises the growing number of FPs reported to undergo photoconversion from one emission wavelength to another (Table 3). Unlike photoactivatable FPs, these probes are readily tracked and imaged in their native emission state prior to photoconversion, making it easier to identify and select regions for optical highlighting. The first report of a photoconvertable highlighter involved a tetrameric FP isolated from the stony Open Brain coral, *Trachyphyllia geoffroyi*, which can be photoconverted from green to red fluorescence emission by illumination with ultraviolet light.¹⁵² The discovery of this highlighter was serendipitous, as are many important discoveries. It occurred when the researchers accidentally left a test tube containing the protein on a laboratory bench near a window, and then astutely observed the shift from green to red. The unusual color transition prompted investigators to name the protein Kaede, after the leaves of the Japanese maple tree that turn from green to red in the fall.

Illumination of the commercially available (MBL) Kaede optical highlighter between 380 and 400 nm results in a rapid spectral shift from principal maxima at 508 nm (absorption) and 518 nm (emission) to longer wavelength peaks at 572 and 582 nm, respectively. Along with photoconversion, there is a dramatic increase in the red-to-green fluorescence ratio (approximately 2000-fold, considering both the decrease in green and the increase in red emission). Photoconversion in Kaede is stable and irreversible under aerobic conditions. Neither exposure to dark for extended periods nor strong illumination at 570 nm can restore green fluorescence to the chromophore. The red fluorescent state of the Kaede chromophore is comparable to the green in brightness and stability, and because the unconverted protein emits very little fluorescence above 550 nm, the appearance of strong red signal provides excellent contrast. The major drawback of Kaede is the tetrameric nature of the protein, which limits its use in most fusion applications in live-cell imaging, although the highlighter has been widely reported to be useful in transgenic studies.^{153–156}

Similar FPs capable of being photoconverted from green to red fluorescence emission by violet and ultraviolet illumination have been discovered in the Great Star coral (mcavRFP; derived from *Montastraea cavernosa*),⁹¹ soft corals (DendFP; derived from members of the genus *Dendronephthya*),¹⁵⁷ and the mushroom coral (rfloRFP; derived from *Ricordea florida*).⁹¹ Each of these optical highlighters (including Kaede, Eos and

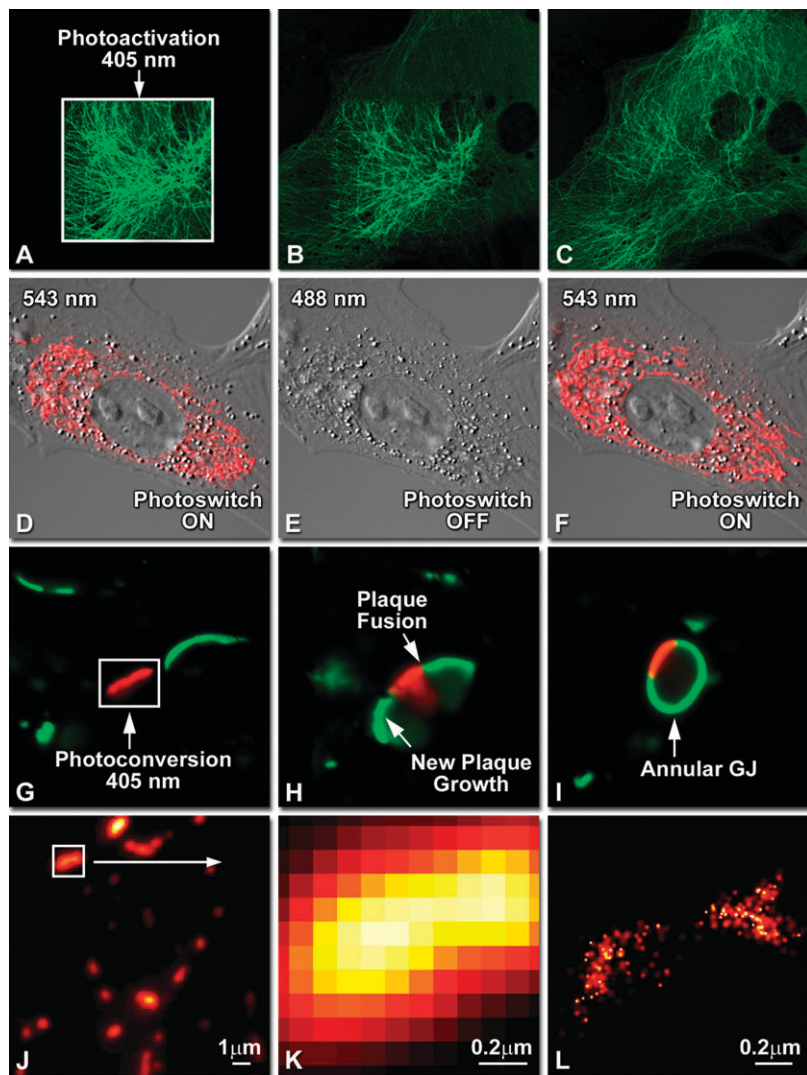


Fig. 15 Optical highlighter FPs in action imaged with laser scanning confocal microscopy. (A–C) Photoactivation of mPA-GFP-tubulin in opossum kidney (OK cell line) epithelial cells, (A) rectangular region of interest is illuminated at 405 nm for 5 s, $t = 0$. (B) The photoactivated tubulin chimera slowly migrates to other portions of the cell, $t = 25$ minutes. (C) The microtubule network gains more intensity at $t = 60$ minutes. (D–F) Photoswitching of the mitochondria with fusion of KFP1 to a mitochondria targeting sequence in fox lung cells. (D) Labeled mitochondria imaged with 543 nm laser in both fluorescence and differential interference contrast, $t = 0$. (E) After completely photoswitching the labeled chimera “off” with 488 nm illumination, the mitochondria now appear devoid of fluorescence, $t = 3$ min. (F) KFP1 label in mitochondria, reactivated with illumination at 543 nm, does not significantly photobleach after 5 rounds of photoswitching. (G–I) Photoconversion of gap junctions labeled with mEos2-Cx43 in HeLa cells. (G) Photoconversion of a gap junction plaque (red) in a selected region (white box) with 405 nm illumination at $t = 0$. (H) New plaque growth and fusion of a non-converted plaque, $t = 50$ min. (I) Formation of annular gap junction with photoconverted region, $t = 80$ min. (J–L) Superresolution microscopy (PALM) imaging of tdEos-mitochondria in fox lung cells. (J) Widefield TIRF image of a mitochondrial field near the nucleus. (K) Summed PALM image of boxed region in (J). (L) PALM image of the mitochondrial fusion.

KikGR, discussed below) contain a chromophore derived from the tripeptide His62-Tyr63-Gly64 that initially emits green fluorescence until driven into a red state by a light-catalyzed cleavage of the polypeptide backbone (Fig. 16C and D). These amino acids form the imidazolinone chromophore (similar to the *Aequorea* proteins). Irradiation induces cleavage between the amide nitrogen and α carbon atoms in the histidine residue with subsequent formation of a highly conjugated dual imidazole ring system, a process requiring catalysis by the intact protein and resulting in the dramatic shift of fluorescence emission to red wavelengths.^{158,159}

The unconventional chemistry involved in this chromophore transition should provide fluorescent protein engineers with an excellent foundation upon which to develop more advanced highlighters. A monomeric variant¹⁶⁰ of the tetrameric DendFP has been developed through random and site-directed mutagenesis and named Dendra (from *Dendronephtha* sp. and red activatable). This highlighter features excitation and emission maxima for the green and red forms of 490/553 nm and 507/573 nm, respectively, and functions well in fusion tags for subcellular localization. The commercial version Dendra2 (Evrogen) is the first monomeric red-to-green

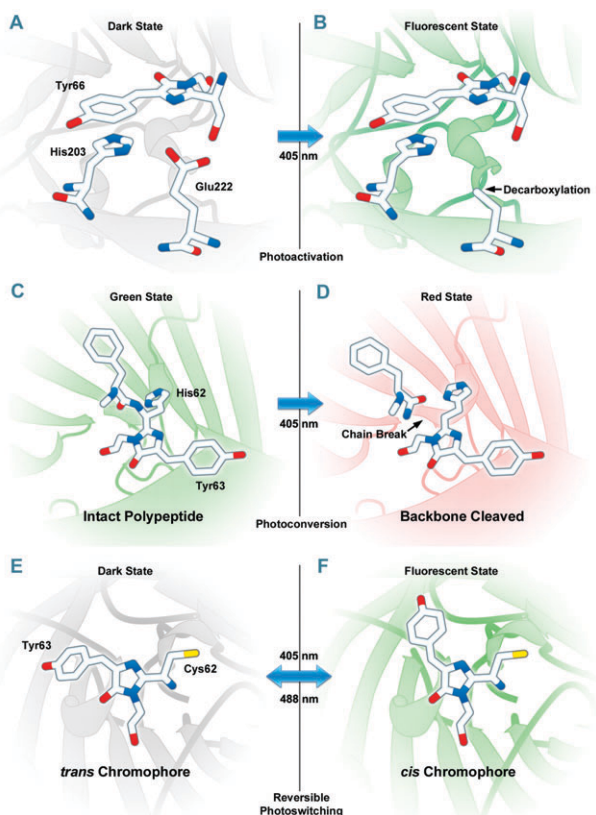


Fig. 16 Photoactivation, photoconversion and photoswitching mechanisms for optical highlighter FPs. (A, B) Photoactivation of PA-GFP (illustrated) and PS-CFP2 is believed to occur due to decarboxylation of Glu222 followed by conversion of the chromophore from a neutral to anionic state. (C, D) Green to red photoconversion for Kaede, KikGR, Dendra2, and Eos, all of which contain the HYG chromophore, occurs when the FP is illuminated with ultraviolet or violet radiation (405 nm) to induce cleavage between the amide nitrogen and α -carbon atoms in the histidine 62 residue leading to subsequent formation of a conjugated dual imidazole ring system. (E, F) Photoswitching of Dronpa involves *cis-trans* photoisomerization induced by alternating radiation between 405 nm and 488 nm. A similar isomerization mechanism is suggested to operate in mTFP0.7 and KFP1.

optical highlighter that has enjoyed widespread use as a tracking tool in live-cell imaging.^{31,161,162}

An optical highlighter isolated from another stony coral (*Lobophyllia hemprichii*), the tetrameric EosFP (named after the goddess of dawn in Greek mythology), behaves similarly to Kaede and the other variants described above. EosFP emits bright green fluorescence at 516 nm (Fig. 17), and can be photoconverted to orange-red (581 nm) fluorescence when illuminated at near-ultraviolet wavelengths.¹⁶³ Random and site-directed mutagenesis of tetrameric EosFP was used to generate two dimers and a true monomeric protein named mEosFP. Unfortunately, the monomeric variant of EosFP can only be expressed efficiently at temperatures below 30 °C, limiting the utility of mEosFP in mammalian systems. To create a pseudo-monomer suitable for imaging fusions at 37 °C, Wiedenmann and colleagues⁸⁵ linked two of the dimeric EosFP units together using a 16-amino acid linker to produce a tandem dimer. tdEosFP has turned out to be one of the most

useful optical highlighters yet developed because of its high functionality as a tag in fusion vectors and for superresolution imaging.^{142–144} Recently, an improved monomeric version that matures at 37 °C, named mEos2, has been reported.¹⁶⁴ Although not as bright as tdEos, mEos2 is an excellent complement for imaging problematic fusions (tubulin, histones, gap junctions; Fig. 15G–I) that localize poorly with tandem dimers.

A third stony coral, *Favia favus*, has yielded a promising tetrameric FP that exhibits efficient photoconversion from green to red fluorescence emission wavelengths (similar to Kaede) upon irradiation with near-ultraviolet or violet light.¹⁶⁵ Genetic engineering efforts based on structural analysis of this protein produced a tetrameric variant, termed KikGR, which is several fold brighter than Kaede in both the green and red states when expressed in mammalian cells. Commercially available (MBL) under the trade name Kikume Green-Red (after Kikume-ishi, the Japanese term for *Favia*), the highlighter has been demonstrated to be successfully photoconverted using multiphoton excitation at 760 nm,¹⁶⁵ which can be used for specific labeling of cells with high spatial resolution in thick tissues. Furthermore, the KikGR highlighter features a wider separation of green and red emission maxima (75 nm *versus* 54 nm) than Kaede. Mutagenesis of the tetrameric KikGR yielded a monomeric derivative containing 21 mutations, which is named mKikGR and has been demonstrated to perform well in fusions that do not tolerate tetramers.¹⁶⁶ Both the green and red form of mKikGR are less photostable and dimmer than mEos2, however, this highlighter might perform better in tubulin and gap junction fusions (Davidson, unpublished).

Of the currently available monomeric green to red optical highlighters (mEos2, Dendra2, and mKikGR), the native and photoconverted species of mEos2 are the brightest followed by Dendra2 and mKikGR, respectively.¹⁶⁴ Dendra2 and mEos2 are almost equivalent in photostability for both the green and red species, and far more photostable than mKikGR. All three of these optical highlighters should be useful in a wide variety of dynamic tracking experiments and can be used for precise localization in superresolution microscopy.¹⁴³ As a significant side note, it appears that photoconversion in FPs is far more widespread than originally suspected as evidenced by observations of alterations to the emission spectral profiles of cyan and yellow FPs following photobleaching experiments.^{101,167,168} In a recent investigation, several of the orange and red Anthozoa proteins, including mOrange, mKate, and HcRed1, have been observed to shift emission to longer or shorter wavelengths upon intense illumination using single and two-photon laser sources, although the contrast ratios between the native and photoconverted species are low.¹⁶⁹ Thus, photoconversion can be harnessed as a tool for cellular dynamics and superresolution microscopy, but investigators should also be aware that this phenomenon could surface as an artifact during photobleaching, FRET, or imaging experiments.

4.3 Photoswitchable fluorescent proteins

The phenomenon of photochromism (the ability to switch between fluorescent and dark states) has been observed in

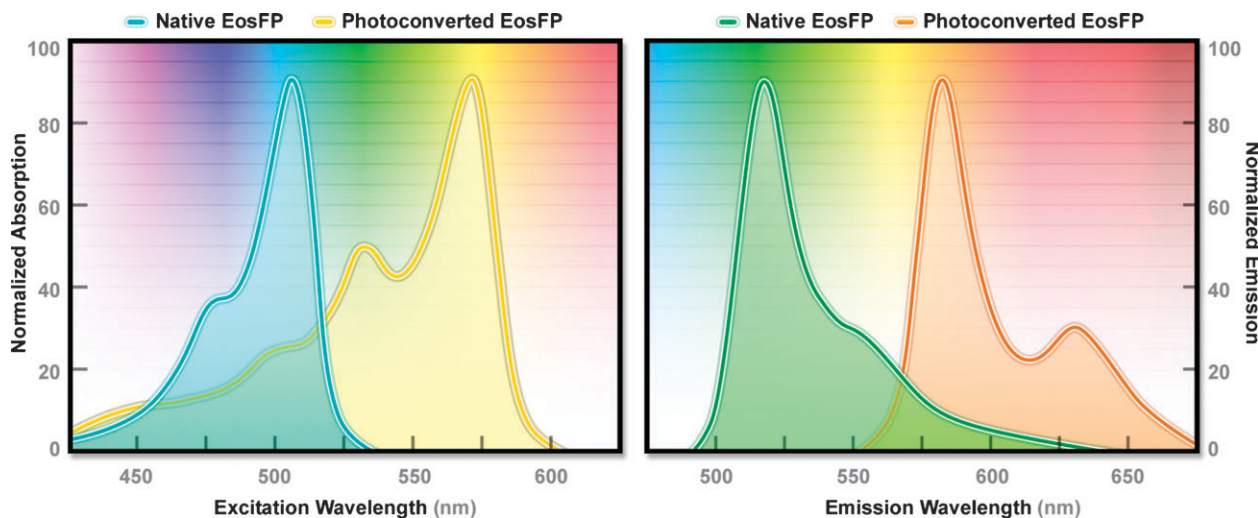


Fig. 17 Absorption and emission spectral profiles of EosFP.

wtGFP and several yellow FP derivatives at the single molecule level;^{138,170} however, none have demonstrated this phenomenon when measured in bulk. In single molecule studies, FPs exhibited fluorescence for several seconds during illumination at 488 nm followed by an equally short interval without fluorescence, after which the fluorescence resumed. The on-and-off switching or “blinking” behavior¹³⁸ was repeated many times before each FP molecule ultimately photobleached. Unfortunately, photoswitching in most of the FPs described above is stochastic, and cannot be used in quantitative experiments. However, some optical highlighters have been isolated that can be reliably toggled on or off by illumination with different excitation wavelengths, and these are called photoswitchable FPs (Table 3).

The most prominent and well-studied member of this class is named Dronpa, which is a monomeric variant derived from a stony coral tetramer.¹⁷¹ Dronpa exhibits an absorption maximum at 503 nm (arising from the anionic, deprotonated chromophore) with a minor peak at 390 nm (from the neutral, protonated chromophore). The anionic chromophore emits green fluorescence with a maximum at 518 nm and has a brightness level almost 2.5 times that of EGFP. Dronpa photoswitching occurs partly by interconversion between the deprotonated (on state; bright) and protonated (off state; dark) forms.¹⁷² Illumination at 488 nm drives Dronpa to the dark species after which the FP can be subsequently switched back on by brief illumination at 405 nm. This cycle can be repeated several hundred times without significant photobleaching.¹⁷³ The primary mechanism of FP photoswitching is thought to also arise from *cis-trans* isomerization of the hydroxybenzilidene (tyrosyl side chain) chromophore moiety that accompanies the changes in the protonation state.¹⁷⁴ Similar to other highlighters, Dronpa is useful both for dynamics and superresolution studies.^{31,143,144} Variants of Dronpa with reversed photoswitching properties and broader spectra have been reported,^{175,176} but application of these rather dim FPs has so far been limited to evaluating their performance in superresolution imaging. Future versions

will no doubt feature higher brightness and should prove useful in dynamics investigations.

Several photoswitching FPs in other regions of the color palette have been developed from anemones and corals. Kindling FP¹⁷⁷ (commercially available from Evrogen as KFP1) is a tetrameric highlighter that emits red fluorescence at 600 nm upon illumination with green or yellow light (525–580 nm). Upon cessation of illumination, KFP1 relaxes back to its initial non-fluorescent state. Irradiation with intense blue light (450–490 nm) completely quenches KFP1 fluorescence immediately, enabling control over the photo-switching (Fig. 15D–F). A cyan FP from coral named mTFP0.7 (an intermediate in mTFP1 mutagenesis) has also been demonstrated to photoswitch, but has not been characterized in living cells. In addition, monomeric photoswitchable variants of mCherry have recently been introduced¹⁷⁸ as potential probes for superresolution microscopy. Termed rsCherry and rsCherryRev, these derivatives display antagonistic switching modes. Here, irradiation of rsCherry with yellow light induces the bright state and blue light drives the FP to the dark state, whereas the reverse is observed with rsCherryRev. Unfortunately, these FPs are only ~10% as bright as mCherry when expressed as ensembles in cells, but are equally bright as mCherry on the single molecule level.

A new and unique optical highlighter derived from wtEosFP couples the properties of photoconversion and photoswitching into a single reporter.¹⁷⁹ Named IrisFP, a single mutation in wtEosFP (F173S) bestows reversible photoswitching induced by *cis-trans* isomerization of the chromophore in both the native (green) and photoconverted (red) species. Similar to the wild-type parent, IrisFP undergoes photoconversion from a green to a red-emitting state upon illumination with violet (405 nm) or UV light resulting from extension of the conjugated π -electron system that accompanies cleavage of the polypeptide backbone. Illumination of the green IrisFP species with 488 nm laser light drives the highlighter to a non-fluorescent dark state, which can then revert to a bright species upon illumination with low-intensity

405 nm light. High intensity 405 nm illumination drives the IrisFP chromophore to the red state. Similar to the green state of IrisFP the red state can be photoswitched off with 532 nm light and back on again with 440 nm light. Although hampered for use in fusions by the tetrameric quaternary structure, IrisFP represents a new class of optical highlighters that could be exploited in the future.

Investigations into the underlying mechanism of FP photoswitching^{174,180,181} indicate that *cis-trans* isomerization of the tyrosine moiety in the chromophore is a key event in the process (see Fig. 16E and F). The *cis* conformation represents the bright fluorescent state, whereas the *trans* conformation reverts the chromophore to the non-fluorescent dark state. These conformational changes are thought to be accompanied by varied chromophore protonation states that also determine the fluorescent properties. In addition, photoswitching is to some degree probably a manifestation of chromophore planarity and structural rearrangements of internal amino acid side chains within the chromophore cavity. These collective features may constitute a fundamental mechanism that is common to all photoactivatable and reversibly photoswitchable FP derivatives.

4.4 Fluorescent timer proteins

A unique, but limited, class of FPs that change spectral properties with time are called *fluorescent timers*, the first example of which was a variant of DsRed.¹⁸² Termed E5, this DsRed derivative effectively functions as a fluorescent clock that slowly changes emission from green to red over a time period of several hours to provide temporal and spatial information on gene activity. Thus, green fluorescent regions indicate recent gene activation, while yellow-orange regions signify continuous activity. Areas exhibiting bright red fluorescence indicate that gene promoter activity has ceased for an extended period. FP timer E5 was used *in vivo* to demonstrate expression in *C. elegans* and *Xenopus* promoters. However, because E5 is an obligate tetramer, it has limited utility as a protein tag.

A recent study focused on improving fluorescent timers¹⁸³ yielded three monomeric variants based on mCherry that change fluorescence from blue to red over time. The mCherry derivatives are divided into distinct classes that exhibit fast, medium, and slow blue to red chromophore maturation rates, which are temperature dependent. The fastest variant exhibits a shift of blue to red fluorescence in approximately 15 minutes, whereas the medium and slow variants have corresponding times of 1.2 and 9.8 hours, respectively. These FP timers were demonstrated to be useful when expressed in bacteria, as well as insect and mammalian cells. Continued development of fluorescent timers should yield multicolored variants with improved brightness and photostability for long-term experiments.

The optical highlighter FPs produced from *Aequorea* GFP derivatives and reef coral proteins show a sufficient promise to warrant aggressive efforts to solve problems associated with oligomerization, limited brightness, and low photostability as well as fine-tuning of their spectral profiles. Further, engineering to generate more advanced optical highlighters should shift

photoactivation wavelengths to the less phototoxic blue and green spectral regions while simultaneously pushing emission wavelengths into the yellow through far-red regions to significantly expand the potential applications of these probes.

5. Specialized techniques using the FPs

Over the past decade, FPs have launched a new and unprecedented era in cell biology by enabling investigators to apply routine molecular cloning methods, fusing these optical probes to a wide variety of protein and enzyme targets, to monitor cellular processes in living systems using fluorescence microscopy and related methodology. The spectrum of applications for fluorescent proteins ranges from reporters of transcriptional regulation and targeted markers for organelles and other subcellular structures (Fig. 18) to fusion proteins designed to monitor motility and dynamics (Fig. 19).

A significant number of fluorescent probes in the FP toolbox are also being applied to some very innovative live-cell imaging investigations. For example, research in Jeff Lichtman's laboratory¹⁸⁴ recently combined the sequences encoding several different FPs into common reporter cassettes, which were then used to generate transgenic mice. Here, *lox* recombination sites were inserted between the sequences encoding the different FPs. This arrangement permitted *Cre*-mediated recombination to randomly determine which of the FPs would be expressed from a particular cassette. Remarkably, when multiple copies of the cassette were targeted to the mouse neurons, many different random color combinations were generated that allowed individual neurons within entire neural networks to be distinguished from their neighbors.¹⁸⁴ This *Cre-lox* system, appropriately termed *Brainbow*, is allowing the investigators to determine how cellular connections are established in neural circuits; information that will be critical for understanding how the nervous system works. Aside from multicolor imaging a variety of optical methods are now used to exploit the characteristics of the FPs.

5.1 Photobleaching techniques

The use of photobleaching techniques to visualize and quantify dynamic processes in cells was introduced in the 1970's.^{185,186} The strategy is straightforward: fluorescence recovery after photobleaching (FRAP) exploits the ability of laser scanning confocal microscopes to rapidly and irreversibly photobleach a small region of interest (ROI) within the cell. The recovery of fluorescence in the bleached region is then measured as a function of time while non-bleached FPs migrate into the ROI from adjacent regions (Fig. 20). Provided the FPs are in equilibrium, the rate of influx of the non-bleached proteins provides an estimation of the mobility of the labeled protein population. However, although the methodology is well established and easily conducted, the interpretation of photobleaching data can be challenging. For instance, incomplete recovery of fluorescence can indicate the presence of one or more immobile populations of proteins that are bound stably to structures within the photobleached region. In addition, it may not be possible to completely photobleach the ROI in a brief time period, allowing highly

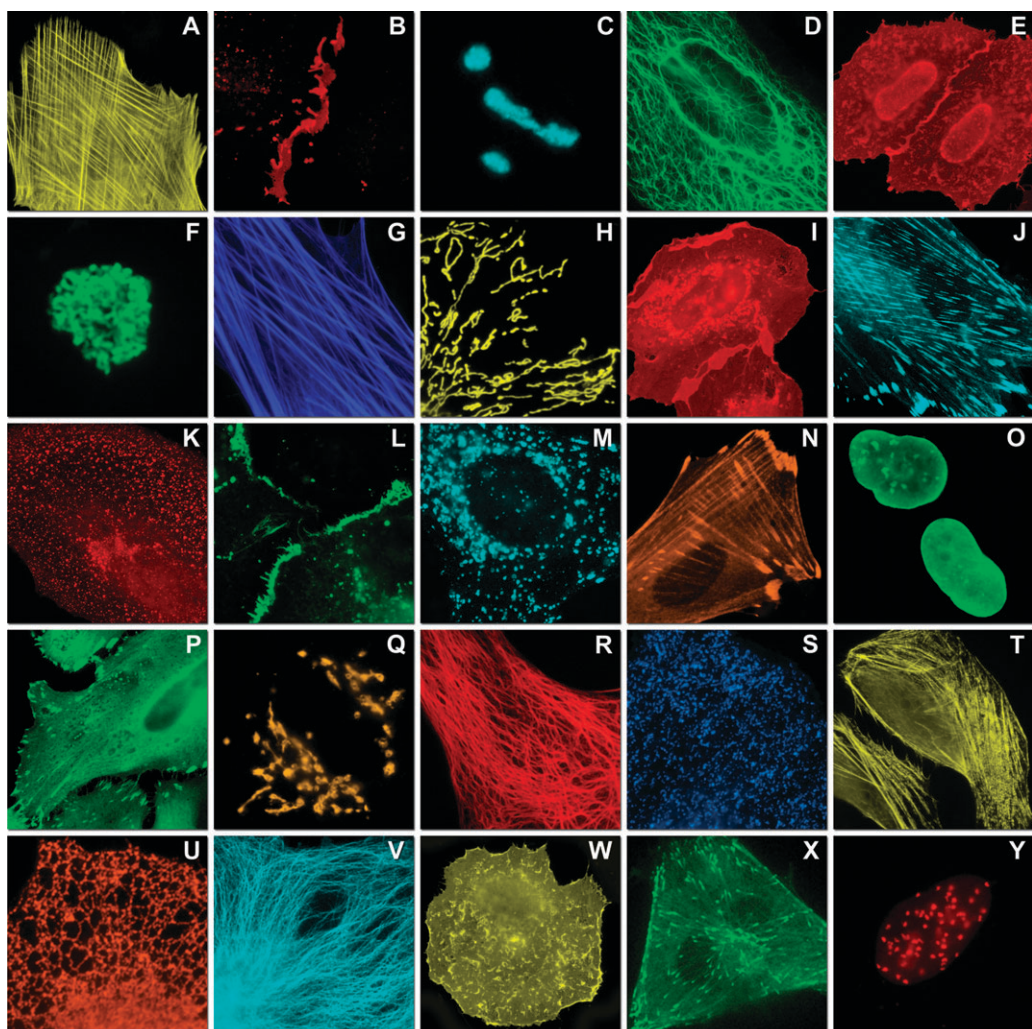


Fig. 18 Fluorescence imaging of FP fusion constructs targeting subcellular locations. Construct images are listed as: FP-fusion partner-N- or C-terminal (with respect to the FP)—number of linker amino acids. (A) mOrange2- β -actin-C-7. (B) mApple-Cx43-N-7. (C) mTFP1-fibrillarin-C-7. (D) mWasabi-cytokeratin-N-17. (E) mRuby-annexin (A4)-C-12. (F) mEGFP-H2B-N-6. (G) EBFP2- β -actin-C-7. (H) mTagRFP-T-mitochondria-N-7. (I) mCherry-C-Src-N-7. (J) mCerulean-paxillin-N-22. (K) mKate-clathrin (light chain)-C-15. (L) mCitrine-VE-cadherin-N-10. (M) TagCFP-lysosomes-C-20. (N) TagRFP-zyxin-N-7. (O) superfolderGFP-lamin B1-C-10. (P) EGFP- α -v-integrin-N-9. (Q) tdTomato-Golgi-N-7. (R) mStrawberry-vimentin-N-7. (S) TagBFP-Rab-11a-C-7. (T) mKO2-LC-myosin-N-7. (U) DsRed2-endoplasmic reticulum-N-5. (V) ECFP- α -tubulin-C-6. (W) tdTurboRFP-farnesyl-C-5. (X) mEmerald-EB3-N-7. (Y) mPlum-CENP-B-N-22.

mobile proteins to exchange with the unbleached compartment during the photobleach period. Therefore, proteins that are extremely mobile can be difficult to measure using photo-bleaching techniques, and a better approach might encompass using the photoactivation techniques described below (Section 5.2). Moreover, there can be unwanted photo-bleaching while monitoring the recovery phase that must be corrected for during data analysis, and there is always the potential for photodamage to light sensitive cellular processes. The behavior of proteins in intact cells is highly complex, and the mobilities that are determined by FRAP experiments are at best described as the average of many interactions and influences.^{187,188}

Related photobleaching approaches, termed fluorescence loss after photobleaching (FLIP) and inverse FRAP (iFRAP), are modifications of the original FRAP technique that measure the loss of fluorescence from a ROI after photobleaching of an

adjacent region. The FLIP technique involves repeated bleaching of an area within the cell to deplete fluorescent proteins that move through that area (reviewed in ref. 189 and 190). The fluorescence in the ROI is monitored during the bleaching of the adjacent area, and if the regions are linked, fluorescence will decrease in the ROI as the FP migrates out and into the region of continuous bleaching. Proteins that are stably associated with a cellular structure will bleach more slowly than those that are more freely mobile. The FLIP and iFRAP approaches reduce concerns about photodamage artifacts possible in FRAP experiments, since the measurements are acquired from regions of cells that are not photobleached.¹⁸⁷

5.2 Photoactivation and photoconversion techniques

The optical highlighter proteins can be ideal for the investigation of protein dynamics in live-cell imaging because

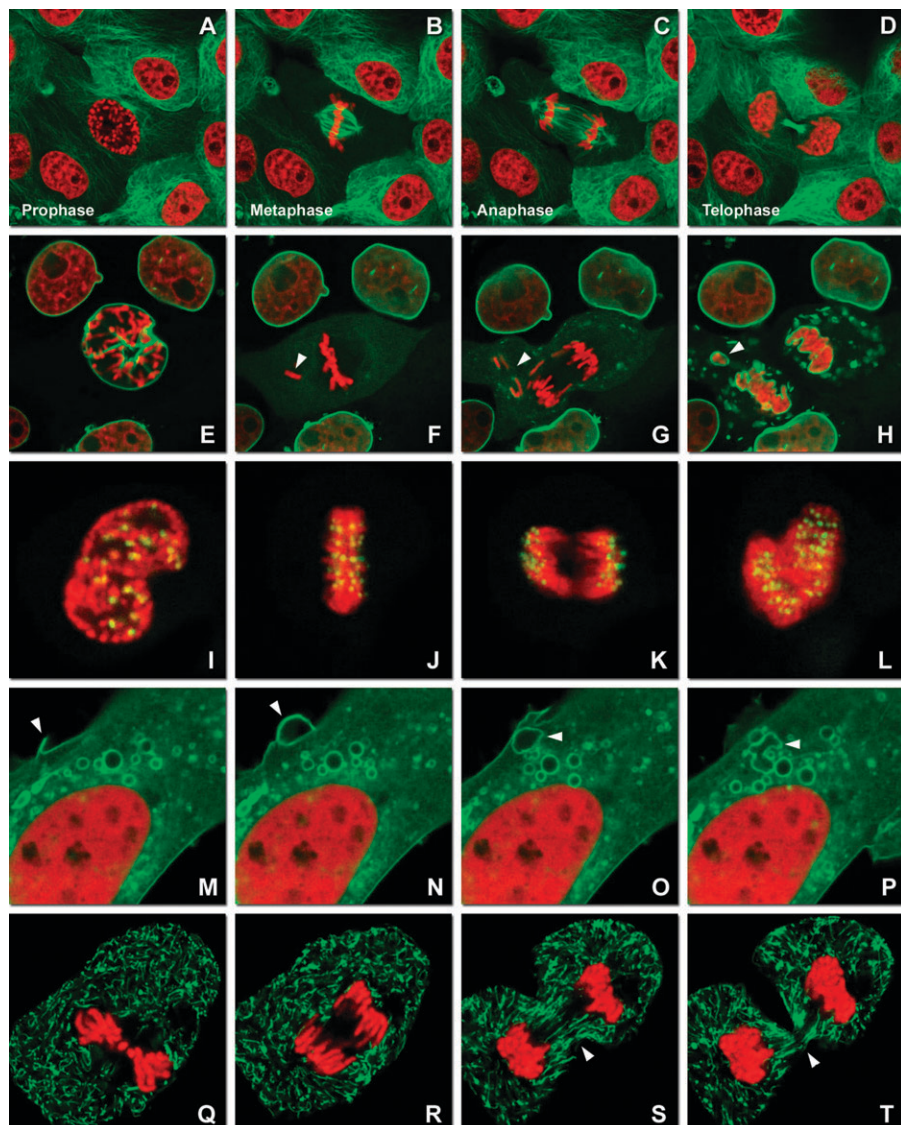


Fig. 19 Fluorescent protein reporters in action imaged with spinning disk confocal and widefield microscopy. (A–D) Observing mitosis in dual-labeled normal pig kidney (LLC-PK1 cell line) epithelial cells stably expressing mCherry-H2B (histones) and mEmerald- α -tubulin. (A) A cell in prophase is captured adjacent to cells in interphase, $t = 0$. (B) The cell forms a spindle and enters metaphase, $t = 20$ min. (C) During anaphase, the spindle poles translocate to opposite sides of the cell, pulling the condensed chromosomes along, $t = 60$ min. (D) The chromosomes begin to decondense during telophase as the daughter cells recover from cell division (mid-body visible). (E–H) Dispersion of the nuclear envelope during mitosis. HeLa cells expressing mRuby-H2B and mEmerald-lamin-B1 are imaged undergoing mitosis. (E) Late prophase with the nuclear envelope intact. (F) In metaphase, the nuclear envelope signal is dispersed in the cytoplasm. Note the detached chromosome (arrow). (G) During late anaphase, the nuclear envelope begins to reform. Note the independent mitosis event for the detached chromosome (arrow). (H) Telophase nuclei decondense and the nuclear envelope reforms. Note the separate nuclear envelope formation on the detached chromosomes (arrow). (I–L) HeLa cells labeled with mApple-H2B and mEmerald-CENPB undergoing mitosis. (I) Prophase nucleus showing labeled condensed chromosomes (red) and centromeres (green). Centromeres and chromosomes are visible during cell division in metaphase (J), anaphase (K), and telophase (L). (M–P) Vesicle formation by C-Src in U2OS cells labeled with mEmerald-C-Src and mRuby-H2B. Arrows denote formation of a vesicle at the periphery of the plasma membrane. (Q–T) Mitosis in opossum kidney cells labeled with mCherry-H2B and mEGFP-mitochondria. Arrows denote localization of mitochondria to the mid-body region during cell division.

photoactivation or photoconversion provides for controlled highlighting of distinct molecular pools within the cell (reviewed in ref. 128, 139 and 140). Since only a limited population of photoactivated molecules exhibits noticeable fluorescence, their lifetime and behavior can be followed independently. Ideal optical highlighters (see Table 3) should be readily photoactivatable/photoconvertible to generate a high level of contrast, and should be monomeric for optimal

performance as fusion tags. These probes offer a gentler alternative to the relatively harsh photobleaching techniques, such as FRAP and FLIP (Section 5.1), which generally require high laser powers and repeated illumination to completely eradicate active fluorophores from the region of interest. Furthermore, measurements are not influenced by freshly synthesized or non-converted FPs, which either remain invisible or continue to emit the original wavelengths.

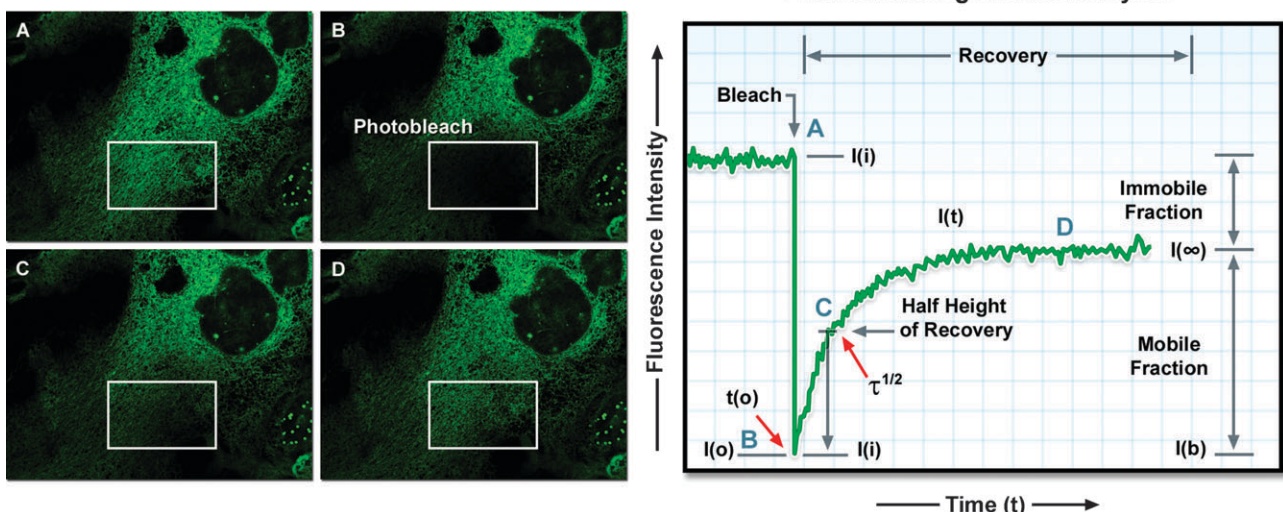


Fig. 20 Opossum kidney epithelial cell labeled with EGFP fused to an endoplasmic reticulum targeting sequence. A region of interest (white box) is photobleached with high laser power for 5 seconds (B), effectively quenching all of the fluorescence. Continued monitoring of the cell enables visualization of fluorescence recovery in the photobleached region (C) and (D). A plot of fluorescence intensity *versus* time enables quantitative analysis of the recovery kinetics and provides information about the diffusion coefficient and mobility for this fluorescent protein chimera.

The first photoactivatable optical highlighter, PA-GFP, produces a 100-fold increase in green fluorescence (504 nm emission peak) as described above, enabling tracking of the dynamics in molecular subpopulations.¹⁴⁵ PA-GFP is difficult to detect in its non-activated form, which limits its use for some applications, but also gives it a high dynamic range for photoactivation. However, the co-expression of PA-GFP with another FP marker can often be used to overcome this limitation. The ability to “switch on” PA-GFP in a user defined ROI, and then follow the photoactivated protein as it diffuses from the ROI, provides a powerful approach to monitor the dynamic of proteins inside the living cell. PA-GFP is still the best optical highlighter in the green region of the spectrum, and has a far better dynamic range compared to PA-mCherry.¹⁵⁰ The photoconvertible proteins that switch color allow pulse-chase experiments that follow a highlighted population of proteins over time. In terms of brightness and conversion efficiency, the green to red Kaede protein is among the best performers.¹⁵² However, as was discussed above (Section 4), there is a significant need for better performers in the optical highlighter category of FPs.

In addition to their utility in selectively labeling subpopulations of fusion proteins for dynamic studies, optical highlighters are also valuable tools in the recently introduced superresolution microscopy techniques designed to break the traditional Abbe diffraction barrier.^{141,142,191,192} These new methods include photoactivated localization microscopy (PALM) and stochastic optical reconstruction microscopy (STORM), which rely on low levels of illumination to photoactivate selected individual molecules spaced further apart than the diffraction limit so that an array of magnified diffraction spots can be recorded on a highly sensitive camera. Adjacent molecules are not recorded because they still exist in the dark or inactivated state. The calculation of the exact coordinates of the single fluorescent molecules within the photoactivated population enables their localization with precision that

exceeds the optical resolution of the conventional microscope. After switching off (or photobleaching) the registered molecules, a new group can be photoactivated and read out. Thus, the image is assembled one molecule at a time by means of iterative switching cycles. The reconstructed images feature optical resolutions down to 20 nm (see Fig. 15J–L). These techniques are becoming increasingly faster and hold a significant promise for live-cell imaging with remarkable spatial resolution.

5.3 Förster resonance energy transfer

The lateral resolution ($x-y$) of the conventional microscope is limited to approximately 200 nm for blue light illumination and lower for illumination of longer wavelengths. Therefore, considerable distances may actually separate proteins that appear to be co-localized by multicolor fluorescence microscopy, limiting speculation about the interactions of the labeled proteins. The newer optical techniques discussed above promise several fold improvement in the optical resolution,¹⁴¹ but much higher resolution is necessary to detect protein–protein interactions in living cells. One method of gaining the Angstrom-scale resolution that is necessary to detect protein–protein interactions is Förster or fluorescence resonance energy transfer (FRET) microscopy. FRET microscopy measures the direct transfer of excitation energy from a donor fluorophore attached to one protein to an acceptor fluorophore attached to an interacting protein. FRET results from electromagnetic dipolar interactions between the donor and acceptor fluorophores, and this limits the distance over which energy transfer can occur to less than approximately 80–100 Å. Thus, the detection of FRET can provide measurements of the spatial relationship of the fluorophores on the scale of angstroms. The essential requirement for the efficient transfer of energy from a donor to an acceptor fluorophore is a substantial overlap of the donor emission spectrum with the

absorption spectrum of the acceptor (reviewed in ref. 42, 193–195). Many FPs discussed above share overlapping spectra, and some have been proven useful for FRET-based microscopy.

5.3.1 Protein standards for FRET measurements. The wide availability of FPs that emit across the visible spectrum and that have a suitable spectral overlap for FRET-based microscopic measurements has led to broad application of this approach. As will be discussed below, there are several different methods to acquire and verify FRET measurements. However, as it is true for any highly technical approach, the interpretation of the experimental results can be problematic, and it is difficult to directly compare the accuracies of different methods. Indeed, the favorable labeling characteristics of FPs led to a newfound popularity of FRET measurements to detect protein interactions in living cells, but this has resulted in what has been called “degradation in the validity of the interpretations” of these experiments.¹⁹⁶ To address this issue, the Vogel laboratory introduced a set of genetically encoded fusion proteins that could be used to evaluate systems for making FRET measurements by a variety of different methods.^{57,196,197}

Currently, the most commonly used FP combination for FRET-based imaging studies is the pairing of cyan and yellow FPs. Of the available FPs in these spectral regions, Cerulean, in combination with Venus, or Citrine is considered to be among the best FRET pairings. To develop fusion proteins that could serve as “standard” for FRET measurements, Thaler and colleagues¹⁹⁷ created genetic constructs that encoded Cerulean directly coupled to Venus through amino acid linkers of defined length. They generated a genetic construct that encoded Cerulean separated from Venus by a five amino acid linker, producing a fusion protein with consistently high (~45%) FRET efficiency. They also made a genetic construct with a larger linker that encoded the 229-amino acid tumor necrosis factor receptor associated factor (TRAF) domain separating the Cerulean and Venus proteins. This produced a fusion protein with low FRET efficiency (~10%). They then used three different techniques to measure FRET in cells that expressed the “FRET-standard” fusion proteins. For each of the fusion proteins tested there was consensus in the results obtained by the different FRET methods, demonstrating that these genetic constructs could serve as FRET standards. What maybe more important, other laboratories can also use these same genetic constructs to verify and calibrate FRET measurements obtained in their own experimental systems.

Recently, we used the FRET standard approach to directly compare different FPs as donors for FRET measurements.¹⁹⁸ An ideal donor FP for FRET studies should be photostable and have a high quantum yield, preferably close to that of the acceptor. The donor FP also should have comparatively narrow spectra and possess simple lifetime decay kinetics. For intensity-based FRET measurements, the ideal acceptor FP will also be very bright and photostable and have an absorption spectrum that strongly overlaps the emission spectrum for the donor. The new monomeric Teal FP (mTFP1, Section 3.5) has these characteristics, so we use the

FRET standard approach to directly compare mTFP1 to Cerulean as a FRET donor for Venus. Our results showed that mTFP1 was an improved FRET donor for Venus compared to Cerulean.¹⁹⁸

Because of its increased brightness and optimal excitation using the standard 458 nm laser line, mTFP1 should improve the detection of interactions between proteins that are produced at low levels in cells. Furthermore, the improved photostability of mTFP1, and its excellent spectral overlap with acceptor proteins such as Venus or newer generation orange FPs (Section 3, above), makes it an appealing donor fluorophore for FRET measurements. In this regard, Venus suffers from poor photostability. Although this can be an advantage for certain FRET-based imaging approaches that use photobleaching (Section 5.4.3, below), there is a need for improved acceptor FPs. Unfortunately, while many of the evolved orange and red FPs have spectral characteristics that should make them excellent acceptor proteins for FRET, few of these proteins have yet been proven to be good FRET partners for intensity-based measurements. Below, we describe three separate methods for making FRET measurements from living cells using FPs. It is important to emphasize that more than one method should be used to evaluate FRET measurements, and that both positive (FRET standards) and negative FRET controls are critical to validate the experimental system.

5.3.2 Spectral bleed-through correction. The required spectral overlap between fluorophores used for FRET microscopy also leads to significant background fluorescence, contributed by both the donor and acceptor fluorophores, which contaminates the FRET signal and must be removed for quantification of the signal. These fluorescence background signals are collectively referred to as spectral bleed-through (SBT) and must be removed from the image acquired in the FRET channel (donor excitation/acceptor emission) to accurately measure FRET efficiency. Several different computer algorithms have been designed for this purpose.^{199–201} A comprehensive comparison of these and other correction methods has been published.²⁰² The most common approach is to acquire reference images of control cells expressing either the donor- or the acceptor-labeled proteins alone. The resulting information is then used to define and remove the contributions of the donor and acceptor SBT background from the FRET signal obtained from experimental cells that express both the donor- and acceptor-labeled proteins. SBT correction is specific to the collection conditions used on a particular instrument, and control measurements must be made for each experiment. Cell movement, focal plane drift, and a lack of precisely-registered images used for FRET determinations are potential sources of artifacts that will appear as regions of either very high or negative FRET in energy transfer images, and must be critically evaluated.²⁰³

Because subtraction of large SBT contributions can introduce artifacts into the estimates of the corrected FRET signals, these correction approaches will work best when the fluorescence intensities of the donor- and acceptor-labeled proteins are similar, and accurately measured above the background noise.²⁰² In addition, energy transfer from the donor to the acceptor fluorophore is accompanied by a

reduction of the donor fluorescence. Therefore, accurate removal of the donor contribution to the FRET signal requires knowledge of the donor signal that is lost to energy transfer, and the different algorithms mentioned above vary in their methods for accounting for this correction. Significantly, the accuracy of these spectral bleed-through correction methods is degraded as the spectral overlap between the FPs is increased to the point where spectral bleed-through components overwhelm the FRET signal.

5.3.3 Acceptor photobleaching. A method that is commonly used to verify FRET measurements obtained using the SBT correction (Section 5.3.1) is called acceptor photobleaching FRET (pbFRET). When FRET occurs, the excited state energy of the donor fluorophore is directly transferred to the acceptor, resulting in quenching of the donor signal. If the acceptor fluorophore is destroyed by photobleaching, the donor signal will be increased (termed dequenching) because its energy is no longer transferred to the acceptor. Therefore, comparing donor fluorescence intensity before and after photobleaching measures the proportion of donor energy lost to FRET.^{204,205} Measuring FRET efficiency by the photobleaching approach requires selective bleaching of the acceptor, because any bleaching of the donor fluorophore will lead to an underestimation of the donor dequenching.^{203,206,207} Because the acceptor is irreversibly bleached, however, the pbFRET method cannot be repeated on the same cell, so pbFRET is limited to a single experiment and is not useful to track interactions over extended periods of time. The pbFRET method is often used for verifying FRET results obtained by other methods.

5.3.4 Fluorescence decay measurements. An alternative method to measure the effect of FRET on the donor fluorophore detects changes in the fluorescence lifetime of the donor in the presence of the acceptor. Where intensity-based imaging methods measure a time averaged fluorescent signal, fluorescence lifetime imaging microscopy (FLIM) measures the average amount of time the fluorophores spend in the excited state. The excited state lifetime is an intrinsic property of a fluorophore, and is not influenced by probe concentration, excitation light intensity, or light scattering, which makes FLIM particularly useful for biological applications. Furthermore, since FRET is a non-radiative process that depopulates the excited state of the donor fluorophore, it can be detected by FLIM as a reduction in the donor fluorescence lifetime. There is a direct and inverse relationship between the donor fluorescent lifetime and the FRET efficiency. When donor lifetimes are determined in the absence (τ_D) and in the presence of the acceptor (τ_{DA}), the ratio of these determined lifetimes provides a clear-cut method to estimate the efficiency of FRET (E_{FRET}) using the relationship:

$$E_{FRET} = 1 - (\tau_{DA}/\tau_D) \quad (1)$$

The FRET-FLIM approach uses optical filtering to isolate the donor fluorescence emission signal and then measure the fluorescence lifetime.^{58,208–210} When there is non-radiative energy transferred from the donor to the acceptor, the donor excited state energy is dissipated and there will be a shift in the

mean lifetime for the donor population to shorter lifetimes. Thus, when FRET occurs, FLIM will detect at least two donor populations: the unquenched donors (free donor) and the donors that are quenched by the acceptors (bound donor). These different populations will be reflected in the donor fluorescence decay kinetics, which can be described by at least two exponential components. Here, the accurate assignment of the donor populations will be improved if the donor fluorophore exhibits simple decay kinetics. In addition, it is important to choose an optical filter that efficiently collects the donor emission signal while eliminating the acceptor emission bleed-through, but this may be at the expense of photon counts.^{211,212} If these requirements are met, the measurements of the donor lifetime provide a robust method to quantify FRET.^{58,210,213,214}

In practice, however, when expressed in the heterogeneous environments inside living cells, many FPs exhibit multi-exponential fluorescence decays, which complicates the interpretation of fluorescence lifetime measurements. For example, both ECFP and its mutant variant Cerulean were found to exhibit different fluorescent states, which limit their use as donors in FLIM–FRET experiments.^{58,59,215} For these FPs, variations in the protonation state of the chromophore allow multiple decay pathways for the donor fluorophore to exit the excited state. Because the fluorescence decay of the donor alone is already complex, the assignment of the quenched and unquenched donor populations from FRET-FLIM measurements can be difficult. In this regard, there are advantages in using GFP as a donor fluorophore for FLIM-FRET. First, it is the donor quantum yield that determines the R_0 for the FRET pair, and GFPs have a higher intrinsic brightness than Cerulean. Second, GFP is excited in a spectral window that generates less autofluorescence than that for any CFP. Third, as mentioned above, simple decay kinetics represent an important characteristic of donor fluorophores for FLIM studies. The emission decay of GFP is mono-exponential, which allows the unambiguous assignment of quenched and unquenched fractions in FRET studies.^{58,216}

These characteristics have prompted the search for optimal FRET acceptors for GFP and green FPs from reef corals. Because of their spectral overlap with GFP both mRFP1 and its variant, mCherry, have been used as FRET acceptors for EGFP in FLIM studies.^{58,212,216} The low quantum yield of mRFP1 actually improves the signal-to-noise, since there is less bleed-through from the acceptor detected in the donor fluorescence channel.⁵⁸ Still, acceptors that have increased spectral overlap with EGFP emission would increase the range of distance over which FRET could be detected. Recently, novel YFPs have been developed that have a high absorbance coefficient, but have extremely low quantum efficiency. This class of chromophore, called resonance energy-accepting chromoproteins (REACH), permits the optimal use of GFP as a donor for FRET-FLIM.^{217,218} Because the REACH probes have very low quantum yield, there is little concern about acceptor back-bleed-through emission in the donor channel. This allows the use of filters with a wider donor spectral window to collect optimally the donor signal. The measurement of a double-exponential fluorescence lifetime decay curve for EGFP in the presence of the dark

chromoproteins will now accurately reflect the populations of free donor and donor quenched by the REACh probe.^{217,218} Additionally, the absence of fluorescence from REACh probes means that the spectral window normally occupied by the acceptor is now available for the detection of another probe. This opens the possibility of correlating the protein–protein interactions detected by FRET with the behavior of another labeled protein expressed inside the same living cells, the cellular biochemical network.^{217,218}

5.4 FRET-based biosensor proteins

Another important FRET-based approach for characterizing changes in protein structure in living cells involves monitoring energy transfer between donor and acceptor FPs attached to different sites in the same “biosensor” protein (Fig. 21). Similar to the FRET standard approach described above (Section 5.3.1), the biosensor proteins incorporate a bioactive linker between the fluorescent proteins. Here, the binding of a ligand, or the modification of the protein linker, leads to a change in the conformation of the linker, thus changing the FRET signal. The early biosensor probes incorporated calcium sensitive linkers to monitor intracellular calcium fluctuations.^{43,44} These probes have been continually modified to incorporate optimized cyan and yellow FPs, increasing their sensitivity and dynamic range.²¹⁹ Recently, linkers incorporating kinase-sensitive domains that undergo conformational reorganization upon phosphorylation have been developed. Here, dynamic changes in the FRET signal are detected as a change in the emission ratio of the two

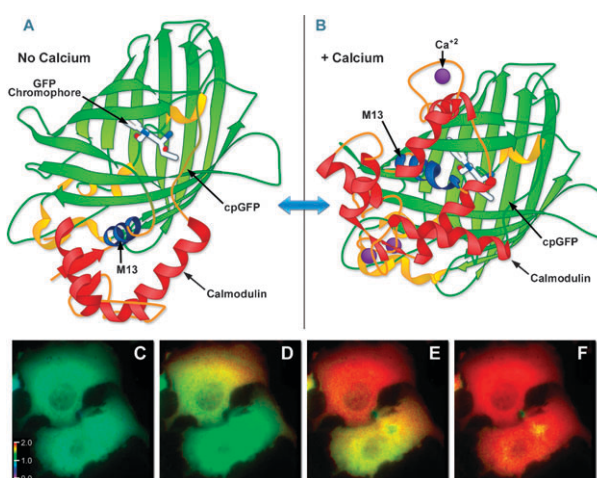


Fig. 21 FP biosensor structure and imaging. (A) GCaMP2, a calcium indicator constructed with a circularly permuted EGFP fused to calmodulin and the calmodulin-binding domain of myosin light chain kinase (M13 domain) in the absence of calcium. (B) GCaMP2 structure when bound to calcium. Drawings based on Protein Data Bank IDs: 3ekj and 3ek4, respectively. (C–F) Widefield fluorescence calcium imaging in the cytosol of HeLa cells expressing a calcium biosensor. (C) Real color image of two cells, $t = 0$, histamine (10 μM) added; (D) pseudocolored ratio image of two HeLa cells as a calcium wave initiates in the upper cell, $t = 10$ s. (E–F) The calcium wave propagates through the cytoplasm of both cells. (E) $t = 10.8$ s. (F) $t = 11.3$ s. The level of FRET is indicated by comparison of the pseudocolor signal to the calibration bar in (C).

fluorophores permitting the direct visualization of kinase activity in live cells.^{78,220}

Ratio imaging of the donor and acceptor signal from the linked probes automatically corrects for the SBT background, greatly simplifying FRET measurements with the biosensor proteins. Continuing efforts in development of new FPs that are suitable as FRET probes will yield new biosensor probes that can be used in different spectral windows.^{221,222} This intramolecular FRET approach has tremendous potential in the development of FRET-based biosensors that can be used for large-scale screening approaches.²²³ However, one caveat to this approach mentioned above (Section 2.5) concerns the potential formation of oligomers of the dual-labeled proteins,^{69,70} where the contributions from both intramolecular and intermolecular FRET will be measured. Another concern is the potential for proteolytic cleavage of the dual-tagged protein over the time course of the experiment, which will lead to separation of the FPs and potential loss of FRET signals. Despite these concerns, the genetically encoded biosensor FRET probes combine the features of subcellular targeting, signal pathway specificity, and detection sensitivity that allow the real-time monitoring of cellular events inside living cells. These FRET-based biosensors have tremendous potential in the development of large-scale screening approaches for the discovery of novel pharmaceuticals and the development of therapeutic strategies.

6. Conclusion and perspectives

It took over thirty years, and the advent of recombinant DNA, and vastly improved molecular biological approaches to see the pioneering work of Osamu Shimomura developed into a useful tool for live-cell imaging by Douglas Prasher and Martin Chalfie. Just in the past decade, however, we have witnessed a truly remarkable expansion in the palette of FPs, largely driven by the innovative studies from Roger Tsien's laboratory. We now have FPs that span almost the entire visible spectrum from deep blue to deep red, providing a wide choice of genetically encoded markers for studies in cell biology. What is more, many FPs have been identified that have optical highlighter characteristics that make them useful reporters of the dynamic behaviors of the proteins they label. Most of the FPs that are commonly used today have been modified through mutagenesis to optimize their expression in biological systems. Continued efforts using directed evolution approaches will no doubt improve the spectral characteristics, photostability, maturation time, brightness, acid resistance, and utility of the FP tags for cellular imaging.

In this critical review, we have described the origins and characteristics of the FPs that we consider to be especially useful or to have the potential for generating useful derivatives for live-cell imaging applications. We should emphasize that when selecting among the many different FPs that are now available, it is important to consider that live-cell imaging is a tradeoff between acquiring adequate signal from the expressed FPs, while limiting cell damage that might be caused by the illumination of the fluorophores. Living systems are more tolerant of longer wavelength illumination, and the newer generations of bright, photostable yellow to red FPs offer

alternatives to the blue and cyan variants that require near UV excitation. Many of the newer generation FPs are very bright, and can be detected with minimal exposure of the living cells to the excitation illumination. Furthermore, if probes in the blue spectrum are necessary, long wavelength excitation of these probes can be achieved with two-photon microscopy, offering a less damaging alternative to near UV excitation. The many new FP probes are allowing non-invasive imaging techniques to complement and extend the results that are obtained by the biochemical analysis of the endogenous cellular proteins. Importantly, the measurements obtained from proteins labeled with the FPs in the natural environment inside living cells provide the most physiologically relevant information about protein behavior currently available.

Acknowledgements

This work would not have been possible without the generous contribution of FPs and technical information from the originating laboratories. These investigators include Eric Betzig, Robert E. Campbell, Dmitriy M. Chudakov, Oliver Griesbeck, George T. Hanson, Harald Hess, Jennifer Lippincott-Schwartz, Konstantin A. Lukyanov, Sergey Lukyanov, Atsushi Miyawaki, Takeharu Nagai, David W. Piston, S. James Remington, Nathan C. Shaner, Roger Y. Tsien, Vladislav V. Verkusha, and Jörg Wiedenmann. We also thank Tony Gines for providing the illustrations.

References

- 1 Pliny, J. Bostock and H. T. Riley, *The natural history of Pliny, Book XXXII. Remedies derived from aquatic animals. Chapter 52—Other aquatic productions. Adarca or Calamochnos: three remedies. Reeds: eight remedies. The ink of the *sæpia*. Gaius Plinius Secundus (Pliny the Elder). AD77.*, H. G. Bohn, London, 1855.
- 2 M. V. Matz, K. A. Lukyanov and S. A. Lukyanov, *Bioessays*, 2002, **24**, 953–959.
- 3 M. Chalfie and S. Kain, *Green fluorescent protein: properties, applications, and protocols*, Wiley-Interscience, Hoboken, NY, 2nd edn, 2006.
- 4 O. Shimomura, F. H. Johnson and Y. Saiga, *J. Cell. Comp. Physiol.*, 1962, **59**, 223–239.
- 5 H. Morise, O. Shimomura, F. H. Johnson and J. Winant, *Biochemistry*, 1974, **13**, 2656–2662.
- 6 M. Zimmer, *Glowing genes: a revolution in biotechnology*, Prometheus Books, Amherst, NY, 2005.
- 7 D. Prasher, R. O. McCann and M. J. Cormier, *Biochem. Biophys. Res. Commun.*, 1985, **126**, 1259–1268.
- 8 D. C. Prasher, V. K. Eckenrode, W. W. Ward, F. G. Prendergast and M. J. Cormier, *Gene*, 1992, **111**, 229–233.
- 9 M. Chalfie, Y. Tu, G. Euskirchen, W. W. Ward and D. C. Prasher, *Science*, 1994, **263**, 802–805.
- 10 S. Inouye and F. I. Tsuji, *FEBS Lett.*, 1994, **341**, 277–280.
- 11 J. D. Plautz, R. N. Day, G. M. Dailey, S. B. Welsh, J. C. Hall, S. Halpain and S. A. Kay, *Gene*, 1996, **173**, 83–87.
- 12 P. van Roessel and A. H. Brand, *Nat. Cell Biol.*, 2002, **4**, E15–E20.
- 13 A. K. Hadjantonakis, M. E. Dickinson, S. E. Fraser and V. E. Papaioannou, *Nat. Rev. Genet.*, 2003, **4**, 613–625.
- 14 C. N. Stewart, Jr., *Trends Biotechnol.*, 2006, **24**, 155–162.
- 15 O. Shimomura, *FEBS Lett.*, 1979, **104**, 220–222.
- 16 C. W. Cody, D. C. Prasher, W. M. Westler, F. G. Prendergast and W. W. Ward, *Biochemistry*, 1993, **32**, 1212–1218.
- 17 R. Heim, D. C. Prasher and R. Y. Tsien, *Proc. Natl. Acad. Sci. U. S. A.*, 1994, **91**, 12501–12504.
- 18 R. Y. Tsien, *Annu. Rev. Biochem.*, 1998, **67**, 509–544.
- 19 M. Zimmer, *Chem. Rev.*, 2002, **102**, 759–781.
- 20 M. Ormo, A. B. Cubitt, K. Kallio, L. A. Gross, R. Y. Tsien and S. J. Remington, *Science*, 1996, **273**, 1392–1395.
- 21 F. Yang, L. G. Moss and G. N. Phillips, Jr., *Nat. Biotechnol.*, 1996, **14**, 1246–1251.
- 22 A. B. Cubitt, R. Heim, S. R. Adams, A. E. Boyd, L. A. Gross and R. Y. Tsien, *Trends Biochem. Sci.*, 1995, **20**, 448–455.
- 23 R. Heim, A. B. Cubitt and R. Y. Tsien, *Nature*, 1995, **373**, 663–664.
- 24 D. A. Zacharias and R. Y. Tsien, *Methods Biochem. Anal.*, 2006, **47**, 83–120.
- 25 T. Nagai, K. Ibata, E. S. Park, M. Kubota, K. Mikoshiba and A. Miyawaki, *Nat. Biotechnol.*, 2002, **20**, 87–90.
- 26 N. C. Shaner, P. A. Steinbach and R. Y. Tsien, *Nat. Methods*, 2005, **2**, 905–909.
- 27 O. Zapata-Hommel and O. Griesbeck, *BMC Biotechnol.*, 2003, **3**, 5.
- 28 M. Chatteraj, B. A. King, G. U. Bublitz and S. G. Boxer, *Proc. Natl. Acad. Sci. U. S. A.*, 1996, **93**, 8362–8367.
- 29 K. Brejc, T. K. Sixma, P. A. Kitts, S. R. Kain, R. Y. Tsien, M. Ormo and S. J. Remington, *Proc. Natl. Acad. Sci. U. S. A.*, 1997, **94**, 2306–2311.
- 30 A. B. Cubitt, L. A. Woollenweber and R. Heim, *Methods Cell Biol.*, 1999, **58**, 19–30.
- 31 N. C. Shaner, G. H. Patterson and M. W. Davidson, *J. Cell Sci.*, 2007, **120**, 4247–4260.
- 32 J. D. Pedelacq, S. Cabantous, T. Tran, T. C. Terwilliger and G. S. Waldo, *Nat. Biotechnol.*, 2006, **24**, 79–88.
- 33 A. Cramer, E. A. Whitehorn, E. Tate and W. P. C. Stemmer, *Nat. Biotechnol.*, 1996, **14**, 315–319.
- 34 R. Heim and R. Y. Tsien, *Curr. Biol.*, 1996, **6**, 178–182.
- 35 G. H. Patterson, S. M. Knobel, W. D. Sharif, S. R. Kain and D. W. Piston, *Biophys. J.*, 1997, **73**, 2782–2790.
- 36 G. Patterson, R. N. Day and D. Piston, *J. Cell Sci.*, 2001, **114**, 837–838.
- 37 T. T. Yang, P. Sinai, G. Green, P. A. Kitts, Y. T. Chen, L. Lybarger, R. Chervenak, G. H. Patterson, D. W. Piston and S. R. Kain, *J. Biol. Chem.*, 1998, **273**, 8212–8216.
- 38 R. Rizzuto, M. Brini, F. De Giorgi, R. Rossi, R. Heim, R. Y. Tsien and T. Pozzan, *Curr. Biol.*, 1996, **6**, 183–188.
- 39 G. H. Patterson, D. W. Piston and B. G. Barisas, *Anal. Biochem.*, 2000, **284**, 438–440.
- 40 R. D. Mitra, C. M. Silva and D. C. Youvan, *Gene*, 1996, **173**, 13–17.
- 41 R. N. Day, *Mol. Endocrinol.*, 1998, **12**, 1410–1419.
- 42 A. Periasamy and R. N. Day, *Methods Cell Biol.*, 1999, **58**, 293–314.
- 43 A. Miyawaki, J. Llopis, R. Heim, J. M. McCaffery, J. A. Adams, M. Ikura and R. Y. Tsien, *Nature*, 1997, **388**, 882–887.
- 44 V. A. Romoser, P. M. Hinkle and A. Persechini, *J. Biol. Chem.*, 1997, **272**, 13270–13274.
- 45 M. Rehm, H. Dussmann, R. U. Janicke, J. M. Tavare, D. Kogel and J. H. Prehn, *J. Biol. Chem.*, 2002, **277**, 24506–24514.
- 46 A. Khodjakov and C. L. Rieder, *Methods*, 2006, **38**, 2–16.
- 47 S. M. Potter, *Curr. Biol.*, 1996, **6**, 1595–1598.
- 48 D. J. Stephens and V. J. Allan, *Science*, 2003, **300**, 82–86.
- 49 M. A. Rizzo and D. W. Piston, in *Live Cell Imaging: A Laboratory Manual*, ed. R. D. Goldman and D. L. Spector, Cold Spring Harbor Laboratory Press, ColdSpring Harbor, 2005, pp. 3–23.
- 50 H. W. Ai, N. C. Shaner, Z. Cheng, R. Y. Tsien and R. E. Campbell, *Biochemistry*, 2007, **46**, 5904–5910.
- 51 G. J. Kremers, J. Goedhart, D. J. van den Heuvel, H. C. Gerritsen and T. W. Gadella, Jr., *Biochemistry*, 2007, **46**, 3775–3783.
- 52 M. A. Mena, T. P. Treynor, S. L. Mayo and P. S. Daugherty, *Nat. Biotechnol.*, 2006, **24**, 1569–1571.
- 53 H. Wallrabe, M. Stanley, A. Periasamy and M. Barroso, *J. Biomed. Opt.*, 2003, **8**, 339–346.
- 54 W. Tomosugi, T. Matsuda, T. Tani, T. Nemoto, I. Kotera, K. Saito, K. Horikawa and T. Nagai, *Nat. Methods*, 2009, **6**, 351–353.
- 55 M. Tramier, I. Gautier, T. Piolot, S. Ravalet, K. Kemnitz, J. Coppey, C. Durieux, V. Mignotte and M. Coppey-Moisan, *Biophys. J.*, 2002, **83**, 3570–3577.
- 56 M. A. Rizzo, G. H. Springer, B. Granada and D. W. Piston, *Nat. Biotechnol.*, 2004, **22**, 445–449.
- 57 S. V. Koushik, H. Chen, C. Thaler, H. L. Puhl, 3rd and S. S. Vogel, *Biophys. J.*, 2006, **91**, L99–L101.

- 58 R. Yasuda, *Curr. Opin. Neurobiol.*, 2006, **16**, 551–561.
- 59 M. Millington, G. J. Grindlay, K. Altenbach, R. K. Neely, W. Kolch, M. Bencina, N. D. Read, A. C. Jones, D. T. Dryden and S. W. Magennis, *Biophys. Chem.*, 2007, **127**, 155–164.
- 60 G. J. Kremers, J. Goedhart, E. B. van Munster and T. W. Gadella, Jr., *Biochemistry*, 2006, **45**, 6570–6580.
- 61 R. M. Wachter, M. A. Elsliger, K. Kallio, G. T. Hanson and S. J. Remington, *Structure (London)*, 1998, **6**, 1267–1277.
- 62 A. Miyawaki, O. Griesbeck, R. Heim and R. Y. Tsien, *Proc. Natl. Acad. Sci. U. S. A.*, 1999, **96**, 2135–2140.
- 63 A. Miyawaki, T. Nagai and H. Mizuno, *Adv. Biochem. Eng. Biotechnol.*, 2005, **95**, 1–15.
- 64 J. Llopis, J. M. McCaffery, A. Miyawaki, M. G. Farquhar and R. Y. Tsien, *Proc. Natl. Acad. Sci. U. S. A.*, 1998, **95**, 6803–6808.
- 65 S. Jayaraman, P. Haggie, R. M. Wachter, S. J. Remington and A. S. Verkman, *J. Biol. Chem.*, 2000, **275**, 6047–6050.
- 66 T. Kuner and G. J. Augustine, *Neuron*, 2000, **27**, 447–459.
- 67 O. Griesbeck, G. S. Baird, R. E. Campbell, D. A. Zacharias and R. Y. Tsien, *J. Biol. Chem.*, 2001, **276**, 29188–29194.
- 68 A. W. Nguyen and P. S. Daugherty, *Nat. Biotechnol.*, 2005, **23**, 355–360.
- 69 T. Ohashi, S. D. Galiacy, G. Briscoe and H. P. Erickson, *Protein Sci.*, 2007, **16**, 1429–1438.
- 70 J. L. Vinkenborg, T. H. Evers, S. W. Reulen, E. W. Meijer and M. Merkx, *ChemBioChem*, 2007, **8**, 1119–1121.
- 71 R. E. Campbell, O. Tour, A. E. Palmer, P. A. Steinbach, G. S. Baird, D. A. Zacharias and R. Y. Tsien, *Proc. Natl. Acad. Sci. U. S. A.*, 2002, **99**, 7877–7882.
- 72 D. A. Zacharias, J. D. Violin, A. C. Newton and R. Y. Tsien, *Science*, 2002, **296**, 913–916.
- 73 W. W. Ward, in *Green Fluorescent Protein: Properties, Applications, and Protocols*, ed. M. Chalfie and S. R. Kain, Wiley-Interscience, New York, 2nd edn, 2006, pp. 39–65.
- 74 G. S. Baird, D. A. Zacharias and R. Y. Tsien, *Proc. Natl. Acad. Sci. U. S. A.*, 2000, **97**, 11984–11989.
- 75 L. A. Gross, G. S. Baird, R. C. Hoffman, K. K. Baldridge and R. Y. Tsien, *Proc. Natl. Acad. Sci. U. S. A.*, 2000, **97**, 11990–11995.
- 76 V. V. Verkhusha and K. A. Lukyanov, *Nat. Biotechnol.*, 2004, **22**, 289–296.
- 77 D. Yarbrough, R. M. Wachter, K. Kallio, M. V. Matz and S. J. Remington, *Proc. Natl. Acad. Sci. U. S. A.*, 2001, **98**, 462–467.
- 78 J. Zhang, R. E. Campbell, A. Y. Ting and R. Y. Tsien, *Nat. Rev. Mol. Cell Biol.*, 2002, **3**, 906–918.
- 79 P. V. Vrzheshch, N. A. Akovbian, S. D. Varfolomeyev and V. V. Verkhusha, *FEBS Lett.*, 2000, **487**, 203–208.
- 80 J. Wiehler, J. von Hummel and B. Steipe, *FEBS Lett.*, 2001, **487**, 384–389.
- 81 H. Mizuno, A. Sawano, P. Eli, H. Hama and A. Miyawaki, *Biochemistry*, 2001, **40**, 2502–2510.
- 82 D. A. Zacharias, *Sci. STKE*, 2002, **2002**, PE23.
- 83 J. Wiedenmann, B. Vallone, F. Renzi, K. Nienhaus, S. Ivanchenko, C. Rocker and G. U. Nienhaus, *J. Biomed. Opt.*, 2005, **10**, 14003.
- 84 A. F. Fradkov, V. V. Verkhusha, D. B. Staroverov, M. E. Bulina, Y. G. Yanushevich, V. I. Martynov, S. Lukyanov and K. A. Lukyanov, *Biochem. J.*, 2002, **368**, 17–21.
- 85 G. U. Nienhaus, K. Nienhaus, A. Holzle, S. Ivanchenko, F. Renzi, F. Oswald, M. Wolff, F. Schmitt, C. Rocker, B. Vallone, W. Weidemann, R. Heilker, H. Nar and J. Wiedenmann, *Photochem. Photobiol.*, 2006, **82**, 351–358.
- 86 Y. G. Yanushevich, D. B. Staroverov, A. P. Savitsky, A. F. Fradkov, N. G. Gurskaya, M. E. Bulina, K. A. Lukyanov and S. A. Lukyanov, *FEBS Lett.*, 2002, **511**, 11–14.
- 87 M. E. Bulina, V. V. Verkhusha, D. B. Staroverov, D. M. Chudakov and K. A. Lukyanov, *Biochem. J.*, 2003, **371**, 109–114.
- 88 U. Lauf, P. Lopez and M. M. Falk, *FEBS Lett.*, 2001, **498**, 11–15.
- 89 D. Shcherbo, C. S. Murphy, G. V. Ermakova, E. A. Solovieva, T. V. Chepurnykh, A. S. Shcheglov, V. V. Verkhusha, V. Z. Pletnev, K. L. Hazelwood, P. M. Roche, S. Lukyanov, A. G. Zaraisky, M. W. Davidson and D. M. Chudakov, *Biochem. J.*, 2009, **418**, 567–574.
- 90 Y. A. Labas, N. G. Gurskaya, Y. G. Yanushevich, A. F. Fradkov, K. A. Lukyanov, S. A. Lukyanov and M. V. Matz, *Proc. Natl. Acad. Sci. U. S. A.*, 2002, **99**, 4256–4261.
- 91 D. A. Shagin, E. V. Barsova, Y. G. Yanushevich, A. F. Fradkov, K. A. Lukyanov, Y. A. Labas, T. N. Semenova, J. A. Ugalde, A. Meyers, J. M. Nunez, E. A. Widder, S. A. Lukyanov and M. V. Matz, *Mol. Biol. Evol.*, 2004, **21**, 841–850.
- 92 A. Salih, A. Larkum, G. Cox, M. Kuhl and O. Hoegh-Guldberg, *Nature*, 2000, **408**, 850–853.
- 93 A. Leutenegger, C. D'Angelo, M. V. Matz, A. Denzel, F. Oswald, A. Salih, G. U. Nienhaus and J. Wiedenmann, *FEBS J.*, 2007, **274**, 2496–2505.
- 94 S. F. Field, M. Y. Bulina, I. V. Kelman, J. P. Bielawski and M. V. Matz, *J. Mol. Evol.*, 2006, **62**, 332–339.
- 95 M. V. Matz, A. F. Fradkov, Y. A. Labas, A. P. Savitsky, A. G. Zaraisky, M. L. Markelov and S. A. Lukyanov, *Nat. Biotechnol.*, 1999, **17**, 969–973.
- 96 S. Karasawa, T. Araki, T. Nagai, H. Mizuno and A. Miyawaki, *Biochem. J.*, 2004, **381**, 307–312.
- 97 D. Shcherbo, E. M. Merzlyak, T. V. Chepurnykh, A. F. Fradkov, G. V. Ermakova, E. A. Solovieva, K. A. Lukyanov, E. A. Bogdanova, A. G. Zaraisky, S. Lukyanov and D. M. Chudakov, *Nat. Methods*, 2007, **4**, 741–746.
- 98 B. J. Bevis and B. S. Glick, *Nat. Biotechnol.*, 2002, **20**, 83–87.
- 99 R. L. Strack, D. E. Strongin, D. Bhattacharyya, W. Tao, A. Berman, H. E. Broxmeyer, R. J. Keenan and B. S. Glick, *Nat. Methods*, 2008, **5**, 955–957.
- 100 N. C. Shaner, R. E. Campbell, P. A. Steinbach, B. N. Giepmans, A. E. Palmer and R. Y. Tsien, *Nat. Biotechnol.*, 2004, **22**, 1567–1572.
- 101 N. C. Shaner, M. Z. Lin, M. R. McKeown, P. A. Steinbach, K. L. Hazelwood, M. W. Davidson and R. Y. Tsien, *Nat. Methods*, 2008, **5**, 545–551.
- 102 L. Wang, W. C. Jackson, P. A. Steinbach and R. Y. Tsien, *Proc. Natl. Acad. Sci. U. S. A.*, 2004, **101**, 16745–16749.
- 103 D. M. Chudakov, S. Lukyanov and K. A. Lukyanov, *Trends Biotechnol.*, 2005, **23**, 605–613.
- 104 H. Masuda, Y. Takenaka, A. Yamaguchi, S. Nishikawa and H. Mizuno, *Gene*, 2006, **372**, 18–25.
- 105 Y. A. L. Mikhail, V. Matz and J. Ugalde, in *Green Fluorescent Protein*, ed. S. R. Kain and M. Chalfie, 2nd edn, 2005, pp. 139–161.
- 106 D. D. Deheyn, K. Kubokawa, J. K. McCarthy, A. Murakami, M. Porrachia, G. W. Rouse and N. D. Holland, *Biol. Bull.*, 2007, **213**, 95–100.
- 107 M. A. Shkrob, Y. G. Yanushevich, D. M. Chudakov, N. G. Gurskaya, Y. A. Labas, S. Y. Poponov, N. N. Mudrik, S. Lukyanov and K. A. Lukyanov, *Biochem. J.*, 2005, **392**, 649–654.
- 108 J. Petersen, P. G. Wilmann, T. Beddoe, A. J. Oakley, R. J. Devenish, M. Prescott and J. Rossjohn, *J. Biol. Chem.*, 2003, **278**, 44626–44631.
- 109 T. Beddoe, M. Ling, S. Dove, O. Hoegh-Guldberg, R. J. Devenish, M. Prescott and J. Rossjohn, *Acta Crystallogr., Sect. D: Biol. Crystallogr.*, 2003, **59**, 597–599.
- 110 S. J. Remington, R. M. Wachter, D. K. Yarbrough, B. Branchaud, D. C. Anderson, K. Kallio and K. A. Lukyanov, *Biochemistry*, 2005, **44**, 202–212.
- 111 X. Shu, N. C. Shaner, C. A. Yarbrough, R. Y. Tsien and S. J. Remington, *Biochemistry*, 2006, **45**, 9639–9647.
- 112 A. Kikuchi, E. Fukumura, S. Karasawa, H. Mizuno, A. Miyawaki and Y. Shiro, *Biochemistry*, 2008, **47**, 11573–11580.
- 113 O. M. Subach, I. S. Gundorov, M. Yoshimura, F. V. Subach, J. H. Zhang, D. Gruenwald, E. A. Souslova, D. M. Chudakov and V. V. Verkhusha, *Chem. Biol.*, 2008, **59**, 1116–1124.
- 114 E. M. Merzlyak, J. Goedhart, D. Shcherbo, M. E. Bulina, A. S. Shcheglov, A. F. Fradkov, A. Gaintzeva, K. A. Lukyanov, S. Lukyanov, T. W. Gadella and D. M. Chudakov, *Nat. Methods*, 2007, **4**, 555–557.
- 115 B. Richards, L. Zharkikh, F. Hsu, C. Dunn, A. Kamb and D. H. Teng, *Cytometry, Part A*, 2002, **48**, 106–112.
- 116 W. W. Ward and M. J. Cormier, *J. Biol. Chem.*, 1979, **254**, 781–788.
- 117 H.-w. Ai, J. N. Henderson, S. J. Remington and R. E. Campbell, *Biochem. J.*, 2006, **400**, 531–540.
- 118 R. N. Day, C. F. Booker and A. Periasamy, *J. Biomed. Opt.*, 2008, **13**, 031203.
- 119 N. G. Gurskaya, A. F. Fradkov, N. I. Pounkova, D. B. Staroverov, M. E. Bulina, Y. G. Yanushevich, Y. A. Labas, S. Lukyanov and K. A. Lukyanov, *Biochem. J.*, 2003, **373**, 403–408.

- 120 S. Karasawa, T. Araki, M. Yamamoto-Hino and A. Miyawaki, *J. Biol. Chem.*, 2003, **278**, 34167–34171.
- 121 M. J. Cormier and C. B. Eckroade, *Biochim. Biophys. Acta*, 1962, **64**, 340–344.
- 122 J. G. Morin and J. W. Hastings, *J. Cell Physiol.*, 1971, **77**, 305–312.
- 123 A. Miyawaki, *Cell Struct. Funct.*, 2002, **27**, 343–347.
- 124 N. G. Gurskaya, A. P. Savitsky, Y. G. Yanushevich, S. A. Lukyanov and K. A. Lukyanov, *BMC Biochem.*, 2001, **2**, 6.
- 125 Y. G. Yanushevich, N. G. Gurskaya, D. B. Staroverov, S. A. Lukyanov and K. A. Lukyanov, *Russ. J. Bioorg. Chem.*, 2003, **29**, 325–329.
- 126 V. E. Zagranichny, N. V. Rudenko, A. Y. Gorokhovatsky, M. V. Zakharov, T. A. Balashova and A. S. Arseniev, *Biochemistry*, 2004, **43**, 13598–13603.
- 127 A. Sakaue-Sawano, H. Kurokawa, T. Morimura, A. Hanyu, H. Hama, H. Osawa, S. Kashiwagi, K. Fukami, T. Miyata, H. Miyoshi, T. Imamura, M. Ogawa, H. Masai and A. Miyawaki, *Cell (Cambridge, Mass.)*, 2008, **132**, 487–498.
- 128 S. J. Remington, *Curr. Opin. Struct. Biol.*, 2006, **16**, 714–721.
- 129 A. Miyawaki, *Nat. Biotechnol.*, 2004, **22**, 1374–1376.
- 130 N. G. Gurskaya, A. F. Fradkov, A. Terskikh, M. V. Matz, Y. A. Labas, V. I. Martynov, Y. G. Yanushevich, K. A. Lukyanov and S. A. Lukyanov, *FEBS Lett.*, 2001, **507**, 16–20.
- 131 J. Wiedenmann, A. Schenk, C. Rocker, A. Girod, K. D. Spindler and G. U. Nienhaus, *Proc. Natl. Acad. Sci. U. S. A.*, 2002, **99**, 11646–11651.
- 132 A. Schenk, S. Ivanchenko, C. Rocker, J. Wiedenmann and G. U. Nienhaus, *Biophys. J.*, 2004, **86**, 384–394.
- 133 S. Kredel, K. Nienhaus, F. Oswald, M. Wolff, S. Ivanchenko, F. Cymer, A. Jeromin, F. J. Michel, K. D. Spindler, R. Heilker, G. U. Nienhaus and J. Wiedenmann, *Chem. Biol.*, 2008, **15**, 224–233.
- 134 S. Kredel, F. Oswald, K. Nienhaus, K. Deuschle, C. Rocker, M. Wolff, R. Heilker, G. U. Nienhaus and J. Wiedenmann, *PLoS One*, 2009, **4**, e4391.
- 135 K. A. Lukyanov, A. F. Fradkov, N. G. Gurskaya, M. V. Matz, Y. A. Labas, A. P. Savitsky, M. L. Markelov, A. G. Zaraisky, X. Zhao, Y. Fang, W. Tan and S. A. Lukyanov, *J. Biol. Chem.*, 2000, **275**, 25879–25882.
- 136 T. Kogure, S. Karasawa, T. Araki, K. Saito, M. Kinjo and A. Miyawaki, *Nat. Biotechnol.*, 2006, **24**, 577–581.
- 137 T. Kogure, H. Kawano, Y. Abe and A. Miyawaki, *Methods*, 2008, **45**, 223–226.
- 138 R. M. Dickson, A. B. Cubitt, R. Y. Tsien and W. E. Moerner, *Nature*, 1997, **388**, 355–358.
- 139 J. Lippincott-Schwartz and G. H. Patterson, *Science*, 2003, **300**, 87–91.
- 140 K. A. Lukyanov, D. M. Chudakov, S. Lukyanov and V. V. Verkhusha, *Nat. Rev. Mol. Cell Biol.*, 2005, **6**, 885–891.
- 141 S. W. Hell, *Science*, 2007, **316**, 1153–1158.
- 142 E. Betzig, G. H. Patterson, R. Sougrat, O. W. Lindwasser, S. Olenych, J. S. Bonifacino, M. W. Davidson, J. Lippincott-Schwartz and H. F. Hess, *Science*, 2006, **313**, 1642–1645.
- 143 M. Fernandez-Suarez and A. Y. Ting, *Nat. Rev. Mol. Cell Biol.*, 2008, **9**, 929–943.
- 144 P. D. M. Heilemann, J. Hofkens and M. Sauer, *Laser Photonics Rev.*, 2009, **3**, 180–202.
- 145 G. H. Patterson and J. Lippincott-Schwartz, *Science*, 2002, **297**, 1873–1877.
- 146 G. H. Patterson and J. Lippincott-Schwartz, *Methods*, 2004, **32**, 445–450.
- 147 D. M. Chudakov, V. V. Verkhusha, D. B. Staroverov, E. A. Souslova, S. Lukyanov and K. A. Lukyanov, *Nat. Biotechnol.*, 2004, **22**, 1435–1439.
- 148 J. N. Henderson, R. Gepstein, J. R. Heenan, K. Kallio, D. Huppert and S. J. Remington, *J. Am. Chem. Soc.*, 2009, **131**, 4176–4177.
- 149 V. V. Verkhusha and A. Sorkin, *Chem. Biol.*, 2005, **12**, 279–285.
- 150 F. V. Subach, G. H. Patterson, S. Manley, J. M. Gillette, J. Lippincott-Schwartz and V. V. Verkhusha, *Nat. Methods*, 2009, **6**, 153–159.
- 151 T. Matsuda, A. Miyawaki and T. Nagai, *Nat. Methods*, 2008, **5**, 339–345.
- 152 R. Ando, H. Hama, M. Yamamoto-Hino, H. Mizuno and A. Miyawaki, *Proc. Natl. Acad. Sci. U. S. A.*, 2002, **99**, 12651–12656.
- 153 M. Tomura, N. Yoshida, J. Tanaka, S. Karasawa, Y. Miwa, A. Miyawaki and O. Kanagawa, *Proc. Natl. Acad. Sci. U. S. A.*, 2008, **105**, 10871–10876.
- 154 T. Sato, M. Takahoko and H. Okamoto, *Genesis (N. Y., NY, U. S.)*, 2006, **44**, 136–142.
- 155 J. M. Davison, C. M. Akitake, M. G. Goll, J. M. Rhee, N. Gosse, H. Baier, M. E. Halpern, S. D. Leach and M. J. Parsons, *Dev. Biol.*, 2007, **304**, 811–824.
- 156 S. Tamaki, S. Matsuo, H. L. Wong, S. Yokoi and K. Shimamoto, *Science*, 2007, **316**, 1033–1036.
- 157 A. A. Pakhomov, N. Y. Martynova, N. G. Gurskaya, T. A. Balashova and V. I. Martynov, *Biochemistry (Moscow)*, 2004, **69**, 901–908.
- 158 H. Mizuno, T. K. Mal, K. I. Tong, R. Ando, T. Furuta, M. Ikura and A. Miyawaki, *Mol. Cell*, 2003, **12**, 1051–1058.
- 159 K. Nienhaus, G. U. Nienhaus, J. Wiedenmann and H. Nar, *Proc. Natl. Acad. Sci. U. S. A.*, 2005, **102**, 9156–9159.
- 160 N. G. Gurskaya, V. V. Verkhusha, A. S. Shcheglov, D. B. Staroverov, T. V. Chepurnykh, A. F. Fradkov, S. Lukyanov and K. A. Lukyanov, *Nat. Biotechnol.*, 2006, **24**, 461–465.
- 161 D. M. Chudakov, S. Lukyanov and K. A. Lukyanov, *BioTechniques*, 2007, **42**, 553–563.
- 162 M. Takeuchi and T. Ozawa, *Anal. Sci.*, 2007, **23**, 25–29.
- 163 J. Wiedenmann, S. Ivanchenko, F. Oswald, F. Schmitt, C. Rocker, A. Salih, K. D. Spindler and G. U. Nienhaus, *Proc. Natl. Acad. Sci. U. S. A.*, 2004, **101**, 15905–15910.
- 164 S. A. McKinney, C. S. Murphy, K. L. Hazelwood, M. W. Davidson and L. L. Looger, *Nat. Methods*, 2009, **6**, 131–133.
- 165 H. Tsutsui, S. Karasawa, H. Shimizu, N. Nukina and A. Miyawaki, *EMBO Rep.*, 2005, **6**, 233–238.
- 166 S. Habuchi, H. Tsutsui, A. B. Kochaniak, A. Miyawaki and A. M. van Oijen, *PLoS One*, 2008, **3**, e3944.
- 167 G. Valentini, C. Verheggen, T. Pirola, H. Neel, M. Coppey-Moisan and E. Bertrand, *Nat. Methods*, 2005, **2**, 801.
- 168 D. Sinnecker, P. Voigt, N. Hellwig and M. Schaefer, *Biochemistry*, 2005, **44**, 7085–7094.
- 169 G.-J. Kremers, K. L. Hazelwood, C. S. Murphy, M. W. Davidson and D. W. Piston, *Nat. Methods*, 2009, **6**, 355–358.
- 170 E. J. G. Peterman, S. Brasselet and W. E. Moerner, *J. Phys. Chem. A*, 1999, **103**, 10553–10560.
- 171 R. Ando, H. Mizuno and A. Miyawaki, *Science*, 2004, **306**, 1370–1373.
- 172 S. Habuchi, R. Ando, P. Dedecker, W. Verheijen, H. Mizuno, A. Miyawaki and J. Hofkens, *Proc. Natl. Acad. Sci. U. S. A.*, 2005, **102**, 9511–9516.
- 173 P. Dedecker, J. Hotta, R. Ando, A. Miyawaki, Y. Engelborghs and J. Hofkens, *Biophys. J.*, 2006, **91**, L45–L47.
- 174 J. N. Henderson, H. W. Ai, R. E. Campbell and S. J. Remington, *Proc. Natl. Acad. Sci. U. S. A.*, 2007, **104**, 6672–6677.
- 175 M. Andresen, A. C. Stiel, J. Folling, D. Wenzel, A. Schonle, A. Egner, C. Eggeling, S. W. Hell and S. Jakobs, *Nat. Biotechnol.*, 2008, **26**, 1035–1040.
- 176 A. C. Stiel, S. Trowitzsch, G. Weber, M. Andresen, C. Eggeling, S. W. Hell, S. Jakobs and M. C. Wahl, *Biochem. J.*, 2007, **402**, 35–42.
- 177 D. M. Chudakov, V. V. Belousov, A. G. Zaraisky, V. V. Novoselov, D. B. Staroverov, D. B. Zorov, S. Lukyanov and K. A. Lukyanov, *Nat. Biotechnol.*, 2003, **21**, 191–194.
- 178 A. C. Stiel, M. Andresen, H. Bock, M. Hilbert, J. Schilde, A. Schonle, C. Eggeling, A. Egner, S. W. Hell and S. Jakobs, *Biophys. J.*, 2008, **95**, 2989–2997.
- 179 V. Adam, M. Lelimousin, S. Boehme, G. Desfonds, K. Nienhaus, M. J. Field, J. Wiedenmann, S. McSweeney, G. U. Nienhaus and D. Bourgeois, *Proc. Natl. Acad. Sci. U. S. A.*, 2008, **105**, 18343–18348.
- 180 M. Andresen, A. C. Stiel, S. Trowitzsch, G. Weber, C. Eggeling, M. C. Wahl, S. W. Hell and S. Jakobs, *Proc. Natl. Acad. Sci. U. S. A.*, 2007, **104**, 13005–13009.
- 181 M. Andresen, M. C. Wahl, A. C. Stiel, F. Grater, L. V. Schafer, S. Trowitzsch, G. Weber, C. Eggeling, H. Grubmuller, S. W. Hell and S. Jakobs, *Proc. Natl. Acad. Sci. U. S. A.*, 2005, **102**, 13070–13074.
- 182 A. Terskikh, A. Fradkov, G. Ermakova, A. Zaraisky, P. Tan, A. V. Kajava, X. N. Zhao, S. Lukyanov, M. Matz, S. Kim, I. Weissman and P. Siebert, *Science*, 2000, **290**, 1585–1588.

- 183 F. V. Subach, O. M. Subach, I. S. Gundorov, K. S. Morozova, K. D. Piatkevich, A. M. Cuervo and V. V. Verkhusha, *Nat. Chem. Biol.*, 2009, **5**, 118–126.
- 184 J. Livet, T. A. Weissman, H. Kang, R. W. Draft, J. Lu, R. A. Bennis, J. R. Sanes and J. W. Lichtman, *Nature*, 2007, **450**, 56–62.
- 185 D. Axelrod, D. E. Koppel, J. Schlessinger, E. Elson and W. W. Webb, *Biophys. J.*, 1976, **16**, 1055–1069.
- 186 D. E. Koppel, D. Axelrod, J. Schlessinger, E. L. Elson and W. W. Webb, *Biophys. J.*, 1976, **16**, 1315–1329.
- 187 R. D. Phair and T. Misteli, *Nat. Rev. Mol. Cell Biol.*, 2001, **2**, 898–907.
- 188 M. Weiss, *Traffic*, 2004, **5**, 662–671.
- 189 J. Lippincott-Schwartz, N. Altan-Bonnet and G. H. Patterson, *Nat. Cell Biol.*, 2003, *Suppl.*, S7–S14.
- 190 J. Lippincott-Schwartz, E. Snapp and A. Kenworthy, *Nat. Rev. Mol. Cell Biol.*, 2001, **2**, 444–456.
- 191 A. Egner, C. Geisler, C. von Middendorff, H. Bock, D. Wenzel, R. Medda, M. Andresen, A. C. Stiel, S. Jakobs, C. Eggeling, A. Schonle and S. W. Hell, *Biophys. J.*, 2007, **93**, 3285–3290.
- 192 S. T. Hess, T. P. Girirajan and M. D. Mason, *Biophys. J.*, 2006, **91**, 4258–4272.
- 193 E. A. Jares-Erijman and T. M. Jovin, *Nat. Biotechnol.*, 2003, **21**, 1387–1395.
- 194 B. A. Pollok and R. Heim, *Trends Cell Biol.*, 1999, **9**, 57–60.
- 195 K. Truong and M. Ikura, *Curr. Opin. Struct. Biol.*, 2001, **11**, 573–578.
- 196 S. S. Vogel, C. Thaler and S. V. Koushik, *Sci. STKE*, 2006, **2006**, re2.
- 197 C. Thaler, S. V. Koushik, P. S. Blank and S. S. Vogel, *Biophys. J.*, 2005, **89**, 2736–2749.
- 198 R. N. Day, C. F. Booker and A. Periasamy, *J. Biomed. Opt.*, 2008, **13**, 031203.
- 199 M. Elangovan, H. Wallrabe, Y. Chen, R. N. Day, M. Barroso and A. Periasamy, *Methods*, 2003, **29**, 58–73.
- 200 G. W. Gordon, G. Berry, X. H. Liang, B. Levine and B. Herman, *Biophys. J.*, 1998, **74**, 2702–2713.
- 201 Z. P. Xia and Y. H. Liu, *Biophys. J.*, 2001, **81**, 2395–2402.
- 202 C. Berney and G. Danuser, *Biophys. J.*, 2003, **84**, 3992–4010.
- 203 A. K. Kenworthy, *Methods*, 2001, **24**, 289–296.
- 204 P. I. Bastiaens and T. M. Jovin, *Proc. Natl. Acad. Sci. U. S. A.*, 1996, **93**, 8407–8412.
- 205 P. I. Bastiaens, I. V. Majoul, P. J. Verveer, H. D. Soling and T. M. Jovin, *EMBO J.*, 1996, **15**, 4246–4253.
- 206 R. N. Day, A. Periasamy and F. Schaufele, *Methods*, 2001, **25**, 4–18.
- 207 A. Miyawaki and R. Y. Tsien, *Methods Enzymol.*, 2000, **327**, 472–500.
- 208 R. N. Day and D. W. Piston, *Nat. Biotechnol.*, 1999, **17**, 425–426.
- 209 A. Periasamy and R. N. Day, *Molecular imaging: FRET microscopy and spectroscopy*, Oxford University Press, Oxford, New York, 2005.
- 210 D. W. Piston and G. J. Kremers, *Trends Biochem. Sci.*, 2007, **32**, 407–414.
- 211 P. I. Bastiaens and A. Squire, *Trends Cell Biol.*, 1999, **9**, 48–52.
- 212 M. Peter, S. M. Ameer-Beg, M. K. Hughes, M. D. Keppler, S. Prag, M. Marsh, B. Vojnovic and T. Ng, *Biophys. J.*, 2005, **88**, 1224–1237.
- 213 C. Y. Dong, T. French, P. T. So, C. Buehler, K. M. Berland and E. Gratton, *Methods Cell Biol.*, 2003, **72**, 431–464.
- 214 R. M. Clegg, O. Holub and C. Gohlke, *Methods Enzymol.*, 2003, **360**, 509–542.
- 215 M. Tramier, K. Kemnitz, C. Durieux and M. Coppey-Moisan, *J. Microsc. (Oxford, U. K.)*, 2004, **213**, 110–118.
- 216 M. Tramier, M. Zahid, J. C. Mevel, M. J. Masse and M. Coppey-Moisan, *Microsc. Res. Tech.*, 2006, **69**, 933–939.
- 217 S. Ganesan, S. M. Ameer-Beg, T. T. Ng, B. Vojnovic and F. S. Wouters, *Proc. Natl. Acad. Sci. U. S. A.*, 2006, **103**, 4089–4094.
- 218 H. Murakoshi, S. J. Lee and R. Yasuda, *Brain Cell Biol.*, 2008, **36**, 31–42.
- 219 T. Nagai, S. Yamada, T. Tominaga, M. Ichikawa and A. Miyawaki, *Proc. Natl. Acad. Sci. U. S. A.*, 2004, **101**, 10554–10559.
- 220 A. Miyawaki, *Neuron*, 2005, **48**, 189–199.
- 221 M. D. Allen and J. Zhang, *Biochem. Biophys. Res. Commun.*, 2006, **348**, 716–721.
- 222 H. W. Ai, K. L. Hazelwood, M. W. Davidson and R. E. Campbell, *Nat. Methods*, 2008, **5**, 401–403.
- 223 X. You, A. W. Nguyen, A. Jabaiah, M. A. Sheff, K. S. Thorn and P. S. Daugherty, *Proc. Natl. Acad. Sci. U. S. A.*, 2006, **103**, 18458–18463.
- 224 N. S. Xia, W. X. Luo, J. Zhang, X. Y. Xie, H. J. Yang, S. W. Li, M. Chen and M. H. Ng, *Mar. Biotechnol.*, 2002, **4**, 155–162.
- 225 H.-w. Ai, S. Olenych, P. Wong, M. Davidson and R. Campbell, *BMC Biol.*, 2008, **6**, 13.
- 226 C. Flors, J. Hotta, H. Uji-I, P. Dedecker, R. Ando, H. Mizuno, A. Miyawaki and J. Hofkens, *J. Am. Chem. Soc.*, 2007, **129**, 13970–13977.
- 227 R. Bizzarri, C. Arcangeli, D. Arosio, F. Ricci, P. Faraci, F. Cardarelli and F. Beltram, *Biophys. J.*, 2006, **90**, 3300–3314.